

The komatiite testimony to ancient mantle heterogeneity

Igor Puchtel, Janne Blichert-Toft, Mary Horan, Mathieu Touboul, Richard Walker

▶ **To cite this version:**

Igor Puchtel, Janne Blichert-Toft, Mary Horan, Mathieu Touboul, Richard Walker. The komatiite testimony to ancient mantle heterogeneity. Chemical Geology, 2022, 594, pp.120776. 10.1016/j.chemgeo.2022.120776 . hal-03589592

HAL Id: hal-03589592
https://hal.science/hal-03589592

Submitted on 25 Feb 2022

HAL is a multi-disciplinary open access archive for the deposit and dissemination of scientific research documents, whether they are published or not. The documents may come from teaching and research institutions in France or abroad, or from public or private research centers.

L'archive ouverte pluridisciplinaire **HAL**, est destinée au dépôt et à la diffusion de documents scientifiques de niveau recherche, publiés ou non, émanant des établissements d'enseignement et de recherche français ou étrangers, des laboratoires publics ou privés.

Revised manuscript with no changes marked

Click here to view linked References

The Komatiite Testimony to Ancient Mantle Heterogeneity

Igor S. Puchtel[1*], Janne Blichert-Toft[2], Mary F. Horan[3],
Mathieu Touboul[2], and Richard J. Walker[1]

[1]Department of Geology, University of Maryland, 8000 Regents Drive, College Park, MD 20742, USA
[2]Laboratoire de Géologie de Lyon, Ecole Normale Supérieure de Lyon, CNRS UMR 5276, Université de Lyon, 46 Allée d'Italie, 69007 Lyon, France
[3]Earth and Planets Laboratory, Carnegie Institution for Science, 5241 Broad Branch Road NW, Washington, DC 20015, USA

*Corresponding author: ipuchtel@umd.edu

Revised for:
Chemical Geology
Invited Review Manuscript

Version: February 06, 2022

Keywords: Komatiites; early Earth; mantle heterogeneity; Hf-W, Sm-Nd, Lu-Hf, Re-Os, Pt-Os isotope systems; highly siderophile elements; grainy late accretion; primordial magma ocean, core-mantle interaction; mixing times of the mantle; Nd-Hf-Os isotope paradox.

Abstract

Komatiites are crystallized samples of high-temperature, high-MgO lavas that were common during the Archean, but became increasingly rarer in the Proterozoic and Phanerozoic. Although the origin of komatiites remains a subject of debate, all komatiites included in this review, ranging in age from 3.6 to 2.0 Ga, are interpreted to have most likely been derived from anhydrous melting in mantle plumes. These plumes are estimated to have been initiated at different depths in the mantle, thus, providing important information about the chemical evolution of the early Earth.

The ^{142,143}Nd, ^{176}Hf, ^{182}W, ^{187}Os, and ^{186}Os systematics and trace- and highly siderophile element (HSE) abundances of these komatiites provide strong evidence for the presence of isotopic and chemical heterogeneities in the mantle during the first half of Earth history. These heterogeneities likely reflect the combined effects of: (1) the co-existence of diverse post-magma ocean silicate domains that were characterized by variably-fractionated lithophile and siderophile element abundances; (2) the presence of distinct reservoirs that included mantles and cores of late accreted, differentiated planetesimals; and (3) isotopic exchange across the core-mantle boundary. These data highlight the complexity of komatiite mantle sources, none of which were similar in composition to estimates for the modern bulk silicate Earth (BSE). Moreover, no single petrogenetic model can account for the remarkably diverse chemical and isotopic compositions of komatiites.

The disappearance of resolvable positive and negative ^{142}Nd anomalies, as well as decoupled ^{143}Nd-^{176}Hf isotopic signatures, in the mafic-ultramafic rock record by ~2.5 Ga indicate that, by the end of the Archean, the earliest silicate reservoirs, formed through primordial magma ocean crystallization, had been largely destroyed as a result of vigorous convective mantle mixing. This implies that, during the Hadean and Archean, it took the mantle ~1.5 Ga to mix away the early formed ^{142}Nd heterogeneities *via* wholesale mantle convection. Similar to ^{142}Nd systematics, there appears to have been a shift from mostly positive ^{182}W anomalies in pre-2.5 Ga komatiite mantle sources to no ^{182}W offsets in post-2.5 Ga komatiite mantle sources. Coupled with the disapperance of projected HSE depletions in komatiite mantle sources at ~2.5 Ga, relative to the modern BSE, this shift may indicate that by the end of the Archean, late accreted planetesimals had become largely homogenized within the mantle, and core-mantle interaction took over as the main driving force of creating ^{182}W isotope anomalies, possibly coincident with the timing of the onset of modern-style plate tectonics on Earth.

1. Introduction

Accurately determining how the distribution of chemical elements within the Earth has changed over time has been, and remains, one of the most fundamental challenges in Earth science; it has far-reaching implications not only for the long-standing debate of how terrestrial planets formed and evolved, but also for understanding ongoing processes on Earth. The information pertaining to the origin and early evolution of Earth comes largely from the geological rock record between ~4.0 and 2.0 Ga, which harbors isotopic and elemental signatures generated in the terrestrial reservoirs *via* early chemical fractionation processes and the radioactive decay of short- and long-lived refractory nuclides, including ^{146,147}Sm, ^{176}Lu, ^{182}Hf, ^{187}Re, and ^{190}Pt.

The mantle is the largest of all the terrestrial reservoirs. Its chemically and isotopically heterogeneous nature has long been established by numerous pioneering studies of the Earth's rock record (*e.g.*, Hart and Brooks, 1977; Hofmann and Hart, 1978; Zindler et al., 1982; Hart and Zindler, 1986; Zindler and Hart, 1986; Jacobsen, 1988; Galer and Goldstein, 1991). Some of the heterogeneities have been argued to be primordial in nature, reflecting initial planetary accretion/differentiation and magma ocean crystallization processes (Goldstein and Galer, 1992; Albarède et al., 2000; Drake, 2000; Boyet and Carlson, 2005; Frost et al., 2008; Caro, 2011; Touboul et al., 2012; Carlson et al., 2015; Jacobsen and Yu, 2015; Puchtel et al., 2016a; Rizo et al., 2016; Boyet et al., 2021). Others likely were formed as a result of a protracted terrestrial accretion history (*e.g.*, Willbold et al., 2011; 2015; Dale et al., 2017; Puchtel et al., 2018; Archer et al., 2019) or later processes associated with the dynamic regime of the planet, especially crustal recycling (*e.g.*, DePaolo, 1980; Armstrong, 1981; Hofmann and White, 1982; Patchett et al., 1984; Shirey and Hanson, 1986; Chase and Patchett, 1988; Galer et al., 1989; Bowring and Housh, 1995; Bennett et al., 1996; Salters and White, 1998; Blichert-Toft et al., 2015).

Despite these decades-long research efforts, still limited insights into the terrestrial mantle mixing history mean that the nature, origin, scale, and longevity of early mantle heterogeneities, in terms of different elements and isotopic systems, remain contentious. This review is intended to fill some of the existing gaps in our understanding of early Earth chemical evolution by synthesizing the existing short- and long-lived refractory radiogenic isotopic and elemental abundance data for a representative set of well-preserved and well-characterized komatiite and basalt systems that are especially advantageous for studying processes that occurred within the first 2.5 billion years of Earth history. In parallel, we

address the question of the complex origins of komatiites and their usefulness as proxies for the chemical composition of the early Earth mantle.

Here, we consider komatiite-basalt systems from 13 different localities around the globe: the 3.55 Ga Schapenburg, 3.48 Ga Komati, and 3.26 Ga Weltevreden komatiites in the Kaapvaal Craton of South Africa; the 3.53 Ga Coonterunah, 3.34 Ga Kelly, and 3.18 Ga Ruth Well and Regal komatiites and basalts in the Pilbara Craton of Western Australia; the 2.82 Ga Kostomuksha, 2.41 Ga Vetreny, and 2.05 Ga Lapland komatiites in the Fennoscandian Shield of northern Europe; the 2.72 Ga Pyke Hill-Alexo and Boston Creek komatiites in the Superior Craton of Canada, and the 2.7 Ga Belingwe komatiites in the Rhodesian Craton of South Africa. These komatiite-basalt systems were chosen because of good preservation of their primary mineralogical and textural features and chemical and isotopic compositions, and because complete sets of published high-precision chemical and isotope data, obtained on the same sample sets, are available for these systems. A schematic world map showing the location of these komatiite-basalt systems is provided in the ***Electronic Supplement***.

2. Komatiites as probes of the early Earth mantle

Komatiites are ultramafic lavas containing more than 18% MgO in the parental liquid (Arndt and Nisbet, 1982). To be classified as a komatiite, the crystallized lava must either contain spinifex texture, or be genetically related to lavas containing spinifex texture. Spinifex texture is a crucial feature that distinguishes komatiites from other ultramafic lavas, such as picrites, boninites, and meimechites. It is characterized by the presence of large, skeletal crystals of olivine that form during rapid, *in situ* crystallization of high-MgO, superheated (*i.e.*, heated to above liquidus temperatures) silicate liquids. Due to the absence of nucleation sites, superheated liquids display a reluctance to nucleate, and olivine crystals that eventually form do so rapidly upon cooling below the liquidus and are typically large and skeletal, leading to the formation of spinifex texture (*e.g.*, Arndt, 1994; Arndt et al., 2008).

Ever since komatiites were first discovered and described in South Africa (Viljoen and Viljoen, 1969), these rocks have served as a source of valuable information bearing on the chemical and thermal evolution of the mantle (*e.g.*, Arndt et al., 2008). Owing to formation *via* the highest degrees of partial melting of all mantle-derived magmas, komatiites have compositions approaching that of mantle peridotite and, thus, represent the closest available approximation of the chemical characteristics of the mantle among volcanic rocks (*e.g.*, Arndt, 1977; Nesbitt et al., 1979; Herzberg, 1992). As high-degree, superheated, and low-viscosity melts, komatiites extracted large proportions of highly siderophile elements (HSE,

including Re, Os, Ir, Ru, Pt, and Pd) from the mantle, experienced little differentiation prior to emplacement, and likely sampled mantle domains on the order of tens of millions of cubic kilometers, as evidenced by the sheer volumes of komatiitic magmas erupted in a number of Archean terrains. Some of these occurrences are argued to be similar in volume to recent and modern oceanic plateaus, such as the Ontong Java plateau (*e.g.*, Condie, 1975; Schubert and Sandwell, 1989; Storey et al., 1991; Kusky and Kidd, 1992; Desrochers et al., 1993; Kimura et al., 1993; Abbott, 1996; Kent et al., 1996; Puchtel et al., 1998; Arndt et al., 2001). During crystallization of komatiite lava flows, major and trace elements, including HSE, behaved in predictable manners relative to indices of magmatic differentiation, making it possible to obtain precise chronological information, estimate element mobility, and determine HSE abundances in the mantle sources of most komatiites. The ability of komatiites to provide a reliable record of the chemical and isotopic characteristics of mantle domains that existed during the first half of Earth history is the key underlying factor for focusing on komatiites in this review, which is intended to summarize what komatiites have taught us about the evolution of early Earth. On the other hand, although basalts are less informative as probes of the HSE characteristics of the mantle, because of their inherently higher Nd, Hf, and W abundances, they are shown here to be reliable recorders of mantle Nd, Hf, and W isotopic compositions and have also been studied in several komatiite-basalt systems.

3. The analytical toolbox to study the chemical evolution of the mantle

The chemical evolution of the mantle has long been studied using radiogenic isotope systems and lithophile and siderophile element abundances in mantle-derived rocks. The lithophile element-based isotopic systems, particularly ^{142,143}Nd and ^{176}Hf, are, by way of their refractory nature and optimal half-lives, powerful tools for examining possible primordial magma ocean processes, as well as subsequent mantle melting and differentiation processes (*e.g.*, DePaolo and Wasserburg, 1976; Jacobsen and Wasserburg, 1979; Patchett and Tatsumoto, 1980; Patchett et al., 1981; White and Patchett, 1984; Zindler and Hart, 1986; Sivell and McCulloch, 1991). Silicate melts have lower Sm/Nd and Lu/Hf than co-existing silicate solids, and after separation, evolve to distinctive ^{143}Nd and ^{176}Hf compositions. If Sm/Nd fractionated prior to ~4.0 Ga, while ^{146}Sm was still extant, variations in ^{142}Nd can also be generated. Hence, application of the combined ^{142,143}Nd systems provides the temporal resolution necessary for deciphering the timing and mechanisms of the earliest mantle differentiation events (Goldstein and Galer, 1992; Harper and Jacobsen, 1992; Boyet et al., 2003; Caro et al., 2003, 2006, 2017; Boyet and Carlson, 2005, 2006; Bennett et al., 2007;

O'Neil et al., 2008, 2012, 2016; Rizo et al., 2012, 2013, 2016; Roth et al., 2013, 2014). Further combining the ^{142,143}Nd with the ^{176}Hf systematics allows identification of specific processes that may have controlled mantle differentiation, including fractionation of the high-pressure bridgmanite (Mg-perovskite) and Ca-perovskite assemblage during crystallization of a primordial magma ocean (Caro et al., 2005; Hoffmann et al., 2011; Rizo et al., 2011; Puchtel et al., 2013; 2016a; Hoffmann and Wilson, 2017; Boyet et al., 2021).

The short-lived ^{182}Hf-^{182}W system can be used to detect fractionation of the lithophile trace element Hf from the siderophile trace element W occurring within the first ~60 Ma of Solar System history. This isotope system constitutes a high-resolution tool for identifying magma ocean crystallization, the effects of late accretion, and, by virtue of its dual lithophile and siderophile nature, potentially core-mantle interaction processes (Kleine et al., 2002, 2004, 2009; Yin et al., 2002, Jacobsen and Yu, 2015; Reimink et al., 2020; Willbold et al., 2011, 2015; Touboul et al., 2012; Puchtel et al., 2018, 2020, 2022; Rizo et al., 2019; Mundl-Petermeier et al., 2019, 2020). Further, application of the combined ^{142}Nd and ^{182}W tools can help discriminate between early magma ocean differentiation processes and the effects of late accretion (Harper and Jacobsen, 1996; Rizo et al., 2016; 2019; Puchtel et al., 2018; Peters et al., 2021).

Abundances of HSE, combined with ^{186}Os and ^{187}Os systematics, provide additional information about the chemical evolution of the mantle and the processes that operated early in Earth history (*e.g.*, Righter et al., 2000; Walker, 2009, 2016; Day, 2013; Puchtel et al., 2014; Day et al., 2016). The behavior of Re, Pt, and Os is governed by their strong partitioning into metal or sulfide liquids relative to silicate melt (Crocket et al., 1997; Righter and Drake, 1997). During mantle melting, Os is moderately to highly compatible with the melting residue, whereas Pt and Re are incompatible to various degrees (*e.g.*, Barnes et al., 1985; Rehkämper et al., 1999; Mallmann and O'Neill, 2007). Thus, the two Os isotopic systems together with HSE abundances provide insight into some primordial processes to which the lithophile element-based isotopic systems are not sensitive, including late-stage planetary accretion and metal-silicate differentiation. Estimates of HSE abundances in komatiite mantle sources can also be used to track the mixing rates of the mantle and the timing of homogenization of late accreted materials within the mantle (*e.g.*, Maier et al., 2009; Puchtel et al., 2018, 2020, 2022). In combination with Os isotope systematics and HSE abundances, the ^{182}Hf-^{182}W isotopic system can be used to discriminate between the effects of early planetary differentiation, late accretion, and core-mantle interaction (*e.g.*, Touboul et al.,

2012; Puchtel et al., 2016a, 2018, 2020, 2022; Archer et al., 2019; Rizo et al., 2019; Tusch et al., 2021).

The water content of a komatiitic lava is also an important parameter for assessing where in the mantle the parental melt originated. Water is highly incompatible during mantle melting (*e.g.*, Moore, 1970; Michael, 1995; Saal et al., 2002; Hauri et al., 2006; Cooper et al., 2012). The water content of a given komatiite mantle source can be derived from that of a komatiite lava provided that effects of secondary alteration can be corrected for. For example, correlations between the abundances of water and other lithophile trace elements, *e.g.*, Ce, in submarine basalt glasses have been used in a number of studies to establish H_2O contents of mantle-derived melts (*e.g.*, Michael, 1995; Saal et al., 2002; Hauri et al., 2006; Cooper et al., 2012). Mid-ocean ridge basalt (MORB) and ocean island basalt (OIB) magmas have $H_2O/Ce \leq 370$ (Hauri et al., 2006), similar to the mantle value of 200±50 (Hirschmann, 2018); the rather large range is due to the fact that during anhydrous mantle melting, spinel lherzolite has a bulk solid/melt $D_{H2O} \approx D_{Ce}$, whereas garnet lherzolite has a bulk solid/melt $D_{H2O} = 0.5 \times D_{Ce}$. By contrast, arc magmas have H_2O/Ce of 2,000 to 3,000, due to variable contributions of H_2O from the subducting slab (Cooper et al., 2012).

The oxidation state of a komatiite magma and its source reflects important information about the location and processes involved in its generation. For example, knowledge of fO_2 can potentially be used to distinguish between a hydrous (*i.e.*, subduction) versus anhydrous (*i.e.*, plume) origin of komatiites. Canil (1997, 1999, 2002) and Canil and Fedortchouk (2001) used V partitioning between liquidus olivine and komatiite liquid as a redox indicator. These authors showed that the major factor controlling the distribution of V between olivine and komatiitic melt $\left(D_V^{ol/liq}\right)$ was oxygen fugacity, fO_2. More oxidized, water-rich island arc magmas (higher fO_2) are invariably characterized by $D_V^{ol/liq} < 0.01$, whereas less oxidized, anhydrous mantle plume-derived magmas (*e.g.*, OIB and MORB) exhibit $D_V^{ol/liq} = 0.025$ - 0.10.

Additional diagnostic features pointing to the origins of komatiites include estimates of potential temperatures of inferred mantle sources and depths of melting initiation. To compare mantle temperatures at various localities, McKenzie and Bickle (1988) proposed the concept of a mantle potential temperature ($\mathbf{T_p}$) as a point of reference. Mantle potential temperature is the temperature that the solid adiabatically-convecting asthenospheric mantle would have had at the surface if it ascended without undergoing melting. Mantle potential temperature determines the depth of melting initiation (*e.g.*, Richter, 1988; Herzberg, 1992, 1995;

Herzberg et al., 2007), which, in turn, governs the style of mantle melting and melt segregation (fractional versus batch). The depth of melting initiation and subsequent melt segregation determines the chemical composition of the resultant komatiite melts, including MgO contents. Pressures >8 GPa (240 km depth) stabilize majorite garnet relative to olivine and pyroxene in the source (e.g., Ohtani, 1984; Herzberg and Ohtani, 1988). If the temperature of a plume core is sufficiently high to initiate melting in the majorite garnet stability field, the melting results in the formation of Al-depleted komatiitic melts with subchondritic Al_2O_3/TiO_2 and Gd/Yb, provided the melt separated from the melting residue while still in the majorite garnet stability field. By contrast, melting and melt segregation at lower pressures, within the spinel lherzolite stability field, produces Al-undepleted komatiitic magmas with chondritic Al_2O_3/TiO_2 and Gd/Yb (*e.g.*, Green, 1975; Ohtani, 1984; Kato et al., 1988; Herzberg, 1995).

4. Which parts of the mantle do komatiites sample?

In order to assess the extents of early mantle isotopic and chemical heterogeneities sampled by komatiites, it is important to determine where in the mantle komatiites originate. The location of komatiite magma generation is almost certainly not the same for all komatiites, given the extent of chemical and isotopic heterogeneity inferred for their mantle sources. This, in turn, requires assessment of diverse komatiite formation models.

Komatiites were most common during the Archean and may, during this eon, have been the volumetrically second most significant constituent among volcanic rocks, comprising as much as 25% of the entire volume of volcanic sequences, the rest being composed mostly of basalts (*e.g.*, Condie, 1975, 1981, 1994; deWit and Ashwal, 1997). Some of these basalts were also derived from komatiites *via* fractional crystallization processes, while others were lower-degree partial melts generated from the same sources as the spatially associated komatiites (Arndt et al., 1977; Campbell et al., 1989; Condie, 2005). The abrupt decline in the abundance of komatiites at the Archean-Proterozoic boundary, as well as the decrease in the MgO contents of emplaced komatiite lavas, have been interpreted as evidence for a significant, up to 300ºC, secular cooling of the mantle over the course of Earth history (*e.g.*, Bickle, 1982; Nisbet et al., 1993; Herzberg et al., 2007; Herzberg and Gazel, 2009). Some authors have linked this to a transition from drip to subduction tectonics (Campbell and Griffiths, 2014), arguing that an increasing abundance of subducted slabs allowed for formation of the core-enveloping D″ insulating layer, which they in turn associate with a step-like drop in maximum komatiite magma MgO contents and mantle potential temperatures between 2.7 and 2.0 Ga.

The origin of komatiites has been a subject of studies for the past half century (*e.g.*, Green, 1975, 1981; Allègre, 1982; Arndt et al., 1998, 2008; Parman et al., 2001, 2004; Berry et al., 2008; Sobolev et al., 2016, 2019; Sossi et al., 2016; Asafov et al., 2018). A common interpretation is that the parental magmas to komatiites were produced in unusually hot upwellings of mantle material, termed mantle plumes (*e.g.*, Cawthorn, 1975; Campbell et al., 1989; Griffith and Campbell, 1990; Richards et al., 1991; Loper, 1991; Herzberg, 1995; Richard et al., 1996). The plumes most likely initiated at one of the two major thermal boundary layers in the mantle, *i.e.*, either the core-mantle boundary (CMB) at 2900 km, or the 660 km discontinuity, with the ensuing rise driven by a buoyancy contrast between the less dense, hot plume material and the cooler and denser surrounding mantle (Campbell and Griffiths, 1990, 1992, 1993; Farnetani and Richards, 1995; Farnetani, 1997). The initially solid mantle plume material was partially melted upon reaching shallower depths as a result of decompression. Based on experimental data, Campbell et al. (1989) argued that komatiites were produced in the hotter plume core containing mostly materials derived from near the thermal boundary layer, whereas spatially associated basalts were generated in the cooler plume head which, upon arrival at the surface, would have contained a substantial amount of entrained upper mantle material. However, later studies (e.g., Farnetani and Richards, 1995) argued that such entrainment was unlikely to contribute significantly to the erupted melts.

Two major types of modern mantle plumes have been proposed based on the depth of their initiation, determined using recent high-resolution seismic tomography imaging data (*e.g.*, Courtillot et al., 2003; Montelli et al., 2004; He et al., 2015; Bao et al., 2022). The first type is “primary”, or Morganian, plumes that are commonly thought to originate in the deepest parts of the lower mantle, perhaps from seismically anomalous regions. Early geophysical studies (*e.g.*, Dziewonski et al., 1977) identified seismically anomalous zones along the core-mantle boundary, the so-called Large Low Shear-Wave Velocity Provinces (LLSVP) and Ultra-Low Velocity Zones (ULVZ). The origin of these regions in the mantle is debated. It has been proposed that LLSVPs may be stratified into primordial bottom domains near the core-mantle boundary, often referred to as the D" layer, and mafic shallow domains that extend from ~1100 to 2300 km depths (*e.g.*, Ballmer et al., 2016; Koppers et al., 2021). These regions in the mantle may serve as nurseries for the majority of "primary" mantle plumes (French and Romanovicz, 2015; Totsvik et al., 2016; Koppers et al., 2021). Ocean island basalt systems that have been associated with this type of plume include Azores, Canary, Coral Sea, Easter, Galapagos, Hawaii, Iceland, Samoa, and Tahiti (Courtillot et al., 2003).

The "secondary" type, or Andersonian, plumes have been proposed to originate at the 660 km discontinuity and, hence, would be an upper mantle feature. Ocean island basalt systems that have been associated with this type of plumes include Ascension, Caroline, McDonald, and Pitcairn islands (Courtillot et al., 2003).

Considering the difficulties in determining even present-day mantle plume characteristics (*e.g.*, Fletcher and Wyman, 2015, and references therein), it is not surprising that there are few reliable estimates of Archean plume parameters (Arndt et al., 2008). This is due to the fact that, unlike modern plumes, ancient plumes are extinct mantle features and, therefore, cannot be examined by geophysical methods. Consequently, indirect approaches must be taken, such as geological field observations. For example, the size of postulated plumes can potentially be constrained by the lateral extent of contemporaneous magmatic activity within a given region. Envisioned parental plume heads of up to 2500 km in diameter for large systems, such as the Yilgarn Craton in Western Australia (Campbell and Hill, 1988; Mole et al., 2014; Barnes and Van Kranendonk, 2014; Barnes et al., 2016), have been argued to be indicative of plumes that originated at the CMB. Smaller plume heads, estimated to range from 200 km to 300 km in diameter, and leading to less widespread volcanism, such as the komatiite-basalt systems of the Pilbara Craton in Western Australia and the Superior Craton in Canada (Arndt et al., 2001; Van Kranendonk, 2008; Hickman and Van Kranendonk, 2012; Dostal and Mueller, 2013; Wyman, 2013, 2018, 2020), are likely to be more typical of upper mantle plumes originated at the 660 km discountinuity.

Puchtel et al. (2009b, 2013, 2016a) calculated H_2O contents of <0.2 wt. % in the Pyke Hill, Belingwe, Schapenburg, Komati, and Weltevreden komatiites, and concluded that their parental magmas were formed under dry, high-temperature melting conditions. Similar estimates of water content have been obtained for the Belingwe komatiites on the basis of the oxidation state of iron in melt inclusions in olivine (*e.g.*, Berry et al., 2008). Thus, it is a common assumption that most komatiites originated from dry, deep-seated mantle sources (Arndt et al., 1998, 2008).

Consistent with the interpretation of an anhydrous, deep mantle origin for most komatiites, Nicklas et al. (2018, 2019) concluded, on the basis of a global survey of partitioning behavior of V between olivine and emplaced komatiitic and picritic melts, that the redox states of a variety of komatiite and OIB sources, ranging in age from 3.48 Ga to present day, were either similar to, or lower than, those of modern MORB.

Recent studies of komatiitic olivine melt inclusions (*e.g.*, Sobolev et al., 2016, 2019; Asafov et al., 2018), while maintaining an anhydrous, deep mantle plume origin for

komatiites, have argued for relatively high water contents in some komatiite magmas, with water being added to rising, dry plume material from a thin hydrous layer located at the top of the mantle transition zone (MTZ), between the 410- and 660- km seismic discontinuities. The origin of these seismic interfaces is attributed to solid- solid phase transitions from olivine to wadsleyite and ringwoodite to perovskite+magnesiowüstite, respectively (*e.g.,* Bina and Helffrich, 1994). The hydrous layer is predicted by Bercovici and Karato (2003) in their MTZ water filter model to occur at the 410 km depth.

Alternatively, it has been argued that komatiites in general, and Komati lavas from the Kaapvaal Craton in South Africa in particular, were produced in a special type of Archean subduction environment *via* hydrous melting of the mantle at shallow depths and at temperatures similar to, or only slightly higher than, those of the ambient upper mantle (*e.g.*, Allègre, 1982; Grove et al., 1997; Parman et al., 1997, 2001, 2004). An important initial condition of this hypothesis is the requirement that the Komati komatiites represent intrusive bodies, since magmatic water escapes outgassing only under pressure (Grove et al., 1997). According to the hydrous komatiite model of Parman et al. (1997, 2001), the presence of water determined both the crystallization sequence and composition of the magmatic minerals of the Komati komatiites. Parman et al. (1997) carried out a detailed experimental study crystallizing material of komatiitic composition under both anhydrous and hydrous conditions, paying particular attention to the composition of the crystallizing pyroxene. Using the pyroxene compositions, these authors estimated that the original Komati komatiite magma contained between 4 and 6 wt. % H_2O. Such a large amount of water would require the temperature in the Komati source to be ~250°C lower than in anhydrous melting models. In their follow-up review paper, Grove and Parman (2004) argued that the Archean mantle was ≤100°C hotter than the modern mantle, hence, offering a view on the thermal evolution of the Earth that contrasts with those that are based on the traditional assumption of a substantially hotter Archean mantle (*e.g.*, Richter, 1985, 1988; Bickle, 1986; Nisbet et al., 1993; Herzberg et al., 2007, 2010).

The summary of estimates of the mantle potential temperatures (**T_p°C)** for the sources of the komatiite systems considered here, as well as the liquidus temperatures of the emplaced komatiite magmas (**T_{liq}°C)** and depths of melting initiation in the respective mantle plumes (**$D_{melt\ init}$**), are presented in **Table 1**. These estimates were generally derived from the studies for the particular komatiite systems referenced in **Table 1** and updated here on the basis of the more recent estimates of the emplaced komatiite lava compositions from Nicklas et al. (2018, 2019), where available, coupled with the previous and more recent mantle melting

parameterization models of McKenzie and Bickle (1988), Herzberg and O'Hara (2002), Herzberg and Asimow (2008), and Herzberg and Gazel (2009).

5. Chemical and isotopic data

A summary of the available chemical and isotopic data for the komatiite systems considered in this review are given in **Tables 1 and 2**.

5.1. Emplaced lava compositions, mantle potential temperatures, and depths of melting

Estimates of emplaced komatiite lava compositions (**MgO_{liq}**), their liquidus temperatures (**T_{liq}°C)**, mantle potential temperatures (**T_p°C)**, and depths of mantle melting initiation (**$D_{melt\ init}$**) are listed in **Table 1**. The details of the methodology used for calculating these parameters are provided in the ***Electronic Supplement***.

The calculated depths of melting initiation range between 605 and 203 km, while liquidus temperatures vary between 1606°C and 1498°C. There is an apparent tendency for a decrease in depth of melting initiation between 3.6 and 2.0 Ga. This is also reflected in the ~100°C decrease in mantle potential temperatures of komatiite sources from 1841 to 1748°C and a corresponding decrease in MgO contents of emplaced komatiite lavas from ~31 to 25 wt.% over the same period of time. Two exceptions are the Coonterunah and Kelly komatiite systems that are less MgO-rich than the other early Archean systems. Therefore, the data place the depths of onset of melting for all komatiite systems considered here within and above the present-day MTZ and provide minimum estimates for the depths of mantle plume initiation. In the following sections, more clues, as to which parts of the mantle the studied komatiite systems sampled (*i.e.*, depths of mantle plume initiation, **$D_{plume\ init}$**), will be considered using the available geochemical and isotopic data (**Table 2**).

5.2. Chemical composition and isotopic systematics

5.2.1. Major and lihophile trace elements

The petrologically most important chemical element in komatiites, along with Mg, is Al; as a result, variations in Al_2O_3, and its rare earth element (REE) behavioral equivalent Yb, form an integral part of all komatiite classifications (*e.g.*, Nesbitt et al., 1979; Jahn et al., 1982). The komatiite systems reviewed here can be subdivided into two major petrological groups on the basis of their Al_2O_3 and Yb contents at a given MgO content, namely Al-depleted/enriched and Al-undepleted. The majority of the early Archean komatiite systems, including the Schapenburg, Komati, Weltevreden, Ruth Well, and Regal systems, belong to the Al-depleted/enriched type of lavas characterized by either sub- or supra-chondritic Al/Ti

and Gd/Yb ratios (**Table 1**). Exceptions are the Coonterunah and Kelly systems that belong to the Al-undepleted type of lavas with Al_2O_3/TiO_2 = 22.8 and 23.1 and Gd/Yb_N = 0.96 and 0.91, respectively (where N denotes BSE-normalized values of Hofmann, 1988). By contrast, the majority of the late Archean komatiite systems, including the Pyke Hill-Alexo, Belingwe, Vetreny, and Lapland systems, belong to the Al-undepleted type of lavas characterized by generally chondritic Al/Ti and Gd/Yb ratios. The Boston Creek (Puchtel et al., 2018) and Kostomuksha komatiites (Puchtel et al., 1998), with Al_2O_3/TiO_2 = 5.1 and 17.2 and Gd/Yb_N = 2.0 and 1.2, respectively, are notable exceptions. Although the Lapland komatiites have low Al_2O_3/TiO_2 = 13.2 and high Gd/Yb_N = 1.5, these features have been shown to be the result of enrichment in Ti and middle REE (MREE), rather than depletions in Al and heavy REE (Puchtel et al., 2020).

Owing to their high liquidus temperatures and low viscosities during their passage through and/or emplacement onto the continental crust, komatiitic liquids are highly susceptible to contamination by upper crustal rocks (Huppert et al., 1984; Huppert and Sparks, 1985). Archean upper crustal rocks are strongly enriched in Th, U, and light REE (LREE), and relatively depleted in Nb (Rudnick and Gao, 2014) as a result of subduction zone processes involving retention of Nb-rich rutile in the eclogitic residue (Foley et al., 2000; Rudnick et al., 2000). Because of that, upper crustal rocks are characterized by negative Nb anomalies relative to elements with similar incompatibility during mantle melting (Th and La), *i.e.*, their Nb/Nb* <<1.0 (where $Nb/Nb^* = Nb_N/\sqrt{(Th_N \times La_N)}$). By contrast, primary komatiitic magmas are expected to have Nb/Nb* ≥ 1.0 (*e.g.*, Hofmann et al., 1986; Jochum et al., 1991). Due to large differences in highly incompatible lithophile trace element concentrations between the upper crust and komatiitic melts, crustal contamination usually leads to sharp increases in the abundances of Th, U, W, and LREE, but much less so of Nb, in the hybrid melts, which acquire negative Nb anomalies in the process. Hence, the Nb/Nb* ratio represents a diagnostic tool that has been utilized to evaluate and mathematically correct for the effects of crustal contamination (*e.g.*, Puchtel et al., 2016b, 2020, 2022).

The majority of the komatiite systems considered here are variably depleted in highly incompatible lithophile trace elements, with the La/Sm_N ratios ranging between 0.14 (the 2.05 Ga Lapland system) and 0.97 (the 3.48 Ga Komati system). The 2.72 Ga Boston Creek lavas are the sole exception (La/Sm_N = 1.9). Furthermore, all komatiite systems examined here have Nb/Nb* ≥ 1.0, reflecting either a lack of crustal contamination, or that the effects of crustal contamination have been mathematically corrected for, as indicated in **Table 2**. The details of the correction protocol are provided in the ***Electronic Supplement***.

5.2.2. Isotopic systems of the lithophile elements

Table 2 presents the initial ε^{143}Nd and ε^{176}Hf values (defined as the deviation in parts per 10,000 of initial ^{143}Nd/^{144}Nd and ^{176}Hf/^{177}Hf in a given sample from those in the chondritic reference at the time of lava emplacement) for each komatiite system, which represent compositions of the respective komatiite-basalt mantle sources. These values were derived from the respective Sm-Nd and Lu-Hf isochrons obtained for each komatiite-basalt system and, where appropriate, corrected for crustal contamination, as indicated in **Table 2**, using the lithophile trace element systematics discussed in the previous section. The resultant initial ε^{143}Nd and ε^{176}Hf values are all positive, ranging between +0.46 and +4.9 and +1.7 and +10.2, respectively, indicating that all the komatiite-basalt systems considered were derived from mantle sources with time-integrated supra-chondritic Sm/Nd and Lu/Hf.

By contrast, Blichert-Toft et al. (2015) reported ^{143}Nd and ^{176}Hf data for a suite of heavily altered Komati drill core samples from several flows. That study produced a much greater scatter, and both positive and negative initial ε^{143}Nd and ε^{176}Hf values for whole-rock samples, than for the initial values obtained from the individual Sm-Nd and Lu-Hf isochrons for the remarkably well preserved Komati komatiite samples from the Puchtel et al. (2013) study reported in **Table 2**. Blichert-Toft et al. (2015) also reported data for variably leached clinopyroxene separates, which yielded initial ε^{143}Nd and ε^{176}Hf values of –2 and +5, respectively. This may indicate more complex magmatic and/or alteration history of the samples studied by Blichert-Toft et al. (2015) than for the Komati samples studied by Puchtel et al. (2013).

The time-integrated Sm/Nd and Lu/Hf ratios in the mantle sources of komatiite systems derived from the respective Sm-Nd and Lu-Hf isochron sets are plotted in **Fig. 1.** These ratios were calculated by assuming the minimum-degree fractionation from either the chondritic values or the values defined by the combined ^{142,143}Nd systematics (where available) to those required to bring the ε^{143}Nd and ε^{176}Hf to the measured initial ε^{143}Nd and ε^{176}Hf of the respective mantle sources by the time of komatiite-basalt system formation. All of these komatiite systems were derived from mantle sources having time-integrated ^{147}Sm/^{144}Nd and ^{176}Lu/^{177}Hf ratios between those of CHUR and DMM. An important feature of the data is that, while all komatiite-basalt systems younger than ~3.0 Ga follow the terrestrial Nd-Hf mantle evolution array, indicating long-term "coupled", or congruent, behavior of the Nd and Hf isotope systematics in the post-3.0 Ga komatiite mantle sources, the komatiite systems older than ~3.0 Ga (with the exception of the Pilbara Craton komatiite-basalt systems) plot above

the terrestrial evolution curve, indicating long-term "decoupled", or incongruent, behavior of the Nd and Hf isotope systematics in their mantle sources. All these early Archean systems are from the Kaapvaal Craton in South Africa. The processes that might have been responsible for producing such Nd-Hf isotope decoupling are discussed in **Section 6.1**.

Relatively limited ^{142}Nd data are available for the komatiite systems reviewed in this study (**Table 2**). The komatiite systems, for which these data are available, mostly exhibit μ^{142}Nd values indistinguishable from the standard reference value, where μ^{142}Nd is defined as the deviation in parts per million of ^{142}Nd/^{144}Nd in a given komatiite sample from the laboratory reference materials (AMES or JNdi), which are considered to represent the composition of the modern BSE. The Schapenburg and Komati komatiite systems have small μ^{142}Nd deficits, averaging –5.0±2.8 (2SD; Puchtel et al., 2016a) and –4.0±4.1 (2SD; Boyet et al., 2021), respectively.

5.2.3. Tungsten abundance and isotope systematics

The ^{182}W data are reported as μ^{182}W, which is the deviation in parts per million of ^{182}W/^{184}W in a given sample from that of the in-house *Alfa Aesar* laboratory W reference material. The μ^{182}W value of 0 for the reference material is considered to represent the composition of the BSE. This is based on the observation that a limited number of data for modern MORB (Willbold et al., 2011; Rizo et al., 2016; Mundl et al., 2017), numerous data for OIB with low ^{3}He/^{4}He (Mundl-Petermeier et al., 2020), and data for Proterozoic and Phanerozoic glacial diamictites and granites (Mundl et al., 2018; Nakanishi et al., 2021) are all characterized by μ^{182}W values of ~0.

In contrast to ^{142}Nd, the majority of komatiite systems examined here exhibit either positive (all the Pilbara, the Kostomuksha, and the Boston Creek komatiite systems), or negative (the Schapenburg and Lapland komatiite systems) ^{182}W anomalies, with only the Komati and Vetreny komatiite systems lacking an ^{182}W anomaly.

The behavior of W during magmatic processes is governed mainly by the redox state of the magmatic system in question (Newsom et al., 1996; Arevalo and McDonough, 2008; König et al., 2011). Under reducing conditions, such as those that likely existed during metallic core formation, W behaves as a moderately siderophile element (MSE), concentrating largely in the metal relative to the silicate melt. During mantle melting under relatively oxidizing conditions in the absence of a metal phase, such as typical of the modern upper mantle, W behaves as a highly incompatible element, concentrating in the silicate melt relative to the melting residue, with a degree of incompatibility similar to that of Th and U.

The Archean mantle was recently shown to be only slightly (by ~1.3 ΔFMQ log units) less oxidized than, whereas the Proterozoic mantle was found to be similarly oxidized to, the modern mantle (Nicklas et al., 2018, 2019). Therefore, it is expected that during the mantle melting that produced the komatiite-basalt systems considered in this review, W behaved similarly to Th and U and, hence, that in undisturbed komatiite-basalt systems, W/Th ≈ W/Th_{BSE}, where W/Th_{BSE} = 0.19 (McDonough and Sun, 1995). Indeed, in modern OIB and MORB, for which W is characterized by a primary, magmatic distribution, the W/Th ratios are similar to the BSE value of 0.19 (*e.g.*, König et al., 2008, 2011; Jenner and O'Neill, 2012). Modern island arc lavas, on the other hand, show uniformly elevated W/Th ratios relative to the BSE value attributed to various constributions of fluid-borne W to the arc mantle from the subducted slab (König et al., 2008, 2011). Although some komatiite systems (*e.g.*, the Komati, Vetreny, and Lapland systems) have average W/Th ratios within the uncertainty limits of the BSE value, and in that respect are similar to modern OIB and MORB, others are variably either enriched (most common) or depleted in W over Th (**Table 1**). In addition, the lack of correlation between W concentrations and indices of magmatic differentiation, such as MgO content, indicates either W mobility after lava emplacement in most komatiite-basalt systems (*e.g.*, Touboul et al., 2012; Puchtel et al., 2016a, 2018, 2020, 2022; Tusch et al., 2021) or involvement of a yet-unaccounted-for magmatic process.

The issue of the origin of W in Archean and Proterozoic komatiite-basalt systems is, therefore, controversial. Recent studies have shown that W abundance and isotopic systematics can be affected by crustal contamination, hydrothermal alteration, and metamorphism (*e.g.*, Touboul et al., 2014; Liu et al., 2016; Puchtel et al., 2016a,b, 2018, 2020, 2022; Tusch et al., 2019, 2021), resulting mostly in W enrichments relative to immobile trace elements with similar degree of incompatibility, *e.g.*, Th. Two mechanisms, based on the origin of W, have been proposed to account for the elevated W/Th ratios in komatiites and basalts. The first mechanism advocates derivation of W from an endogenous source, whereby W originated within the komatiite-basalt system. The second mechanism assumes an exogeneous origin, whereby W is introduced into the komatiite-basalt systems from genetically unrelated sources. We address these two mechanisms in more detail below.

Endogenous origin of W in komatiite-basalt systems have been advocated for the Kostomuksha (Touboul et al., 2012), Schapenburg (Puchtel et al., 2016a), Boston Creek (Puchtel et al., 2018), and the Coonterunah and Kelly systems (Puchtel et al., 2022). In case of the two Pilbara komatiite-basalt systems, the komatiites are characterized by high W/Th ratios, whereas the basalts, that are spatially associated and genetically related to komatiites,

are depleted to only slightly enriched in W relative to Th. In these komatiite-basalt systems, and also in many other Archean komatiite-basalt systems around the globe, komatiites constitute 5-10% of the sequence by volume, the rest consisting of basalts (Condie, 1981; de Wit and Ashwal, 1997; Smithies et al., 2007). Originally, basalts contain significantly higher abundances of all highly incompatible trace elements, including W, compared to komatiites. During secondary alteration, komatiites are turned into serpentinites, whereas basalts are transformed into amphibolites. Serpentine is a major host for W and can accommodate several orders of magnitude more W than the precursor mineral olivine, whereas W shows a lower affinity for amphibole (Liu et al., 2016). Therefore, if W is mobilized and redistributed within a komatiite-basalt volcanic sequence, it is expected to be preferentially captured by komatiites during serpentinization of the primary mineral assemblage. The effect of this relative W enrichment is amplified by the low trace element concentrations in komatiites, resulting in high W/Th ratios (Puchtel et al., 2022).

In the case of the Boston Creek system, samples collected across a differentiated lava flow have remarkably uniform ^{182}W compositions, but show a wide range of W/Th ratios, from enriched in the lower olivine cumulate part to BSE-like in the low-Mg basaltic layer, with strong inverse correlation between MgO content (*i.e.*, amount of modal serpentine) and W/Th (Puchtel et al., 2018). The above features were argued by these authors to reflect an endogenous nature of W in the Boston Creek system, with isotopically uniform W having been redistributed within the lava flow and hence reflecting the primary magmatic signature.

The above scenarios have been argued to be applicable to several other komatiite-basalt systems, including the Kostomuksha (Touboul et al., 2012), and the Schapenburg (Puchtel et al., 2016a) systems.

Exogenous W in the komatiite-basalt systems considered in this review has been shown to be derived from upper crustal rocks either during passage of mafic-ultramafic magmas through the continental crust *en route* to the surface (the Vetreny and Lapland systems: Puchtel et al., 2016b, 2020), or as a result of interaction with upper crustal rocks during both the magmatic stage *via* crustal contamination, and the post-magmatic stage *via* fluid-rock interaction (the Ruth Well and Regal systems: Puchtel et al., 2022).

Due to the generally high W abundances in upper crustal rocks (*e.g.*, Rudnick and Gao, 2014), crustal contamination has the potential to modify both W concentrations and ^{182}W compositions of komatiite-basalt magmas during ascent, as has been argued to be the case for the Vetreny, Lapland, Ruth Well, and Regal systems on the basis of studies of lithophile trace element systematics (Puchtel et al., 2016b, 2020, 2022). In order to mathematically correct for

570 the effects of magmatic crustal contamination, these authors performed un-mixing
571 calculations using the degrees of crustal contamination estimated on the basis of trace element
572 systematics and assumptions about the W isotopic composition and abundances in the most
573 likely potential crustal contaminant.

574 Being a highly fluid-mobile element (*e.g.*, König et al., 2008), W can be transferred from
575 spatially associated granitic rocks to komatiite-basalt sequences *via* W-rich fluids. Such a
576 mechanism has been proposed to affect the W isotopic composition of the Ruth Well and
577 Regal komatiite systems on the basis of the high W/Th ratios in both komatiites and basalts
578 and the similarity in ^{182}W compositions between the most W-enriched komatiites and the
579 spatially associated 3.5 Ga tonalites of the Pilbara Craton (Puchtel et al., 2022). These authors
580 were able to evaluate the W isotopic composition of the primary lavas by assuming that their
581 ^{182}W composition was similar to that of the least affected basalts from Tusch et al. (2021) and
582 Puchtel et al. (2022), with W/Th ratios closest to that in the BSE estimate.

583 After corrections have been applied where needed, the $\mu^{182}W$ values reported in **Table 2**
584 are considered to reflect those in the sources of the respective komatiite-basalt systems.

585 ***5.3. Os isotope systematics and HSE abundances***

586 The $^{186,187}Os$ data are listed in **Table 2** and plotted in **Fig. 2**. The majority of the komatiite
587 systems have $\gamma^{187}Os$ values (defined as percent deviation of the $^{187}Os/^{188}Os$ ratio in a given
588 komatiite sample from a chondritic reference value at the time of komatiite lava
589 emplacement) plotting within the chondritic range, indicating evolution of their mantle
590 sources with time-integrated near-chondritic Re/Os ratios. The only exceptions are the
591 Schapenburg and Kostomuksha komatiite systems that have more radiogenic $\gamma^{187}Os$ values of
592 +3.7 and +2.5, respectively, implying that their mantle sources evolved with long-term
593 slightly suprachondritic Re/Os.

594 The limited ^{186}Os data available indicate that, out of the seven systems studied, only three
595 (the Pyke Hill, Belingwe, and Vetreny systems) have initial $\mu^{186}Os$ values (defined as the
596 deviation in ppm of the $^{186}Os/^{188}Os$ ratio in a given komatiite sample from a chondritic
597 reference value at the time of the komatiite lava emplacement) that plot within the chondritic
598 range, indicating that their mantle sources evolved with time-integrated near-chondritic Pt/Os
599 ratios. The other four komatiite systems have non-chondritic initial $\mu^{186}Os$ values and, thus,
600 evolved with either suprachondritic (the Weltevreden, Kostomuksha, and Lapland systems) or
601 subchondritic (the Komati system) time-integrated Pt/Os ratios. Importantly, among the
602 mantle sources with non-chondritic Re-Os and/or Pt-Os systematics, only in the Kostomuksha

603 komatiite source are these isotope systematics coupled, whereas in the others, they are
604 decoupled.
605 The total HSE abundances in the komatiite mantle sources have been calculated using the
606 bootstrap method of Puchtel et al. (2004b) that was refined in subsequent studies (*e.g.*,
607 Puchtel et al., 2020, 2022). This method combines the ^{186,187}Os isotopic and HSE abundance
608 data for a suite of komatiitic lavas derived from a common primary magma and related by
609 fractional crystallization of olivine after lava emplacement. The details of the analytical
610 protocol used in the bootstrap method of Puchtel et al. (2004b) are provided in the ***Electronic***
611 ***Supplement***.
612 The total HSE abundances in the sources of the komatiite systems considered in this
613 review, calculated as percent of those in the estimates of the modern BSE of Becker et al.
614 (2006), are presented in **Table 2** and plotted as a function of their age in **Fig. 3.** The
615 calculated total HSE abundances range from ~30% in the 3.55 Ga Schapenburg and 3.53 Ga
616 Coonterunah systems to ~120% in the 2.05 Ga Lapland system. Overall, the entire dataset,
617 except for the obvious outliers (*e.g.*, the 2.72 Ga Boston Creek, 2.69 Ga Belingwe, and 2.41
618 Ga Vetreny systems), exhibits a broad trend of increasing HSE abundances in the komatiite
619 mantle sources with time. This trend is generally consistent with that defined by the much
620 more scattered data of Maier et al. (2009).
621 In the following sections, the data reviewed in **Section 5** will be discussed in light of the
622 possible mechanisms responsible for creating these early chemical and isotopic
623 heterogeneities in the mantle.

624 **6. Mechanisms for creating early mantle heterogeneities**

625 ***6.1. Primordial differentiation of the mantle***

626 Crystallization of a primordial magma ocean(s) is one possible mechanism for generating
627 early chemical and isotopic heterogeneities in the mantle (*e.g.*, Boyet et al., 2003, 2021; Boyet
628 and Carlson, 2005, 2006; Caro et al., 2005, 2017; Brown et al., 2014; Puchtel et al., 2016a;
629 Byerly et al., 2017; Morino et al., 2017). Periodic magma oceans are likely a direct
630 consequence of planetary growth due to gravitational energy release from core formation and
631 high-energy collisions during final stages of accretion (*e.g.*, Tonks and Melosh, 1993; Bottke
632 et al., 2010; Rubie et al., 2011). Crystallization of a magma ocean results in stratification
633 controlled by fractionation of mineral assemblages, the composition of which depends on the
634 depth of the magma ocean and the composition of the melted domain. Some studies have
635 argued for occasional, near-complete melting of the silicate Earth, such as may have occurred

during the putative giant impact that led to formation of the Moon (Rubie et al., 2011; Canup, 2012; Elkins-Tanton, 2012; Young et al., 2016). The pressures and temperatures near the bottom of such a magma ocean would have stabilized bridgmanite (Mg-perovskite) and Ca-perovskite (Kato et al., 1988; Abe, 1997; Walter et al., 2004). Because most trace elements are variably compatible in Ca-perovskite, with the degree of compatibility decreasing in the order Lu>Hf>Sm>Nd (Corgne et al., 2005), the presence of Ca-perovskite in the fractionating assemblage would result in stronger fractionation of Lu/Hf relative to Sm/Nd than that observed under upper mantle conditions. Over time, this would result in Nd-Hf isotopic decoupling in the mantle domains derived from magma ocean differentiation products, relative to the coupling of these two isotope systems observed in the sources of modern MORB and most OIB, which together define the modern Nd-Hf mantle array, or terrestrial evolution curve (e.g., Salters and White, 1998).

The Nd-Hf mantle array owes its origin to the coupled, or congruent, Nd-Hf isotope systematics of most terrestrial rocks that arise from similar partitioning behavior of the parent (^{147}Sm, ^{176}Lu) and daughter (^{143}Nd, ^{176}Hf) isotopes of the Sm-Nd and Lu-Hf systems during upper mantle differentiation and crust-forming processes (*e.g.*, Patchett et al., 1981; Salters and White, 1998; Vervoort and Blichert-Toft, 1999; Vervoort et al., 1999, 2000). During mantle melting, both parent isotopes are less incompatible with the melt fraction than the daughter isotopes, which results in higher Sm/Nd and Lu/Hf ratios in the melting residue compared to the melt; over time, the residual mantle evolves to more radiogenic Nd and Hf isotopic compositions than the extracted melts. Both isotope systems are lithophile, refractory, insensitive to redox conditions, and largely immobile during alteration and metamorphism. These properties make them useful for investigating the interplay between the formation and recycling of oceanic and continental crust in driving the geochemical evolution of the mantle.

The decoupling of the Nd and Hf isotope systematics (and, thus, deviation from the terrestrial Nd-Hf array) in the early Archean komatiite-basalt systems from the Kaapvaal Craton, such as Schapenburg, Weltevreden, and Komati, have been interpreted to reflect the involvement of primordial magma ocean processes.

Based on the combined ^{142,143}Nd and ^{176}Hf systematics, Puchtel et al. (2013) developed a model of formation of the mantle silicate reservoirs that gave rise to the Komati and Weltevreden komatiites *via* crystallization of a primordial magma ocean. According to their model, during magma ocean differentiation, the lower three quarters of the magma column (from depths of ~2900 to ~700 km) were largely dominated by bridgmanite, with subordinate amounts of ferropericlase and Ca-perovskite, Ca-Pv (Trønnes and Frost, 2002; Ito et al., 2004;

Caro et al., 2005; Elkins-Tanton, 2008). Puchtel et al. (2013) used an equilibrium crystallization model based on the high-pressure and -temperature partitioning studies of Corgne and Wood (2002; 2004), Corgne et al. (2005), Liebske et al. (2005), and Walter et al. (2004), and assumed a completely molten mantle with a composition corresponding to that of the early depleted reservoir (EDR) of Boyet and Carlson (2006) that crystallized within the first 150 Ma of the Solar System history, i.e., by 4400 Ma.

Since the study of Puchtel et al. (2013) has been published, the EDR model of Boyet et al. (2006) has been proven untenable. This model was based on the data available at the time that the accessible Earth has a greater $^{142}Nd/^{144}Nd$ ratio than chondrites (Carlson et al., 2007). This ^{142}Nd difference required a higher-than-chondritic Sm/Nd ratio for the accessible Earth. This ratio must have been acquired during global silicate differentiation within the first 30 million years of Solar System formation (Boyet and Carlson, 2006) and implied the formation of a complementary ^{142}Nd-depleted reservoir that is either hidden in the deep Earth, or lost to space by impact erosion (Caro et al., 2008). However, Burkhardt et al. (2016) showed that, compared to chondrites, Earth's building blocks were enriched in ^{142}Nd that was produced by the s-process of nucleosynthesis, which leads to higher $^{142}Nd/^{144}Nd$ ratios. After these authors corrected for this effect, the ^{142}Nd composition of chondrites and the accessible Earth were shown to be indistinguishable. The results of Burkhardt et al. (2016), therefore, obviate the need for a hidden-reservoir or ^{142}Nd-superchondritic Earth models and imply a chondritic Sm/Nd ratio for the BSE.

In view of the new data of Burkhardt et al. (2016), we have modified the model of Puchtel et al. (2013), as illustrated in **Fig. 4**; the methodology used in these model calculations are available as an ***Electronic Supplement*****.** The composition of the primordial magma ocean, unlike in our previous model, is now represented by that of the chondritic uniform reservoir (CHUR).

Figure 4 shows the time-integrated $^{147}Sm/^{144}Nd$ and $^{176}Lu/^{177}Hf$ ratios in the sources of the Komati and Weltevreden komatiite systems formed as a result of the 4400 Ma magma ocean differentiation and cryslallization event specified above, depending on the relative proportions of fractionating bridgmanite and Ca-Pv. The upper panel of the diagram represents aggregate compositions of the magma ocean cumulates, while the lower panel represents the compositions of the residual liquids. As mentioned in the previous model, the contrasting partitioning behavior of Lu and Hf between bridgmanite and Ca-Pv results in differentiation trends that are highly affected by the relative proportions of these two phases. According to this model, the Komati and Weltevreden mantle domains represent solidification

products of a bridgmanite-Ca-Pv cumulate that was derived from ~20% and 12% accumulation of a bridgmanite:Ca-Pv assemblage in the proportions of 93:7 and 80:20, respectively. These proportions and the degrees of magma ocean crystallization are within the range of those envisaged for lower mantle conditions during the Hadean (*e.g.*, Caro et al., 2005). If the modified model of Puchtel et al. (2013) presented here is correct, the mantle plumes that gave rise to the Komati and Weltevreden komatiites must have originated in the lower mantle (**Table 1**).

Boyet et al. (2021) obtained a slightly negative average μ^{142}Nd value of –4.0±4.1 for a set of Komati drill core samples. As noted above, that study combined their ^{142}Nd results with the ^{143}Nd and ^{176}Hf data of Blichert-Toft et al. (2015) for clinopyroxene separates from the same rocks. In order to explain the negative μ^{142}Nd and ε^{143}Nd values and the corresponding positive ε^{176}Hf value, Boyet et al. (2021) proposed a four-stage model for the formation of these lavas, whereby the negative μ^{142}Nd value and low Hf/Sm ratios developed during the crystallization of a deep magma ocean soon after Earth accretion. The material that ultimately became the source of the komatiites was a residual liquid produced by 50% crystallization of a bridgmanite/ferropericlase/Ca-Pv mineral assemblage in the proportions 79:16:5, which resulted in decoupling of the Nd and Hf isotope systematics. Thus, the model of Boyet et al. (2021) also supports a lower mantle origin for the plume that gave rise to the Komati komatiites.

Metal-silicate fractionation processes operating at the high temperatures and pressures characterizing the first ~60 Ma of Solar System history at the base of an early transient magma ocean, or in a partially molten zone at or near the core-mantle boundary (Labrosse et al., 2007), while ^{182}Hf was still extant, have also been argued to be capable of generating coupled ^{182}W and ^{186,187}Os heterogeneities in the mantle (Touboul et al., 2012). To explain the enriched ^{182}W and $^{186, 187}$Os compositions of the Kostomuksha komatiite system, Touboul et al. (2012) envisioned a lower mantle magma ocean reservoir where silicate melt could potentially equilibrate with metal that represented either the growing core or the metal passing through the molten region on its way to the core. This model is based on experimental data of substantially reduced metal-silicate partitioning for Re and Pt, relative to Os, at high temperatures and pressures (Righter and Drake, 1997; Cottrell and Walker, 2006; Fortenfant et al., 2006; Yokoyama et al., 2009; Brenan and McDonough, 2009), and on the more siderophile behavior of W under the somewhat more reducing conditions that likely existed in the lower mantle during core formation compared to the present-day upper mantle (Wade and

Wood, 2005). The model of Touboul et al. (2012) requires the long-term survival of some portion of the mantle in which HSE and MSE were set by high-temperature and -pressure metal-silicate partitioning under reducing conditions. In order to achieve the $^{186,\ 187}$Os and ^{182}W isotopic and elemental characteristics of the Kostomuksha komatiite source, Touboul et al. (2012) envisioned a mantle plume tapping this reservoir and mixing material from it with overlying mantle characterized by Os isotopic compositions and HSE concentrations similar to those in estimates of the BSE of Meisel et al. (2001) and Becker et al. (2006), in the proportions of ~1:1 (**Fig. 5**). If the model of Touboul et al. (2012) is correct, it implies that the plume, which gave rise to the Kostomuksha komatiites, originated in the lowermost mantle.

Isotopic heterogeneities involving the HSE-based isotopic systems have also been argued to be related to primordial magma ocean crystallization processes by Puchtel et al. (2014) in their study of the HSE abundances and $^{186,\ 187}$Os compositions of the Komati and Weltevreden komatiite systems considered above. These authors used the experimental partitioning data of Borisov and Palme (1997) and Mallmann and O'Neill (2007) indicating that under the highly reducing conditions that may have existed during crystallization of a primordial magma ocean immediately following the main stage of core formation (Frost et al., 2008), solubility of Pt in silicate melts, unlike the other HSE, may have been low and Pt, hence, would have had a strong tendency to form alloys. Fractionation and subsequent heterogeneous dispersal of Pt alloys within the mantle could have resulted in the formation of both Pt-enriched and -depleted domains. These would then have evolved with supra- and subchondritic Pt/Os ratios, respectively, which over time would have resulted in the decoupling of the ^{186}Os and ^{187}Os systems in these domains (Puchtel et al., 2014).

A model of silicate-silicate fractionation during primordial mantle magma ocean crystallization, involving early removal of bridgmanite and Ca-Pv, was also proposed by Puchtel et al. (2016a) to explain the coupled ^{182}W, ^{142,143}Nd, and ^{176}Hf isotope systematics of the Schapenburg komatiite source. In their model, the authors recognized that crystal-liquid fractionation in a purely silicate system of a global primordial magma ocean would lead to high Hf/W, Sm/Nd, and Lu/Hf in early-formed cumulates and low Hf/W, Sm/Nd, and Lu/Hf in the residual liquid. If these fractionation processes occurred while ^{182}Hf and ^{146}Sm were still extant, the residual silicate liquid would have developed a coupled deficit in ^{182}W and ^{142}Nd, compared to the ambient mantle, which is what has been observed in the 3.55 Ga Schapenburg komatiites. If the model of Puchtel et al. (2016a) is applicable, it places the mantle domain that served as the sources for the Schapenburg mantle plume in the lowermost mantle.

6.2. Late accretion

The term "late veneer" was first introduced by Turekian and Clark (1969) and later elaborated on by Chou et al. (1978; 1983) to explain the excess of HSE abundances in the terrestrial mantle compared to what would otherwise be expected after core formation on the basis of the low pressure and -temperature metal-silicate experimental partitioning data available at the time (*e.g.*, Kimura et al., 1974). Late accretion is defined as the accretion of 0.5-1% (Walker, 2009) of Earth's mass of a chondritic component after cessation of core formation. In earlier studies, it was assumed that this chondritic component was added to the surface of the Earth in the form of relatively small objects to create a thin layer initially coating the entire planet (thus the term "veneer"). It has also been proposed that a slow downward mixing of this putative thin layer into the mantle was responsible for the apparent trend of increasing HSE abundances in Archean komatiites over time (Maier et al., 2009). Studies by Bottke et al. (2002, 2007), however, have concluded that it is unlikely that late accretion in the form of small objects could have achieved an Earth/Moon late accretionary mass influx ratio of ~1200 required on the basis of the Re-Os isotopic and HSE abundance studies of terrestrial (Meisel et al., 2001; Becker et al., 2006; Fischer-Gödde et al., 2011) and lunar (Walker et al., 2004, 2014; Day et al., 2007; Day and Walker, 2015) samples. Bottke et al. (2010) proposed that late accretion to Earth was dominated by addition of a few large projectiles, with a mean diameter of ~2500 km, and that HSE were added to the Moon through the accretion of much smaller bodies, ~250 km in diameter. Projectiles with a diameter of 2500 km hitting the Earth likely have been differentiated into HSE-rich cores and HSE-stripped silicate mantles (Marchi et al., 2018). As a result, mantle domains with low HSE abundances and positive ^{182}W anomalies, on the one hand, and high HSE abundances and negative ^{182}W anomalies, on the other hand, would have been generated. In the absence of modern-style plate tectonics prior to ~2.5 Ga (*e.g.*, Brown and Johnson, 2018), these mantle domains would be expected to survive for extended periods of time before eventually becoming homogenized within the mantle *via* wholesale mantle convection.

Heterogeneous distribution of HSE in the early Earth's mantle has been recognized from ^{186,187}Os and HSE abundance studies of komatiites (*e.g.*, Maier et al., 2009; Puchtel et al., 2004a,b, 2005, 2009a,b, 2014, 2016a,b, 2018, 2020, 2022). As noted in **Section 5**, available high-precision ^{187}Os data for komatiitic systems worldwide indicate that most komatiite sources were characterized by initial γ^{187}Os values ranging from only −0.1 to +1.3, implying that these komatiitic systems evolved with long-term Re/Os well within the range of chondritic meteorites (**Fig. 2a**). Only two exceptions have been identified so far, which are

the Schapenburg and Kostomuksha komatiite systems. The more limited ^{186}Os dataset indicates a somewhat greater variability outside of the chondritic range, but, nevertheless, suggests that the mantle sources of the late Archean Pyke Hill, Belingwe, and Vetreny komatiite systems evolved with time-integrated Pt/Os within the chondritic range (**Fig. 2b**). By contrast, the high initial μ^{186}Os and γ^{187}Os values in the mantle source of the Kostomuksha komatiites require long-term suprachondritic Pt/Os and Re/Os ratios. Originally, these coupled ^{186,187}Os enrichments were interpreted to be the result of core-mantle interaction processes (Puchtel et al., 2005). However, the ^{182}W data obtained by Touboul et al. (2012) for these komatiites rendered this interpretation implausible and these authors instead proposed that the combined ^{186,187}Os and ^{182}W systematics were the result of metal-silicate fractionation in a primordial magma ocean, as discussed earlier. Additional contrasts are the Komati and Weltevreden (Puchtel et al., 2014) and the Lapland (Puchtel et al., 2020) komatiite systems, which evolved with non-chondritic time-integrated Pt/Os ratios and chondritic time-integrated Re/Os ratios, thereby displaying decoupling of the ^{186}Os and ^{187}Os systematics. For the Komati and Weltevreden komatiite systems, this decoupled behavior has been interpreted to be the result of fractionation of Pt-Fe alloys in a primordial magma ocean during the first 150 Ma of Earth history, followed by slow homogenization of the crystallized post-magma ocean mantle domains characterized by fractionated Pt/Os ratios (Puchtel et al., 2014). For the Lapland komatiite system, derivation from a mantle domain characterized by an excess of late accreted, differentiated planetesimal core metal, the so-called "grainy" late accretion (Walker, 2016), were considered to be one of the two plausible models for explaining the decoupled ^{186}Os and ^{187}Os systematics (Puchtel et al., 2020).

On the basis of variable Pt and Ru contents in komatiites of various ages, Maier et al. (2009) argued for a gradual increase in HSE abundances in the presumed deep mantle sources of komatiites between ~3.5 and ~2.9 Ga due to slow downward mixing of a "late veneer" of chondritic materials. However, the ^{186,187}Os and ^{182}W isotopic and HSE abundance studies of Puchtel et al. (2020; 2022, and references therein) of the best preserved early Archean to early Proterozoic komatiite systems worldwide revealed a somewhat more complex picture. As attested to by the plot of the calculated total HSE abundances in the sources of these komatiite systems as percent of those in the estimates of the modern BSE of Becker et al. (2006) versus age (**Fig. 3**), this trend has been argued unlikely to be the result of simple "slow downward mixing of a late veneer of chondritic materials", although a broad trend of increasing HSE abundances in komatiite sources over time is apparent (*e.g.*, Puchtel et al., 2016a, 2018, 2020, 2022). The argument is two-fold. First, as is evident from **Fig. 3**, the total HSE abundances in

839 the sources of some late Archean komatiite systems were even lower than those in some early
840 Archean komatiite systems. Second, for some of the komatiite systems considered here, *e.g.*,
841 the Schapenburg and Kostomuksha komatiites, the calculated total HSE abundances were
842 shown to be inconsistent with the proportion of late accreted materials estimated to have been
843 added to their sources based on the ^{186,187}Os and ^{182}W data (Touboul et al., 2012; Puchtel et
844 al., 2016a).

845 These observations are illustrated in **Fig. 6**, where the μ^{182}W values of komatiite systems
846 are plotted against the calculated total HSE abundances in their mantle sources normalized to
847 those in the estimates for the modern BSE of Becker et al. (2006). This proportion
848 corresponds to the fraction of the total HSE budget of the modern BSE added during late
849 accretion, assuming an essentially HSE-free BSE immediately following core formation.
850 According to this model, the HSE budgets, taking into account their respective uncertainties,
851 of those komatiitic systems that plot within the segment constrained by the blue lines in **Fig.**
852 **6,** are consistent with having been established *via* addition of late accreted materials to their
853 mantle source regions. By contrast, the HSE budgets of the komatiite systems that plot outside
854 this segment are presumed to have been affected by additional primordial processes, such as
855 metal-silicate (*e.g.*, the Kostomuksha komatiites: Touboul et al., 2012) or silicate-silicate
856 (*e.g.*, the Schapenburg komatiites: Puchtel et al., 2016a) fractionation in a primordial magma
857 ocean within the first 60 Ma of Solar System history. Furthermore, the combined ^{187,186}Os-
858 ^{182}W and HSE abundance data for the Lapland komatiite system (**Fig. 6)** are consistent with
859 involvement of fractionated metal derived from cores of differentiated planetesimals during
860 late accretion processes and formation of Os-W isotope and HSE abundance heterogeneities
861 in the early mantle (Puchtel et al., 2020).

862 It has been argued that the impactors that created the largest impact basins on the Moon,
863 Mars, and presumably also the Earth, were hundreds of km in diameter (Ryder, 2002; Strom
864 et al., 2005; Bottke et al., 2010) and possibly dominated by differentiated planetesimals.
865 Impacts of such bodies would be capable of generating large ^{182}W and HSE anomalies in
866 portions of the mantle as a result of such "grainy" late accretion (Walker, 2016; Marchi et al.,
867 2018; 2020). Cores of differentiated planetesimals would have up to two orders of magnitude
868 higher W abundances, and up to 350 ppm less radiogenic ^{182}W/^{184}W, than the modern BSE
869 (Kleine et al., 2002, 2004; Schoenberg et al., 2002; Yin et al., 2002). Hence, any mantle
870 domain to which an excess of this material was added would be ^{182}W-depleted and would also
871 be expected to be enriched in HSE, compared to BSE, as is observed for the Lapland
872 komatiite system (Puchtel et al., 2020). On the other hand, the mantle domain to which less of

a late accretionary HSE component was added, *e.g.*, in the form of the HSE-stripped silicate mantles of differentiated planetesimals, would be ^{182}W-enriched, compared to those mantle domains to which a full HSE complement of late accretionary material was added, and would also be depleted in HSE relative to BSE. A typical example of a komatiite system derived from such a mantle domain is the Boston Creek komatiites (Puchtel et al., 2018).

Using the data for the komatiite systems, for which late accretion has been argued to be the main cause for the observed ^{182}W versus source HSE abundance relationships (**Fig. 6**), and assuming that the ^{182}W excesses were due entirely to a deficit of late accreted materials in their mantle sources, Puchtel et al. (2022) estimated μ^{182}W of the pre-late accretionary BSE to be +17±7 (**Fig. 6**). This estimate is consistent with the ^{182}W excess in the pre-late accretion BSE of +18±9 ppm obtained by Kleine and Walker (2017) using an independent approach and to the estimates for the ^{182}W composition of the pre-late accretionary Moon of +25±5 ppm (Kruijer et al., 2015; Touboul et al., 2015; Kruijer and Kleine, 2017). These similarities provide further support to the hypothesis that the Earth and the Moon formed from material with identical W isotopic compositions (Kleine and Walker, 2017), in concert with earlier observations of similarity of O, Si, and Ti isotopic compositions between the Earth and the Moon (*e.g.*, Dauphas et al., 2014), as well as additional evidence that the Moon likely formed mainly from terrestrial, rather than impactor, material.

6.3. Core-mantle boundary processes

Core-mantle exchange is yet another process that may have been responsible for creating large ^{182}W and $^{186, 187}$Os isotope and HSE abundance heterogeneities in the mantle. Originally, the idea was proposed by Walker et al. (1995) based on their studies of the Re, Pt, and Os partitioning behavior in group IIAB magmatic iron meteorites. Walker et al. (1995) noted that during magmatic differentiation, solid metal – liquid metal partition coefficients decrease in the order $D_{Os}>D_{Re}>D_{Pt}$, so that after crystallization of the inner core, the liquid outer core would end up with supra-chondritic Re/Os and Pt/Os and, given enough time, would develop coupled $^{186, 187}$Os enrichments. Walker et al. (1997) observed a coupled radiogenic $^{186, 187}$Os signature in the Noril'sk sulfide ores, which they interpreted as having originated from interaction of the starting 251 Ma Siberian superplume (*e.g.*, Campbell, 2007) with the liquid outer core at the CMB.

The concept of core-mantle interaction was further elaborated upon by Brandon et al. (1998, 1999, 2003) and Puchtel et al. (2005) in their studies of plume-derived ocean island basalts and komatiites. These authors proposed that the type of correlation between the initial

906 $\mu^{186}Os$ and $\gamma^{187}Os$ values observed in plume-derived Hawaiian picrites and Gorgona Island
907 and Kostomuksha komatiites is unique to mixtures with fractionated liquid outer core metal
908 (Pt/Re ~100), whereas common crustal materials have Pt/Re <30.

909 The major drawback of the original core-mantle interaction model stems from the fact that
910 the onset of inner core crystallization is poorly constrained, ranging from <1.0 to 3.5 Ga given
911 the uncertainties in estimates of present-day heat flux at the CMB which vary from 3 to 10
912 TW (see review in Nakagawa, 2020, and references therein), as well as currently insufficient
913 knowledge of the partition coefficients of radioactive elements (*e.g.*, K) under the CMB
914 conditions. Another issue concerns the fact that the core-mantle interaction model of Walker
915 et al. (1995) and Brandon et al. (1998, 1999) calls for physical addition of ~1% of the outer
916 core liquid metal to the silicate lower mantle. Because the liquid outer core has up to three
917 orders of magnitude higher HSE abundances compared to the mantle, the $^{186,\ 187}Os$
918 composition of the resulting hybrid mantle source would be dominated by that of the outer
919 core, and this source would also have had an order of magnitude higher HSE abundances
920 compared to those in the BSE. Most OIB, including Hawaiian picrites, are sulfur-saturated
921 melts and likely to have lost a significant part of their HSE inventory to either immiscible
922 sulfide liquid fractionation or to retaining residual sulfide in their melting source regions (*e.g.*,
923 Shirey and Walker, 1998; Bennett et al., 2000; Jamais et al., 2008; Ireland et al., 2009). Such
924 loss of HSE during magma generation and ascent would not be the case for komatiites,
925 however, which are strongly sulfur-undersaturated magmas and, therefore, reliably record the
926 HSE abundances in their mantle source regions upon emplacement. Yet, those komatiites for
927 which input from the outer core has been advocated to explain their coupled $^{186,187}Os$
928 enrichments, *e.g.*, Gorgona Island (Brandon et al., 2003) and Kostomuksha (Puchtel et al.,
929 2005) komatiites, have calculated HSE abundances in their mantle source regions similar to
930 those in estimates for the modern BSE.

931 To reconcile the $^{186,187}Os$ and HSE abundance data for the Kostomuksha komatiites with
932 this apparent inconsistency, Puchtel and Humayun (2000) proposed a mechanism of core-
933 mantle interaction *via* isotopic exchange at the core-mantle interface, without any significant
934 mass transfer from the core to the mantle. This idea has been further advanced by Humayun
935 (2011). The mechanism of core-mantle interaction of Humayun (2011) requires the outer core
936 liquid to be trapped in a cumulate pile of Fe-rich non-metallic precipitates (FeO, FeS, Fe_3Si)
937 at the top of the core, then undergo fractional crystallization by precipitating solid metal
938 grains and leaving behind the residual metallic liquid. The residual liquid is then incorporated
939 into the base of the mantle, where it subsequently may be entrained by mantle plumes.

Based on the discovery of negative $\mu^{182}W$ values in some modern ocean island basalts, Mundl et al. (2017), Rizo et al. (2019), and Mundl-Petermeier et al. (2019, 2020) have also argued for some form of core-mantle exchange/equilibration in order to transfer the inferred negative $\mu^{182}W$ value of the core of –220 to plumes rising from the CMB. Although the $^{186,187}Os$ and ^{182}W data obtained on the same samples are still limited, all Hawaiian lavas with negative $\mu^{182}W$ (ranging between –7.8 and –20.2) are also characterized by positive $\mu^{186}Os$ (ranging between +18.6 and +62.8) and positive $\gamma^{187}Os$ (ranging between +2.0 and +7.2). Furthermore, Puchtel et al. (2020) obtained a negative $\mu^{182}W$ value of –10 for the Lapland komatiites, which is within the range of the $\mu^{182}W$ values obtained for Hawaii, and proposed that Lapland komatiites could be early Proterozoic equivalents of Hawaiian picrites. A core-mantle interaction process, as put forward by Puchtel et al. (2020), would be expected to have decreased the ^{182}W value in the Lapland komatiite source relative to the ambient mantle, and also have increased the HSE abundances in this source over ambient mantle levels, which is consistent with the observations (**Fig. 6**). That study further proposed that if the residual metal in the model of Humayun (2011) had a composition similar to that of fractionated iron meteorites, its entrainment into the mantle plume that gave rise to the Lapland komatiites could explain the decoupled $^{186,187}Os$ systematics of these komatiites.

6.4. Crustal recycling processes

Yet another important mechanism for creating mantle chemical heterogeneities is recycling of Earth's mantle lithosphere, oceanic crust, and sedimentary layers back into the mantle (Hofmann and White, 1982; Shirey and Hanson, 1986; Chase and Patchett, 1988; Campbell and Griffiths, 1992; Hart et al., 1992; Carlson, 1994; Roy-Barman and Allègre, 1995; Widom, 1997; Lassiter and Hauri, 1998; Blichert-Toft et al., 1999; Lassiter, 2006). This recycling may occur via subduction – a process by which one tectonic plate moves under another and sinks into the mantle as the plates converge; subduction is the driving force behind modern plate tectonics. The subducted material may age in the mantle for hundreds of millions of years until entrained in mantle plumes. Although there is little agreement on the timing of the onset or even existence of modern-style plate tectonics in the Hadean and Archean (e.g., Brown, 2007; Shirey et al., 2008; Gerya, 2014; Sizova et al., 2015; Johnson et al., 2017; Bédard, 2018), several lines of geochemical evidence put forward by Shirey et al. (2008) require that some version of modern-style plate tectonics already operated as far back in Earth history as 3.5 billion years ago, followed by a transition from the stagnant-lid to mobile-lid plate tectonic regimes sometime in the late Archean (O'Neill and Debaille, 2014).

Crustal recycling, e.g., in the form of subduction of pelagic sediments into the mantle, may also cause decoupling of Nd and Hf isotope systematics of lavas from the Nd-Hf mantle array, as has been argued to be the case for a suite of drill core Komati komatiite samples (Blichert-Toft et al., 2015). This is due to the fact that the Lu/Hf ratio is strongly fractionated relative to Sm/Nd in the Earth's sedimentary system (Patchett et al., 1984). This is caused by high resistance to chemical weathering of the mineral zircon, which contains most of the Hf budget of continental crustal rocks. During weathering of continental crustal rocks, they break down into zircon-bearing sandy sediments with very low Lu/Hf and fine-grained clay material with up to three times the chondritic Lu/Hf ratio. During sediment transport via turbidity currents, sandy sediments stay on or near the continent, while the pelagic material is carried out onto the ocean floor, where it may eventually be subducted into the mantle.

7. The Nd-Hf-Os isotope paradox and its implications for early Earth history

As noted above, there is evidence for decoupling between the radiogenic lithophile ^{143}Nd and ^{176}Hf systems in certain komatiites mantle sources, but there is also apparent decoupling between these lithophile isotope systems and the highly siderophile ^{187}Os system in some komatiite mantle sources. The majority of the Archean and Proterozoic komatiite systems are characterized by variable, and generally strong, long-term depletions in more incompatible lithophile trace elements relative to less incompatible elements, *e.g.*, Nd versus Sm and Hf versus Lu (**Fig. 1**), yet they retain chondritic time-integrated Re/Os (**Fig. 2**). These komatiite mantle sources must have experienced relatively early melt depletion events that fractionated the Sm/Nd and Lu/Hf ratios to suprachondritic values high enough to bring the ^{143}Nd and ^{176}Hf compositions to the variably positive ε^{143}Nd and ε^{176}Hf values. Since Re is generally moderately to highly incompatible during mantle melting, whereas Os is moderately to highly compatible (*e.g.*, Barnes et al., 1985; Mallmann and O'Neill, 2007), these melt extraction events should have also decreased the Re/Os ratio in the komatiite-basalt mantle sources. This would have resulted in retardation of ^{187}Os ingrowth and, thus, evolution of the sources to variably negative γ^{187}Os values. However, such isotopic relationships are not observed in the global komatiite record.

Puchtel et al. (2022) named this phenomenon the Nd-Hf-Os isotope paradox, to which Puchtel et al. (2020, 2022) offered a solution by developing a model whereby the komatiite-basalt mantle sources underwent early (~100 Ma into Solar System history), low-degree (F = 1.5-2.0%) partial melting and melt extraction events that would have sufficiently fractionated the Sm/Nd and Lu/Hf ratios in the mantle sources, but would have had little effect on the

Re/Os ratio due to the significantly lower incompatibility of Re compared to Nd and Hf during low-degrees of partial mantle melting.

Because this depleted reservoir is apparently persistent throughout the Archean and is globally distributed, it requires early formation and subsequent complete isolation of a complementary basaltic crust enriched in incompatible lithophile trace elements. Calculations by Puchtel et al. (2022) indicate that such crust formed as a result of 1.5-2.0% batch melting of a BSE-like mantle would contain 31-27 ppm Nd, 7.1-6.5 ppm Sm, 0.62-0.59 ppm Lu, and 5.2-4.7 ppm Hf, and would have $^{147}Sm/^{144}Nd$ = 0.140-0.145 and $^{176}Lu/^{177}Hf$ = 0.0166-0.0174 (compared to 0.1967 and 0.0336 in the BSE, respectively). Based on these estimates of Sm and Nd concentrations in the early crust, the mass of this reservoir must have represented ≤2.0% of the mass of the BSE, which is consistent with this reservoir being the size of the D" layer. The existence of such crust has been previously advocated for by Galer and Goldstein (1991). Alternatively, this earliest mafic crust could have served as the source of the oldest tonalite-trondhjemite-granodiorite (TTG) complexes (Carlson et al., 2019), such as those from the Nuvvuagittuq Greenstone Belt in Québec (O'Neil et al., 2008, 2016) or the Vodla Block TTG complex in the Fennoscandian Shield (Puchtel et al., 2016b).

The residence time of this early mafic crust in the mantle is difficult to constrain. The available komatiite-basalt record would require its isolation through at least the late Archean, *i.e.*, when the ^{142}Nd anomalies were still present in the mantle (Debaille et al., 2013). However, there is no evidence that this crust was stored in the mantle until the present day, based on the generally chondritic ^{138}Ce, $^{142,143}Nd$, and ^{176}Hf composition estimates for the BSE (Jackson and Carlson, 2012; Horan et al., 2018; Willig and Stracke, 2019; Willig et al., 2020; Hyung and Jacobsen, 2020).

8. Komatiite constraints on early mixing rates of the terrestrial mantle

It has been proposed that the mixing rates of the mantle, or the average time of mantle homogenization, can be evaluated through studies of short-lived radiogenic isotope systematics and HSE abundances in mantle-derived rocks (*e.g.*, Jacobsen and Yu, 2015; Carlson et al., 2019; Hyung and Jacobsen, 2020; Tusch et al., 2021; Puchtel et al., 2022). Isotopic variations due to the decay of the now extinct ^{146}Sm and ^{182}Hf nuclides recorded processes in the Earth that fractionated Sm/Nd and Hf/W ratios between different terrestrial reservoirs at the times when these parent nuclides were still alive. When these events occurred during the first ~600 and ~60 Ma of Earth history, respectively, the differentiation processes resulted in formation of ^{142}Nd and ^{182}W anomalies in these terrestrial reservoirs. Due to the

protracted, violent accretion history of the Earth accompanied by vigorous convective mixing during the Hadean and Archean eons, these reservoirs and, thus, the isotopic anomalies they hosted, were gradually erased from the geological record. Hence, tracing the variations in the magnitude of these isotopic anomalies over geological time can be used to determine the mixing rates of the terrestrial mantle (*e.g.*, Jacobsen and Yu, 2015; Hyung and Jacobsen, 2020).

Early mantle convection models (*e.g.*, Blichert-Toft and Albarède, 1994; Coltice and Schmalzl, 2006) concluded that the mixing times in the hot Hadean and Archean mantle were 10 times faster than today, and that any large-scale primordial chemical and isotopic heterogeneities in the mantle would have been erased within ~100 Ma of their creation. However, during the past two decades, numerous ^{142}Nd and ^{182}W anomalies have been discovered in the terrestrial mantle-derived rock record (**Fig. 7**). The largest ^{142}Nd anomalies (μ^{142}Nd up to +20 ppm and down to −20 ppm) have been reported for Eo- to Paleoarchean supracrustal rocks from the Isua Greenstone Belt, Greenland (Boyet et al., 2003; Caro et al., 2006; Bennett et al., 2007; Rizo et al., 2011; 2012; 2013; O'Neil et al., 2016), the Nuvvuagittuq Greenstone Belt, Québec (O'Neil et al., 2008; 2012; Roth et al., 2013), the Acasta Gneiss Complex, Canada (Roth et al., 2014; Reimink et al., 2018), and the Barberton Greenstone Belt, Kaapvaal Craton, South Africa (Puchtel et al., 2016a; Boyet et al., 2021). These isotopic anomalies must have been created before ~4.0 Ga by silicate-silicate differentiation and, thus, have survived for >1.0 Ga, implying much slower mixing times of the mantle for ^{142}Nd than was predicted by the early mantle convection models. Following these discoveries, more recent mantle convection models argue for complete homogenization of the mantle by the end of the Archean (*e.g.*, Rosas and Korenaga, 2018; Korenaga, 2021). Only few terrestrial samples with ages between 3.0 and 2.7 Ga have μ^{142}Nd values deviating from the terrestrial standard by more than ±5 ppm, the only known exception being 2.72 Ga tholeiites from the Abitibi Greenstone Belt, Canada (Debaille et al., 2013). Although there is a significant gap in the mafic-ultramafic rock record for ^{142}Nd data between ~2.7 Ga and the present day, it indeed appears that ^{142}Nd anomalies largely disappeared by the end of the Archean (**Fig. 7**). As a result, on the basis of the now much larger ^{142}Nd record and using a mathematical mantle mixing box model, Hyung and Jacobsen (2020) concluded that the relationships in **Fig. 7** are consistent with mantle mixing rates of ~400 Ma that operated since the early Hadean. These authors further argued that such fast mixing rates are consistent with Earth's thermal and chemical evolution having been largely regulated by plate tectonics for most of its history.

Nonetheless, recent studies have shown that some modern plume-derived OIB (**Fig. 7)** have ^{142}Nd compositions resolved, albeit marginally, from the terrestrial standard (*e.g.*, Horan et al., 2018; Peters et al., 2018), indicating that some ^{142}Nd isotopic signatures dating back to Earth's earliest differentiation events may still be preserved in deepest parts of the modern mantle.

In contrast to the earliest ^{142}Nd record, mostly positive ^{182}W anomalies, of up to ~+20 ppm, have been reported for mafic-ultramafic rocks ranging in age from 4.0 to 2.7 Ga (**Fig. 7b**). The only exceptions are komatiites from the Schapenburg system (Puchtel et al., 2016a), which have a negative ^{182}W anomaly of –8 ppm. On the other hand, some recent and modern OIB, such as Hawaii, Samoa, Iceland, Galapagos, Heard, Pitcairn (Mundl et al., 2017; Mundl-Petermeier et al., 2019, 2020), and Kerguelen and Reunion (Rizo et al., 2019) are characterized by negative ^{182}W anomalies down to –25 ppm, although the volumetrically dominant signature in OIB is most likely ^{182}W = 0. The very limited data available (Puchtel et al., 2016b, 2020) provide a hint that there may be a transition at ~2.5 Ga from mostly positive μ^{182}W-dominated to no-anomaly μ^{182}W-dominated mantle (**Fig. 7b**). With the relatively young 2.05 Ga Lapland komatiites already registering a negative ^{182}W anomaly of –10 ppm (Puchtel et al., 2020), and some OIB sources registering negative ^{182}W anomalies down to –25 ppm, this transition may indicate the combined effects of the onset of modern-style plate tectonics and core-mantle interaction taking over as the main driving forces controlling the W isoltopic composition of the deep plume mantle sources (*e.g.*, Rizo et al., 2019; Carlson et al., 2019).

The different behavior of the two short-lived isotopic systems in the mantle may be possible to reconcile when the mechanisms behind the origin of ^{142}Nd and ^{182}W anomalies are considered. Because both Sm and Nd are uniformly strongly lithophile elements under the redox conditions applicable to Earth's formation, ^{142}Nd anomalies are solely the result of primordial silicate-silicate planetary differentiation (*e.g.*, Boyet and Carlson, 2005). No new ^{142}Nd anomalies could have been created in the BSE after ~4.0 Ga, when ^{146}Sm became extinct. In contrast to the ^{146}Sm-^{142}Nd system, Hf is strongly lithophile, while W is moderately siderophile. Hafnium, therefore, can be fractionated from W during metal-silicate differentiation, such as that which occurred during planetary core segregation. During silicate-silicate differentiation, W is more incompatible than Hf, which can result in fractionation of Hf from W in purely silicate systems. Both processes are considered to be capable of creating ^{182}W anomalies within the first 60 Ma of Earth's history, while ^{182}Hf was still extant. The additional processes that are thought to be capable of introducing ^{182}W heterogeneities to the

mantle and to which the ^{142}Nd system was insensitive, were late accretion and core-mantle interaction, as discussed in **Section 6**. As a result of the combination of all these factors in variable, and generally unconstrained, proportions, the use of the ^{182}Hf-^{182}W isotopic system for tracing mixing times of the mantle appears to be of lesser value than the ^{146}Sm-^{142}Nd systematics.

Mantle mixing rates in terms of HSE have been studied *via* tracing the changes in HSE abundances in the mantle over the span of geological time (*e.g.*, Maier et al., 2009; Puchtel et al., 2018, 2020, 2022). Because the lunar highland crust, which was formed at ~4.4 Ga (*e.g.*, Borg et al., 2014), is only negligibly contaminated by meteoritic material (*e.g.*, Day et al., 2010), late accretion must have been largely complete prior to 4.4 Ga, *i.e.*, within the first ~150 Ma of the Solar System history. Puchtel et al. (2022) used the estimated HSE abundances in the sources of the Archean and Proterozoic komatiite systems plotted in **Fig. 3** as a function of their ages and *Isoplot* regression analysis to calculate the average time by which the late accreted materials would have been completely homogenized within the mantle, and found 2.5±0.2 Ga. These data require that survival times of the late accreted planetesimals within the mantle, before complete homogenization, were on average 1.9±0.2 Ga (*i.e.*, the time interval between 4.4 and 2.5 Ga), thus constraining the average mixing rates of the terrestrial mantle in terms of siderophile element abundances in the Hadean and the Archean. This period in time coincides with the timing of onset of modern-style plate tectonics on Earth, as argued by some (Brown, 2007; Brown and Johnson, 2018), and with the near-complete disappearance of all ^{142}Nd and positive ^{182}W anomalies in the mantle (Carlson et al., 2019; Reimink et al., 2020, Tusch et al., 2021).

It is possible that some inefficient mixing could be due to early Earth tectonic regimes differing from those of modern-style plate tectonics (O'Neill and Debaille, 2014). A stagnant-lid, or episodic, subduction regime in the Hadean is consistent with the persistence of short-lived isotopic anomalies and compositional heterogeneities, although more recent modeling indicates that such mantle heterogeneities can survive for billions of years, even under a mobile-lid tectonic regime (Foley and Rizo, 2017).

9. The diverse nature of komatiite sources reflects on the complexity of the terrestrial mantle

As is evident from the chemical and isotopic data summarized in **Tables 1** and **2** and discussed throughout this review, komatiite mantle sources were characterized by extreme diversity throughout the Archean and early Proterozoic in terms of both trace- and HSE

abundances and radiogenic isotope systematics. Early Archean komatiites were likely derived from lower mantle domains that were created very early in Earth history as a result of deep-seated magma ocean crystallization processes. These mantle domains were characterized by highly variable, and often strong, long-term depletions in the highly incompatible lithophile trace elements and generally large deficits in the late accreted component, as attested to by their HSE abundance and ^{182}W systematics.

The late Archean and Proterozoic komatiites show evidence in their mantle sources for limited variability of long-term depletions in highly incompatible lithophile trace elements as a result of prior melt extractions. With the exception of the Kostomuksha and possibly Lapland systems, these komatiites were derived from mantle plumes that originated in the upper mantle, most likely in the MTZ. These komatiite sources were characterized by smaller deficits to excesses in the late accreted component, as testified to by their HSE abundance and ^{182}W systematics.

Finally, our compliation of the geochemical data relevant to the mantle sources of Archean and early Proterozoic komatiites reveals that none of the projected sources were similar in composition to estimates for the BSE. The komatiite systems considered here, which span wide geographical and temporal distributions, further demonstrate that no single petrogenetic model can account for all the diverse chemical compositions of komatiites.

10. Conclusions

Komatiites, due to their unique properties and, with a few exceptions, very old ages, are among the best samples to constrain the evolution of the chemical composition of the early Earth's mantle. Isotopic and elemental signatures created in early-formed silicate reservoirs *via* radioactive decay of short- and long-lived nuclides, including $^{146,147}Sm$, ^{176}Lu, ^{182}Hf, ^{187}Re, and ^{190}Pt, have been sampled by komatiitic magmas and preserved in the geological rock record. These signatures have been used here to constrain the nature and timing of formation of these, by now largely vanished, mantle reservoirs.

The komatiites considered in the present review are interpreted to have been derived from anhydrous melting in mantle plumes that were initiated in both the lower and upper mantle, although, in contrast to modern plumes, all evidence for the depths of ancient mantle plume initiation is circumstantial in nature.

The data for the existing 3.6-2.0 Ga komatiite record provide robust evidence for the presence of remarkably ancient isotopic and chemical heterogeneities in the mantle at that time interval in Earth history. These heterogeneities have been shown here to reflect the

combined effects of (i) the co-existence of diverse post-magma ocean silicate domains characterized by variably-fractionated lithophile and siderophile element abundances; (ii) the presence of distinct reservoirs representing mantles and cores of large, differentiated planetesimals delivered to Earth during late accretion; and (iii) isotopic exchange across the core-mantle boundary.

The near-complete disappearance of resolvable ^{142}Nd anomalies and of decoupled ^{143}Nd-^{176}Hf isotopic signatures in the mafic-ultramafic rock record by ~2.5 Ga indicates that the earliest silicate reservoirs, formed as a result of primordial magma ocean crystallization, had been largely destroyed by that time through vigorous, convective mantle mixing, implying mixing rates of the mantle on the order of ~1.5 Ga. The shift from mostly positive ^{182}W offsets in the pre-2.5 Ga mantle sources of mafic-ultramafic lavas to no ^{182}W offsets at ~2.5 Ga, as well as disapperance of HSE abundance anomalies at ~2.5 Ga, may indicate the combined effects of the onset of modern-style plate tectonics and core-mantle interaction that took over as the main driving force of creating ^{182}W isotopic heterogeneities in the mantle.

This review further emphasizes the great compositional complexity of early Archean to early Proterozoic komatiite mantle sources in terms of both lithophile and siderophile element abundances and isotope systematics; apparently, none of these sources were similar in composition to that of the BSE. Obviously, no single petrogenetic model can fully account for the chemical and isotopic diversity of komatiites.

Acknowledgements

This work was supported by NSF Petrology and Geochemistry grant EAR 1754186 to ISP. We are grateful to Al Hofmann and Maud Boyet for thorough and constructive reviews of the initial version of this manuscript and to Catherine Chauvel for editorial handling. This work greatly benefitted from close collaborations with Carl Anhaeusser, Nick Arndt, Gary Byerly, Eero Hanski, Al Hofmann, Munir Humayun, Vyacheslav and Victoria Kulikov, Mike Lesher, Marek Locmelis, Euan Nisbet, and Andi Mundl-Petermeier.

References

Abbott, D., 1996. Plumes and hotspots as sources of greenstone belts. Lithos 37 (2-3): 113-127.

Abe, Y., 1997. Thermal and chemical evolution of the terrestrial magma ocean. Physics of the Earth and Planetary Interiors 100 (1-4): 27-39.

Agee, C.B. and Walker, D., 1988. Static compression and olivine flotation in ultrabasic silicate liquid. Journal of Geophysical Research 93 (B4): 3437-3449.

Albarède, F., Blichert-Toft, J., Vervoort, J. D., Gleason, J. D., Rosing, M., 2000. Hf-Nd isotope evidence for a transient dynamic regime in the early terrestrial mantle. Nature **404** (6777): 488-490.

Allègre, C.J., 1982. Genesis of Archaean komatiites in a wet ultramafic subducted plate. In: Arndt, N.T. and Nisbet, E.G. (Eds.), Komatiites, George Allen and Unwin, London, pp. 495-500.

Andreasen, R., Sharma, M., Subbarao, K.V., and Viladkar, S.G., 2008. Where on Earth is the enriched Hadean reservoir? Earth and Planetary Science Letters 266 (1-2): 14-28.

Archer, G.J., Brennecka, G.A., Gleißner, P., Stracke, A., Becker, H., and Kleine, T., 2019. Lack of late-accreted material as the origin of ^{182}W excesses in the Archean mantle: Evidence from the Pilbara Craton, Western Australia. Earth and Planetary Science Letters, 528: 115841.

Arevalo, R., McDonough, W. F., 2008. Tungsten geochemistry and implications for understanding the Earth's interior. Earth and Planetary Science Letters **272** (3-4): 656-665.

Armstrong, R. L., 1981. Radiogenic isotopes: the case for crustal recycling on a near-steady-state no-continental-growth. Philosophical Transactions of the Royal Society of London **A301**: 443-472.

Arndt, N.T., 1994. Archean Komatiites. In: Condie, K.C. (Ed.). Archean Crustal Evolution, Elsevier, Amsterdam, pp. 11-44.

Arndt, N.T. and Nisbet, E.G., 1982. Komatiites. Allen and Unwin, London, 582 pp.

Arndt, N.T., Lesher, C.M., and Barnes, S.J., 2008. Komatiite. Cambridge University Press, Cambridge, UK, 467 pp.

Arndt, N.T., Naldrett, A.J., Pyke, D.R., 1977. Komatiitic and iron-rich tholeiitic lavas of Munro Township, northeast Ontario. Journal of Petrology **18**: 319-369.

Arndt, N.T., 1977. Ultrabasic magmas and high-degree melting of the mantle. Contributions to Mineralogy and Petrology 64 (2): 205-221.

Arndt, N.T., Ginibre, C., Chauvel, C., Albarède, F., Cheadle, M., Herzberg, C., Jenner, G., and Lahaye, Y., 1998. Were komatiites wet? Geology 26 (8): 739-742.

Arndt, N., Bruzak, G., and Reischmann, T., 2001. The oldest continental and oceanic plateaus: Geochemistry of basalts and komatiites of the Pilbara Craton, Australia. Geological Society of America Special Paper 352: 359-387.

Asafov, E.V., Sobolev, A.V., Gurenko, A.A., Arndt, N.T., Batanova, V.G., Portnyagin, M.V., Garbe-Schönberg, D., and Krasheninnikov, S.P., 2018. Belingwe komatiites (2.7 Ga) originate from a plume with moderate water content, as inferred from inclusions in olivine. Chemical Geology 478: 39-59.

Ballmer, M.D., Schumacher, L., Lekic, V., Thomas, C., and Ito, G., 2016. Compositional layering within the large low shear-wave velocity provinces in the lower mantle. Geochemistry, Geophysics, Geosystems 17 (12): 5056-5077.

Bao, X., Lithgow-Bertelloni, C.R., Jackson, M.G., and Romanowicz, B., 2022. On the relative temperatures of Earth's volcanic hotspots and mid-ocean ridges. Science 373 (6576): 57-61.

Barnes, S.-J., Naldrett, A.J., Gorton, M.P., 1985. The origin of the fractionation of platinum-group elements in terrestrial magmas. Chemical Geology 53 (3-4): 303-323.

Barnes, S.J. and Van Kranendonk, M.J., 2014. Archean andesites in the east Yilgarn craton, Australia: Products of plume-crust interaction? Lithosphere 6 (2): 80-92.

Barnes, S.J., Mole, D., Wyche, S., and Dering, G., 2016. Komatiites and associated rocks of the Kalgoorlie–Leonora region. Geological Survey of Western Australia Record 2016/12, 70 pp.

Becker, H., Horan, M.F., Walker, R.J., Gao, S., Lorand, J.-P., and Rudnick, R.L., 2006. Highly siderophile element composition of the Earth's primitive upper mantle: Constraints from new data on peridotite massifs and xenoliths. Geochimica et Cosmochimica Acta 70 (17): 4528-4550.

Bédard, J.H., 2018. Stagnant lids and mantle overturns: Implications for Archaean tectonics, magmagenesis, crustal growth, mantle evolution, and the start of plate tectonics. Geoscience Frontiers 9 (1): 19-49.

Bennett, V.C., Esat, T.M., and Norman, M.D., 1996. Two mantle-plume components in Hawaiian picrites inferred from correlated Os-Pb isotopes. Nature **381** (6579): 221-224.

Bennett, V.C., Norman, M.D., and Garcia, M.O., 2000. Rhenium and platinum group element abundances correlated with mantle source components in Hawaiian picrites: sulphides in the plume. Earth and Planetary Science Letters 183 (3-4): 513-526.

Bennett, V.C., Brandon, A.D., and Nutman, A.P., 2007. Coupled ^{142}Nd-^{143}Nd isotopic evidence for Hadean mantle dynamics. Science 318 (5858): 1907-1910.

Bercovici, D. and Karato, S., 2003. Whole-mantle convection and the transition-zone water filter. Nature 425 (6953): 39-44.

Berry, A.J., Danyushevsky, L.V., O'Neill, H.S.C., Newville, M., and Sutton, S.R., 2008. Oxidation state of iron in komatiitic melt inclusions indicates hot Archaean mantle. Nature 455 (7215): 960-963.

Bickle, M.J., 1982. The magnesium contents of komatiitic liqiuds. In: Komatiites. George Allen and Unwin, London, pp. 479-494.

Bickle, M.J., 1986. Implications of melting for stabilisation of lithosphere and heat loss in the Archaean. Earth and Planetary Science Letters 80 (3-4): 314-324.

Bina, C.R. and Helffrich, G., 1994. Phase transition Clapeyron slopes and transition zone seismic discontinuity topography. Journal of Geophysical Research 99 (B8): 15853-15860.

Blichert-Toft, J. and Albarède, F., 1994. Short-lived chemical heterogeneities in the Archean mantle with implications for mantle convection. Science 263: 1593-1596.

Blichert-Toft, J. and Arndt, N.T., 1999. Hf isotope compositions of komatiites. Earth and Planetary Science Letters 171(3): 439-451.

1285 Blichert-Toft, J., Frey, F.A., and Albarède, F., 1999. Hf isotope evidence for pelagic
1286 sediments in the source of Hawaiian basalts. *Science* **285**: 879-882.
1287 Blichert-Toft, J. and Puchtel, I.S., 2010. Depleted mantle sources through time: Evidence
1288 from Lu-Hf and Sm-Nd isotope systematics of Archean komatiites. Earth and Planetary
1289 Science Letters 297 (3-4): 598-606.
1290 Blichert-Toft, J., Arndt, N.T., Wilson, A., and Coetzee, G., 2015. Hf and Nd isotope
1291 systematics of early Archean komatiites from surface sampling and ICDP drilling in the
1292 Barberton Greenstone Belt, South Africa. American Mineralogist 100: 2396-2411.
1293 Borg, L.E., Gaffney, A.M., and Shearer, C.K., 2014. A review of lunar chronology revealing
1294 a preponderance of 4.34–4.37 Ga ages. Meteoritics and Planetary Science **50** (4): 715-732.
1295 Borisov, A. and Palme, H., 1997. Experimental determination of the solubility of platinum in
1296 silicate melts. Geochimica et Cosmochimica Acta 61 (20): 4349-4357.
1297 Bottke, W.F., Morbidelli, A., Jedicke, R., Petit, J.-M., Levison, H.F., Michel, P., Metcalfe,
1298 T.S., 2002. Debiased Orbital and Absolute Magnitude Distribution of the Near-Earth
1299 Objects. Icarus 156 (2): 399-433.
1300 Bottke, W.F., Levison, H.F., Nesvorny, D., Dones, L., 2007. Can planetesimals left over from
1301 terrestrial planet formation produce the lunar Late Heavy Bombardment? Icarus 190 (1):
1302 203-223.
1303 Bottke, W.F., Walker, R.J., Day, J.M.D., Nesvorny, D., and Elkins-Tanton, L., 2010.
1304 Stochastic Late Accretion to Earth, the Moon, and Mars. Science 330 (6010): 1527-1530.
1305 Bouvier, A., Vervoort, J.D., and Patchett, P.J., 2008. The Lu-Hf and Sm-Nd isotopic
1306 composition of CHUR: Constraints from unequilibrated chondrites and implications for
1307 the bulk composition of terrestrial planets. Earth and Planetary Science Letters 273 (1-2):
1308 48-57.
1309 Boyet, M., Blichert-Toft, J., Rosing, M., Storey, M., Télouk, P., and Albarède, F., 2003. ^{142}Nd
1310 evidence for early Earth differentiation. Earth and Planetary Science Letters 214 (3-4):
1311 427-442.
1312 Boyet, M., and Carlson, R.W., 2005. ^{142}Nd evidence for early (>4.53 Ga) global
1313 differentiation of the silicate Earth. Science **309** (5734): 576-581.
1314 Boyet, M., and Carlson, R.W., 2006. A new geochemical model for the Earth's mantle
1315 inferred from ^{146}Sm-^{142}Nd systematics. Earth and Planetary Science Letters 250 (1-2):
1316 254-268.
1317 Boyet, M., Garçon, M., Arndt, N.T., Carlson, R. W., and Konc, Z., 2021. Residual liquid from
1318 deep magma ocean crystallization in the source of komatiites from the ICDP drill core in
1319 the Barberton Greenstone Belt. Geochimica et Cosmochimica Acta 304: 141-159.
1320 Brenan, J.M. and McDonough, W.F., 2009. Core formation and metal-silicate fractionation of
1321 osmium and iridium from gold. Nature Geoscience 2: 798-801.
1322 Brown, M. and Johnson, T., 2018. Secular change in metamorphism and the onset of global
1323 plate tectonics. American Mineralogist 103 (2): 181-196.
1324 Brown, M., 2007. Metamorphism, Plate Tectonics, and the Supercontinent Cycle. Earth
1325 Science Frontiers 14 (1): 1-18.
1326 Brown, S.M., Elkins-Tanton, L.T., and Walker, R.J., 2014. Effects of magma ocean
1327 crystallization and overturn on the development of ^{142}Nd and ^{182}W isotopic

heterogeneities in the primordial mantle. Earth and Planetary Science Letters 408: 319-330.
Bowring, S. A., Housh, T., 1995. The Earth's early evolution. Science **269** (5230): 1535-1540.
Boyet, M., Blichert-Toft, J., Rosing, M., Storey, M., Télouk, P., Albarède, F., 2003. ^{142}Nd evidence for early Earth differentiation. Earth and Planetary Science Letters **214**: 427-442.
Brandon, A.D., Walker, R.J., Morgan, J.W., Norman, M.D., and Prichard, H.M., 1998. Coupled ^{186}Os and ^{187}Os evidence for core-mantle interaction. Science 280 (5369): 1570-1573.
Brandon, A.D., Norman, M.D., Walker, R.J., and Morgan, J.W., 1999. ^{186}Os-^{187}Os systematics of Hawaiian picrites. Earth and Planetary Science Letters 174 (1-2): 25-42.
Brandon, A.D., Walker, R.J., Puchtel, I.S., Becker, H., Humayun, M., and Revillon, S., 2003. ^{186}Os-^{187}Os systematics of Gorgona Island komatiites: Implications for early growth of the inner core. Earth and Planetary Science Letters 206 (3-4): 411-426.
Brandon, A.D., Humayun, M., Puchtel, I.S., and Zolensky, M., 2005. Re-Os isotopic systematics and platinum group element composition of the Tagish Lake carbonaceous chondrite. Geochimica et Cosmochimica Acta **69** (6): 1619-1631.
Brandon, A.D., Walker, R.J., and Puchtel, I.S., 2006. Platinum-osmium isotope evolution of the Earth's mantle: Constraints from chondrites and Os-rich alloys. Geochimica et Cosmochimica Acta 70 (8): 2093-2103.
Burkhardt, C., Borg, L.E., Brennecka, G.A., Shollenberger, Q.R., Dauphas, N., and Kleine, T., 2016. A nucleosynthetic origin for the Earth's anomalous ^{142}Nd composition. Nature 537: 394-398.
Byerly, B.L., Kareem, K., Bao, H., and Byerly, G.R., 2017. Early Earth mantle heterogeneity revealed by light oxygen isotopes of Archaean komatiites. Nature Geoscience 10: 871-876.
Campbell, I.H., Griffiths, R.W., and Hill, R.I., 1989. Melting in an Archaean mantle plume: head it's basalts, tails it's komatiites. Nature 339 (6227): 697-699.
Campbell, I.H. and Hill, R.I., 1988. A two stage model for the formation of the granite-greenstone terrains of the Kalgoorlie-Norseman area, Western Australia. Earth and Planetary Science Letters 90 (1): 11-25.
Campbell, I.H. and Griffiths, R.W., 1990. Implications of mantle plume structure for the evolution of flood basalts. Earth and Planetary Science Letters 99 (1-2): 79-93.
Campbell, I.H. and Griffiths, R.W., 1992. The changing nature of mantle hotspots through time: Implications for the chemical evolution of the mantle. Journal of Geology 92 (5): 497-523.
Campbell, I.H. and Griffiths, R.W., 1993. The evolution of the mantle's chemical structure. Lithos 30 (3): 389-399.
Campbell, I.H., 2007. Testing the plume theory. Chemical Geology 241 (3-4): 153-176.
Campbell, I.H. and Griffiths, R.W., 2014. Did the formation of D" cause the Archaean-Proterozoic transition? Earth and Planetary Science Letters 388: 1-8.
Canil, D., 1997. Vanadium partitioning and the oxidation state of Archaean komatiite magmas. Nature 389 (6653): 842-845.

Canil, D., 1999. Vanadium partitioning between orthopyroxene, spinel and silicate melt and the redox states of mantle source regions for primary magmas. Geochimica et Cosmochimica Acta 63 (3-4): 557-572.

Canil, D., 2002. Vanadium in peridotites, mantle redox and tectonic environments: Archean to present. Earth and Planetary Science Letters 195 (1-2): 75-90.

Canil, D. and Fedortchouk, Y., 2001. Olivine-liquid partitioning of vanadium and other trace elements, with applications to modern and ancient picrites. Canadian Mineralogist 39: 319-330.

Canup, R.M., 2012. Forming a Moon with an Earth-like Composition via a Giant Impact. Science 338 (6110): 1052-1055.

Carlson, R.W., 1994. Mechanisms of Earth differentiation: consequences for the chemical structure of the mantle. Review of Geophysics 32 (4): 337-361.

Carlson, R.W., Boyet, M., and Horan, M., 2007. Chondrite barium, neodymium, and samarium isotopic heterogeneity and early earth differentiation. Science 316 (5828): 1175-1178.

Carlson, R. W., Boyet, M., O'Neil, J., Rizo, H., and Walker, R. J., 2015. Early Differentiation and Its Long-Term Consequences for Earth Evolution. In: The Early Earth. Hoboken, New Jersey, John Wiley & Sons, Inc.: 143-172.

Carlson, R.W., Garçon, M., O'Neil, J., Reimink, J., and Rizo, H., 2019. The nature of Earth's first crust. Chemical Geology 530: 119321.

Caro, G., Bourdon, B., Birck, J.-L., and Moorbath, S., 2003. ^{146}Sm-^{142}Nd evidence from Isua metamorphosed sediments for early differentiation of the Earth's mantle. Nature 423 (6938): 428-432.

Caro, G., Bourdon, B., Wood, B.J., and Corgne, A., 2005. Trace-element fractionation in Hadean mantle generated by melt segregation from a magma ocean. Nature 436 (7048): 246-249.

Caro, G., Bourdon, B., Birck, J.-L., and Moorbath, S., 2006. High-precision ^{142}Nd/^{144}Nd measurements in terrestrial rocks: Constraints on the early differentiation of the Earth's mantle. Geochimica et Cosmochimica Acta 70 (1): 164-191.

Caro, G., Bourdon, B., Halliday, A.N., and Quitte, G., 2008. Super-chondritic Sm/Nd ratios in Mars, the Earth and the Moon. Nature 452 (7185): 336-339.

Caro, G., 2011. Early Silicate Earth Differentiation. Annual Review of Earth and Planetary Sciences 39 (1): 31-58.

Caro, G., Morino, P., Mojzsis, S.J., Cates, N.L., and Bleeker, W., 2017. Sluggish Hadean geodynamics: Evidence from coupled ^{146,147}Sm-^{142,143}Nd systematics in Eoarchean supracrustal rocks of the Inukjuak domain (Québec). Earth and Planetary Science Letters 457: 23-37.

Cawthorn, R.G, 1975. Degrees of melting in mantle diapirs and the origin of ultrabasic liquids. Earth and Planetary Science Letters 27 (1): 113-120.

Chase, C.G., Patchett, P.J., 1988. Stored mafic/ultramafic crust and early Archaean mantle differentiation. Earth and Planetary Science Letters **91** (1-2): 66-72.

Chou, C.-L., 1978. Fractionation of siderophile elements in the earth's upper mantle. Proceedings of the 9th Lunar and Planetary Science Conference, pp. 219-230.

Chou, C.-L., Shaw, D.M., Crocket, J.H., 1983. Siderophile trace elements in the Earth's oceanic crust and upper mantle. Journal of Geophysical Research 88 (S2): A507-A518.

Coltice, N. and Schmalzl, J., 2006. Mixing times in the mantle of the early Earth derived from 2-D and 3-D numerical simulations of convection. Geophysical Research Letters 33 (23): L23304.

Condie, K.C., 1975. Mantle-plume model for the origin of Archaean greenstone belts based on trace element distributions. Nature 258 (5534): 413-414.

Condie, K.C., 1981. Archaean greenstone belts. Elsevier, Amsterdam, 434 pp.

Condie, K.C., 1994. Greenstones through time. In: Condie, K.C. (Ed.). Archean Crustal Evolution. Elsevier, Amsterdam, pp. 85-120.

Condie, K.C., 2005. High field strength element ratios in Archean basalts: a window to evolving sources of mantle plumes? Lithos 79 (3-4): 491-504.

Cooper, L.B., Ruscitto, D.M., Plank, T., Wallace, P.J., Syracuse, E.M., and Manning, C.E., 2012. Global variations in H_2O/Ce: 1. Slab surface temperatures beneath volcanic arcs. Geochemistry Geophysics Geosystems 13 (3): Q03024.

Corgne, A. and Wood, B.J., 2002. $CaSiO_3$ and $CaTiO_3$ perovskite-melt partitioning of trace elements: Implications for gross mantle differentiation. Geophysical Research Letters 29 (19): 39.1-39.4.

Corgne, A. and Wood, B.J., 2004. Trace element partitioning between majoritic garnet and silicate melt at 25 GPa. Physics of the Earth and Planetary Interiors 143: 407-419.

Corgne, A., Liebske, C., Wood, B.J., Rubie, D.C., and Frost, D.J., 2005. Silicate perovskite-melt partitioning of trace elements and geochemical signature of a deep perovskitic reservoir. Geochimica et Cosmochimica Acta 69 (2): 485-496.

Cottrell, E. and Walker, D., 2006. Constraints on core formation from Pt partitioning in mafic silicate liquids at high temperatures. Geochimica et Cosmochimica Acta 70 (6): 1565-1580.

Courtillot, V., Davaille, A., Besse, J., and Stock, J., 2003. Three distinct types of hotspots in the Earth's mantle. Earth and Planetary Science Letters 205 (3): 295-308.

Crocket, J.H., Fleet, M.E., and Stone, W.E., 1997. Implications of composition for experimental partitioning of platinum-group elements and gold between sulfide liquid and basalt melt: The significance of nickel content. Geochimica et Cosmochimica Acta 61 (19): 4139-4149.

Dale, C.W., Kruijer, T.S., and Burton, K.W., 2017. Highly siderophile element and ^{182}W evidence for a partial late veneer in the source of 3.8 Ga rocks from Isua, Greenland. Earth and Planetary Science Letters 458: 394-404.

Dauphas, N., Burkhardt, C., Warren, P. H., Fang-Zhen, T., 2014. Geochemical arguments for an Earth-like Moon-forming impactor. Philosophical Transactions of the Royal Society: **372** (2024): 20130244.

Day, J.M.D., Walker, R.J., James, O.B., and Puchtel, I.S., 2010. Osmium isotope and highly siderophile element systematics of the lunar crust. Earth and Planetary Science Letters 289 (3-4): 595-605.

Day, J.M.D., 2013. Hotspot volcanism and highly siderophile elements. Chemical Geology 341: 50-74.

1456 Day, J.M.D., Pearson, D.G., Taylor, L.A., 2007. Highly siderophile element constraints on
1457 accretion and differentiation of the Earth-Moon system. Science 315 (5809): 217-219.
1458 Day, J.M.D. and Walker, R.J., 2015. Highly siderophile element depletion in the Moon. Earth
1459 and Planetary Science Letters 423: 114-124.
1460 Day, J.M.D., Brandon, A.D., and Walker, R.J., 2016. Highly Siderophile Elements in Earth,
1461 Mars, the Moon, and Asteroids. Reviews in Mineralogy and Geochemistry 81 (1): 161-
1462 238.
1463 Debaille, V., O'Neill, C., Brandon, A.D., Haenecour, P., Yin, Q.-Z., Mattielli, N., and
1464 Treiman, A.H., 2013. Stagnant-lid tectonics in early Earth revealed by ^{142}Nd variations in
1465 late Archean rocks. Earth and Planetary Science Letters 373: 83-92.
1466 DePaolo, D. J., 1980. Crustal growth and mantle evolution: inferences from models of
1467 element transport and Nd and Sr isotopes. Geochimica et Cosmochimica Acta **44** (8):
1468 1185-1196.
1469 DePaolo, D.J. and Wasserburg, G.J., 1976. Nd isotopic variations and petrogenetic models.
1470 Geophysical Research Letters 3 (5): 249-252.
1471 Desrochers, J.-P., Hubert, C., Ludden, J.N., and Pilote, P., 1993. Accretion of Archaean
1472 oceanic plateau fragments in the Abitibi greenstone belt, Canada. Geology **21** (5): 451-
1473 454.
1474 De Wit, M.J. and Ashwal, L.D., 1997. Greenstone Belts. Clarendon Press, Oxford, 809 pp.
1475 Dostal, J. and Mueller, W.U., 2013. Deciphering an Archean mantle plume: Abitibi
1476 greenstone belt, Canada. Gondwana Research 23 (2): 493-505.
1477 Drake, M. J., 2000. Accretion and primary differentiation of the Earth: A personal journey.
1478 Geochimica et Cosmochimica Acta **64** (14): 2363-2370.
1479 Dupré, B., Chauvel, C., and Arndt, N.T., 1984. Pb and Nd isotopic study of two Archean
1480 komatiitic flows from Alexo, Ontario. Geochimica et Cosmochimica Acta **48** (10): 1965-
1481 1972.
1482 Dziewonski, A.M., Hager, B.H., and O'Connell, R.J., 1977. Large-scale heterogeneities in the
1483 lower mantle. Journal of Geophysical Research 82 (2): 239-255.
1484 Elkins-Tanton, L.T., Parmentier, E.M., and Hess, P.C., 2003. Magma ocean fractional
1485 crystallization and cumulate overturn in terrestrial planets: Implications for Mars.
1486 Meteoritics & Planetary Science 38 (12): 1753-1771.
1487 Elkins-Tanton, L.T., 2008. Linked magma ocean solidification and atmospheric growth for
1488 Earth and Mars. Earth and Planetary Science Letters 271 (1-4): 181-191.
1489 Elkins-Tanton, L.T., 2012. Magma Oceans in the Inner Solar System. Annual Review of
1490 Earth and Planetary Sciences 40 (1): 113-139.
1491 Farnetani, C.G. and Richards, M.A., 1995. Thermal entrainment and melting in mantle
1492 plumes. Earth and Planetary Science Letters 136 (4): 251-267.
1493 Farnetani, C.G., 1997. Excess temperature of mantle plumes: the role of chemical
1494 stratification across "D". Geophysical Research Letters 24 (13): 1583-1586.
1495 Fischer-Gödde, M., Becker, H., and Wombacher, F., 2010. Rhodium, gold and other highly
1496 siderophile element abundances in chondritic meteorites. Geochimica et Cosmochimica
1497 Acta **74** (1): 356-379.

Fischer-Gödde, M., Becker, H., Wombacher, F., 2011. Rhodium, gold and other highly siderophile elements in orogenic peridotites and peridotite xenoliths. Chemical Geology 280 (3-4): 365-383.

Fletcher, M. and Wyman, D.A., 2015. Mantle plume-subduction zone interactions over the past 60 Ma. Lithos 233: 162-173.

Foley, S.F., Barth, M.G., and Jenner, G.A., 2000. Rutile/melt partition coefficients for trace elements and an assessment of the influence of rutile on the trace element characteristics of subduction zone magmas. Geochimica et Cosmochimica Acta 64 (5): 933-938.

Foley, B.J. and Rizo, H., 2017. Long-term preservation of early formed mantle heterogeneity by mobile lid convection: Importance of grainsize evolution. Earth and Planetary Science Letters 475: 94-105.

Fortenfant, S.S., Gunther, D., Dingwell, D.B., and Rubie, D.C., 2003. Temperature dependence of Pt and Rh solubilities in a haplobasaltic melt. Geochimica et Cosmochimica Acta 67 (1): 123-131.

French, S.W. and Romanowicz, B., 2015. Broad plumes rooted at the base of the Earth's mantle beneath major hotspots. Nature 525 (7567): 95-99.

Frost, D. J., Mann, U., Asahara, Y., Rubie, D. C., 2008. The redox state of the mantle during and just after core formation. Philosophical Transactions of the Royal Society **366** (1883): 4315-4337.

Galer, S. J. G., Goldstein, S. L., O'Nions, R. K., 1989. Limits on chemical and convective isolation in the Earth's interior. Chemical Geology **75** (4): 257-290.

Galer, S. J. G., Goldstein, S. L., 1991. Early mantle differentiation and its thermal consequences. Geochimica et Cosmochimica Acta **55** (1-2): 227-239.

Gerya, T., 2014. Precambrian geodynamics: Concepts and models. Gondwana Research 25 (2): 442-463.

Gangopadhyay, A. and Walker, R.J., 2003. Re-Os systematics of the ca. 2.7 Ga komatiites from Alexo, Ontario, Canada. Chemical Geology 196 (1-4): 147-162.

Goldstein, S.L., O'Nions, R.K., and Hamilton, P.J., 1984. A Sm-Nd Isotopic Study of Atmospheric Dusts and Particulates from Major River Systems. Earth and Planetary Science Letters 70 (2): 221-236.

Goldstein, S.L., Galer, S.J.G., 1992. On the trail of early mantle differentiation: $^{142}Nd/^{144}Nd$ ratios of early Archean rocks. Eos **73** (30): 323.

Green, D.H., 1975. Genesis of Archean peridotitic magmas and constraints on Archean geothermal gradients and tectonics. Geology 3 (1): 15-18.

Green, D.H., 1981. Petrogenesis of Archean ultramafic magmas and implications for Archean tectonics. In: Precambrian Plate Tectonics, Kröner, A. (Ed.), Elsevier, Amsterdam, pp. 469-480.

Grove, T.L., de Wit, M.J., and Dann, J., 1997. Komatiites from the Komati type section, Barberton, South Africa. In: de Wit, M.J. and Ashwal, L.D. (Eds.). Greenstone Belts. Oxford Science Publications, Oxford, pp. 422-437.

Grove, T.L. and Parman, S.W., 2004. Thermal evolution of the Earth as recorded by komatiites. Earth and Planetary Science Letters 219 (3-4): 173-187.

Hamilton, P.J., O'Nions, R.K., Bridgwater, D., and Nutman, A.P., 1983. Sm-Nd studies of Archaean metasediments and metavolcanics from West Greenland and their implications for the Earth's early history. Earth and Planetary Science Letters 62 (2): 263-272.

Harper, C.L. and Jacobsen, S.B., 1992. Evidence from coupled ^{147}Sm-^{143}Nd and ^{146}Sm-^{142}Nd systematics for very early (4.5-Gyr) differentiation of the Earth's mantle. Nature 360 (6406): 728-732.

Harper, C.L. and Jacobsen, S.B., 1996. Evidence for ^{182}Hf in the early Solar System and constraints on the timescale of terrestrial accretion and core formation. Geochimica et Cosmochimica Acta 60 (7): 1131-1153.

Hart, S. R., Brooks, S., 1977. The geochemistry and evolution of Early Precambrian mantle. Contributions to Mineralogy and Petrology **61** (2): 109-128.

Hart, S. R., Zindler, A., 1986. In search of a bulk-earth composition. Chemical Geology **57** (3-4): 247-267.

Hart, S.R., Hauri, E.H., Oschmann, L.A., and Whitehead, J.A., 1992. Mantle plumes and entrainment: isotopic evidence. Science 256 (5056): 517-520.

Hauri, E.H., Gaetani, G.A., and Green, T.H., 2006. Partitioning of water during melting of the Earth's upper mantle at H_2O-undersaturated conditions. 248 (3-4): 715-734.

He, Y., Wen, L., Capdeville, Y., and Zhao, L., 2015. Seismic evidence for an Iceland thermo-chemical plume in the Earth's lowermost mantle. Earth and Planetary Science Letters 417: 19-27.

Herzberg, C.T. and Ohtani, E., 1988. Origin of komatiite at high pressures. Earth and Planetary Science Letters 88 (3-4): 321-329.

Herzberg, C.T., 1992. Depth and degree of melting of komatiites. Journal of Geophysical Research 97 (B4): 4521-4540.

Herzberg, C.T., 1995. Generation of plume magmas through time: an experimental perspective. Chemical Geology 126 (1): 1-16.

Herzberg, C. and O'Hara, M.J., 2002. Plume-associated ultramafic magmas of Phanerozoic age. Journal of Petrology 43 (10): 1857-1883.

Herzberg, C., Asimow, P.D., Arndt, N.T., Niu, Y.L., Lesher, C.M., Fitton, J.G., Cheadle, M.J., and Saunders, A.D., 2007. Temperatures in ambient mantle and plumes: Constraints from basalts, picrites, and komatiites. Geochemistry Geophysics Geosystems 8: Q02006.

Herzberg, C. and Gazel, E., 2009. Petrological evidence for secular cooling in mantle plumes. Nature 458 (7238): 619-622.

Herzberg, C., Condie, K., and Korenaga, J., 2010. Thermal history of the Earth and its petrological expression. Earth and Planetary Science Letters 292 (1-2): 79-88.

Hickman, A. and Kranendonk, M.V., 2012. Early Earth Evolution: Evidence from the 3.5-1.8 Ga Geological History of the Pilbara Region of Western Australia. Episodes 35 (1): 283-297.

Hirschmann, M.M., 2018. Comparative deep Earth volatile cycles: The case for C recycling from exosphere/mantle fractionation of major (H_2O, C, N) volatiles and from H_2O/Ce, CO_2/Ba, and CO_2/Nb exosphere ratios. Earth and Planetary Science Letters 502: 262-273.

Hoffmann, J.E., Münker, C., Polat, A., Rosing, M.T., and Schulz, T., 2011. The origin of decoupled Hf-Nd isotope compositions in Eoarchean rocks from southern West Greenland. Geochimica et Cosmochimica Acta 75 (21): 6610-6628.

Hoffmann, J.E. and Wilson, A.H., 2017. The origin of highly radiogenic Hf isotope compositions in 3.33 Ga Commondale komatiite lavas (South Africa). Chemical Geology 455: 6-21.

Hofmann, A.W. and Hart, S., 1978. An assessment of local and regional isotopic equilibrium in the mantle. Earth and Planetary Science Letters 38 (1): 44-62.

Hofmann, A.W. and White, W.M., 1982. Mantle plumes from ancient oceanic crust. Earth and Planetary Science Letters 57 (2): 421-436.

Hofmann, A.W., Jochum, K.P., Seufert, M., and White, W.M., 1986. Nb and Pb in oceanic basalts: New constraints on mantle evolution. Earth and Planetary Science Letters 79 (1-2): 33-45.

Hofmann, A.W., 1988. Chemical differentiation of the Earth: The relationship between mantle, continental crust and oceanic crust. Earth and Planetary Science Letters 90 (3): 297-314.

Horan, M.F., Walker, R.J., Morgan, J.W., Grossman, J.N., and Rubin, A.E., 2003. Highly siderophile elements in chondrites. Chemical Geology **196** (1-4): 5-20.

Horan, M.F., Carlson, R.W., Walker, R.J., Jackson, M., Garçon, M., and Norman, M., 2018. Tracking Hadean processes in modern basalts with 142-Neodymium. Earth and Planetary Science Letters 484: 184-191.

Humayun, M., 2011. A model for osmium isotopic evolution of metallic solids at the core-mantle boundary. Geochemistry Geophysics Geosystems 12 (3): 1-23.

Huppert, H.E., Sparks, R.S.J., Turner, J.S., and Arndt, N.T., 1984. Emplacement and cooling of komatiite lavas. Nature 309 (5963): 19-22.

Huppert, H.E. and Sparks, R.S.J., 1985. Cooling and contamination of mafic and ultramafic magmas during ascent through continental crust. Earth and Planetary Science Letters 74 (4): 371-386.

Hyung, E. and Jacobsen, S.B., 2020. The $^{142}Nd/^{144}Nd$ variations in mantle-derived rocks provide constraints on the stirring rate of the mantle from the Hadean to the present. Proceedings of the National Academy of Sciences: 117 (26): 14738-14744.

Ireland, T.J., Walker, R.J., and Garcia, M.O., 2009. Highly siderophile element and 187Os isotope systematics of Hawaiian picrites: Implications for parental melt composition and source heterogeneity. Chemical Geology 260 (1-2): 112-128.

Ito, E., Kubo, A., Katsura, T., Walter, M.J., 2004. Melting experiments of mantle materials under lower mantle conditions with implications for magma ocean differentiation. Physics of the Earth and Planetary Interiors 143: 397-406.

Jackson, M.G. and Carlson, R.W., 2012. Homogeneous superchondritic $^{142}Nd/^{144}Nd$ in the mid-ocean ridge basalt and ocean island basalt mantle. Geochemistry Geophysics Geosystems 13 (6): Q06011.

Jacobsen, S.B., and Wasserburg, G.J., 1980. Sm-Nd isotopic evolution of chondrites. Earth and Planetary Science Letters 50 (1): 139-155.

Jacobsen, S. B., 1988. Isotopic and chemical constraints on mantle-crust evolution. Geochimica et Cosmochimica Acta **52** (6): 1341-1350.

Jacobsen, S.B. and Yu, G., 2015. Extinct isotope heterogeneities in the mantles of Earth and Mars: Implications for mantle stirring rates. Meteoritics & Planetary Science 50 (4): 555-567.

Jahn, B.-M., Gruau, G., and Glikson, A.Y., 1982. Komatiites of the Onverwacht Group, South Africa: REE geochemistry, Sm-Nd age and mantle evolution. Contributions to Mineralogy and Petrology 80 (1): 25-40.

Jamais, M., Lassiter, J.C., and Brügmann, G., 2008. PGE and Os-isotopic variations in lavas from Kohala Volcano, Hawaii: Constraints on PGE behavior and melt/crust interaction. Chemical Geology 250 (1-4): 16-28.

Jenner, F.E. and O'Neill, H.St.C.C.Q., 2012. Major and trace analysis of basaltic glasses by laser-ablation ICP-MS. Geochemistry, Geophysics, Geosystems 13 (3): Q03003.

Jochum, K.P., Arndt, N.T., and Hofmann, A.W., 1991. Nb-Th-La in komatiites and basalts: constraints on komatiite petrogenesis and mantle evolution. Earth and Planetary Science Letters 107 (2): 272-289.

Johnson, T.E., Brown, M., Gardiner, N.J., Kirkland, C.L., and Smithies, R.H., 2017. Earth's first stable continents did not form by subduction. Nature 543 (7644): 239-242.

Kato, T., Ringwood, A.E., and Irifune, T., 1988. Experimental determination of element partitioning between silicate perovskite, garnet and liquid: constraints on early differentiation of the mantle. Earth and Planetary Science Letters 89 (1): 123-145.

Kent, R.W., Hardarson, B.S., Saunders, A.D., and Storey, M., 1996. Plateaux ancient and modern: Geochemical and sedimentological perspectives on Archaean oceanic magmatism. Lithos 37 (2-3): 129-142.

Kimura, G., Ludden, J.N., Desroshers, J.-P., and Hori, R., 1993. A model of ocean-crust accretion for the Superior province, Canada. Lithos 30 (3-4): 337-355.

Kimura, K., Lewis, R.S., Anders, S., 1974. Distribution of gold and rhenium between nickel-iron and silicate melts; implications for abundance of siderophile elements on the Earth and Moon. Geochimica et Cosmochimica Acta 38 (5): 683-701.

Kleine, T., Münker, C., Mezger, K., Palme, H., 2002. Rapid accretion and early core formation on asteroids and the terrestrial planets from Hf-W chronometry. Nature 418 (6901): 952-955.

Kleine, T., Mezger, K., Palme, H., Münker, C., 2004. The W isotope evolution of the bulk silicate Earth: constraints on the timing and mechanisms of core formation and accretion. Earth and Planetary Science Letters 228 (1-2): 109-123.

Kleine, T., Touboul, M., Bourdon, B., Nimmo, F., Mezger, K., Palme, H., Jacobsen, S.B., Yin, Q.-Z., and Halliday, A.N., 2009. Hf-W chronology of the accretion and early evolution of asteroids and terrestrial planets. Geochimica et Cosmochimica Acta 73 (17): 5150-5188.

Kleine, T., Walker, R. J., 2017. Tungsten Isotopes in Planets. Annual Review of Earth and Planetary Sciences **45** (1): 389-417.

König, S., Münker, C., Schuth, S., and Garbe-Schönberg, D., 2008. Mobility of tungsten in subduction zones. Earth and Planetary Science Letters 274 (1-2): 89-92.

König, S., Münker, C., Hohl, S., Paulick, H., Barth, A. R., Lagos, M., Pfander, J., Büchl, A., 2011. The Earth's tungsten budget during mantle melting and crust formation. Geochimica et Cosmochimica Acta **75** (8): 2119-2136.

Koppers, A.A.P., Becker, T.W., Jackson, M.G., Konrad, K., Müller, R.D., Romanowicz, B., Steinberger, B., and Whittaker, J.M., 2021. Mantle plumes and their role in Earth processes. Nature Reviews 2: 382-401.

Korenaga, J., 2021. Hadean geodynamics and the nature of early continental crust. Precambrian Research 359: 106178.
Kruijer, T.S., Kleine, T., Fischer-Gödde, M., Sprung, P., 2015. Lunar tungsten isotopic evidence for the late veneer. Nature 520 (7548): 534-537.
Kruijer, T. S., Kleine, T., 2017. Tungsten isotopes and the origin of the Moon. Earth and Planetary Science Letters **475** (Supplement C): 15-24.
Kusky, T.M. and Kidd, W.S.F., 1992. Remnants of an Archean oceanic plateau, Belingwe greenstone belt, Zimbabwe. Geology 20 (1): 43-46.
Labrosse, S., Hernlund, J.W., and Coltice, N., 2007. A crystallizing dense magma ocean at the base of the Earth's mantle. Nature 450 (7171): 866-869.
Lassiter, J.C. and Hauri, E.H., 1998. Osmium-isotope variations in Hawaiian lavas: evidence for recycled oceanic lithosphere in the Hawaiian plume. Earth and Planetary Science Letters 164 (3-4): 483-496.
Lassiter, J.C., 2006. Constraints on the coupled thermal evolution of the Earth's core and mantle, the age of the inner core, and the origin of the $^{186}Os/^{188}Os$ "core signal" in plume-derived lavas. Earth and Planetary Science Letters 250 (1-2): 306-317.
Liebske, C., Corgne, A., Frost, D.J., Rubie, D.C., and Wood, B.J., 2005. Compositional effects on element partitioning between Mg-silicate perovskite and silicate melts. Contributions to Mineralogy and Petrology 149 (1): 113-128.
Liu, J., Touboul, M., Ishikawa, A., Walker, R.J., and Pearson, D.G., 2016. Widespread tungsten isotope anomalies and W mobility in crustal and mantle rocks of the Eoarchean Saglek Block, northern Labrador, Canada: Implications for early Earth processes and W recycling. Earth and Planetary Science Letters 448: 13-23.
Loper, D.E., 1991. Mantle plumes. Tectonophysics 187 (4): 373-384.
Maier, W.D., Barnes, S.J., Campbell, I.H., Fiorentini, M.L., Peltonen, P., Barnes, S.-J., Smithies, R.H., 2009. Progressive mixing of meteoritic veneer into the early Earth's deep mantle. Nature 460 (7255): 620-623.
Mallmann, G. and O'Neill, H.St.C., 2007. The effect of oxygen fugacity on the partitioning of Re between crystals and silicate melt during mantle melting. Geochimica et Cosmochimica Acta 71 (11): 2837-2857.
Marchi, S., Canup, R.M., Walker, R.J., 2018. Heterogeneous delivery of silicate and metal to the Earth by large planetesimals. Nature Geoscience 11: 77-81.
Marchi, S., Walker, R.J., and Canup, R.M., 2020. A compositionally heterogeneous martian mantle due to late accretion. Science Advances 6 (7): eaay2338.
Maya, J.M., Bhutani, R., Balakrishnan, S., and Rajee Sandhya, S., 2017. Petrogenesis of 3.15 Ga old Banasandra komatiites from the Dharwar craton, India: Implications for early mantle heterogeneity. Geoscience Frontiers 8 (3): 467-481.
McDonough, W.F. and Sun, S.S., 1995. The composition of the Earth. Chemical Geology 120 (3-4): 223-253.
McKenzie, D. and Bickle, M.J., 1988. The volume and composition of melt generated by extension of the lithosphere. Journal of Petrology 29 (3): 625-679.
Meisel, T., Walker, R.J., Irving, A.J., Lorand, J.-P., 2001. Osmium isotopic compositions of mantle xenoliths: A global perspective. Geochimica et Cosmochimica Acta 65 (8): 1311-1323.

Michael, P., 1995. Regionally Distinctive Sources of Depleted MORB - Evidence from Trace-Elements and H_2O. Earth and Planetary Science Letters 131 (3-4): 301-320.

Mole, D.R., Fiorentini, M.L., Thebaud, N., Cassidy, K.F., McCuaig, T.C., Kirkland, C.L., Romano, SS., Doublier, M.P., Belousova, E.A., Barnes, S.J., and Miller, J., 2014. Archean komatiite volcanism controlled by the evolution of early continents. Proceedings of the National Academy of Sciences 111 (28): 10083-10088.

Montelli, R., Nolet, G., Dahlen, F.A., Masters, G., Engdahl, E.R., and Hung, S.-H., 2004. Finite-Frequency Tomography Reveals a Variety of Plumes in the Mantle. Science 303 (5656): 338-343.

Moore, J.G., 1970. Water Content of Basalt Erupted on the ocean floor. Contributions to Mineralogy and Petrology 28 (4): 272-279.

Morino, P., Caro, G., Reisberg, L., and Schumacher, A., 2017. Chemical stratification in the post-magma ocean Earth inferred from coupled ^{146,147}Sm-^{142,143}Nd systematics in ultramafic rocks of the Saglek block (3.25-3.9 Ga; northern Labrador, Canada). Earth and Planetary Science Letters 463: 136-150.

Mundl, A., Touboul, M., Jackson, M.G., Day, J.M.D., Kurz, M.D., Lekic, V., Helz, R.T., and Walker, R.J., 2017. Tungsten-182 heterogeneity in modern ocean island basalts. Science 356 (6333): 66-69.

Mundl, A., Walker, R.J., Reimink, J.R., Rudnick, R.L., and Gaschnig, R.M., 2018. Tungsten-182 in the upper continental crust: Evidence from glacial diamictites. Chemical Geology 494: 144-152.

Mundl-Petermeier, A., Walker, R.J., Jackson, M.G., Blichert-Toft, J., Kurz, M.D., and Haldórsson, S.A. (2019) Temporal evolution of primordial tungsten-182 and ^{3}He/^{4}He signatures in the Iceland mantle plume. Chemical Geology 525, 245-259.

Mundl-Petermeier, A., Walker, R.J., Fischer, R.A., Lekic, V., Jackson, M.G., and Kurz, M.D., 2020. Anomalous μ^{182}W signatures in high ^{3}He/^{4}He ocean island basalts – fingerprints of Earth's core? Geochimica et Cosmochimica Acta 271: 194-211.

Murphy, D.T., Brandon, A.D., Debaille, V., Burgess, R., and Ballentine, C., 2010. In search of a hidden long-term isolated sub-chondritic ^{142}Nd/^{144}Nd reservoir in the deep mantle: Implications for the Nd isotope systematics of the Earth. Geochimica et Cosmochimica Acta 74 (2): 738-750.

Murphy, D., Rizo, H., O'Neil, J., Hepple, R., Wiemer, D., Kemp, A., and Vervoort, J., 2021. Combined Sm-Nd, Lu-Hf, and ^{142}Nd study of Paleoarchean basalts from the East Pilbara Terrane, Western Australia. Chemical Geology 578: 120301.

Nakagawa, T., 2020. A coupled core-mantle evolution: review and future prospects. Progress in Earth and Planetary Science 7 (1): 57.

Nakanishi, N., Giuliani, A., Carlson, R.W., Horan, M.F., Woodhead, J., Pearson, D. G., and Walker, R.J., 2021. Tungsten-182 evidence for an ancient kimberlite source. Proceedings of the National Academy of Sciences 118 (23): e2020680118.

Newsom, H.E., Sims, K.W.W., Noll, P.D., Jaeger, W.L., Maehr, S.A., and Beserra, T.B., 1996. The depletion of tungsten in the bulk silicate Earth: Constraints on core formation. Geochimica et Cosmochimica Acta 60 (5): 1155-1169.

Nicklas, R.W., Puchtel, I.S., and Ash, R.D., 2018. The Redox Evolution of the Archean Mantle: Evidence from Komatiites. Geochimica et Cosmochimica Acta 222: 447-466.

Nicklas, R.W., Puchtel, I.S., Ash, R.D., Piccoli, P.M., Hanski, E., Nisbet, E.G., Waterton, P., Pearson, D.G., and Anbar, A.D., 2019. Secular mantle oxidation across the Archean-Proterozoic boundary: Evidence from V partitioning in komatiites and picrites. Geochimica et Cosmochimica Acta 250: 49-75.

Nesbitt, R.W., Sun, S.S., and Purvis, A.C., 1979. Komatiites: geochemistry and genesis. Canadian Mineralogist 17 (2): 165-186.

Nisbet, E.G., Cheadle, M.J., Arndt, N.T., and Bickle, M.J., 1993. Constraining the potential temperature of the Archaean mantle: a review of the evidence from komatiites. Lithos 30: 291-307.

Ohtani, E., 1984. Generation of komatiite magma and gravitational differentiation in the deep upper mantle. Earth and Planetary Science Letters 67 (2): 261-272.

O'Neil, J., Carlson, R.W., Francis, D., and Stevenson, R.K., 2008. Neodymium-142 evidence for Hadean mafic crust. Science 321 (5897): 1828-1831.

O'Neil, J., Carlson, R.W., Paquette, J.-L., and Francis, D., 2012. Formation age and metamorphic history of the Nuvvuagittuq Greenstone Belt. Precambrian Research 220-221: 23-44.

O'Neil, J., Rizo, H., Boyet, M., Carlson, R.W., Rosing, M.T., 2016. Geochemistry and Nd isotopic characteristics of Earth's Hadean mantle and primitive crust. Earth and Planetary Science Letters 442: 194-205.

O'Neill, C. and Debaille, V., 2014. The evolution of Hadean-Eoarchaean geodynamics. Earth and Planetary Science Letters 406: 49-58.

Parman, S.W., Dann, J.C., Grove, T.L., and de Wit, M.J., 1997. Emplacement conditions of komatiite magmas from the 3.49 Ga Komati Formation, Barberton greenstone belt, South Africa. Earth and Planetary Science Letters 150 (3-4): 303-323.

Parman, S.W., Grove, T.L., and Dann, J.C., 2001. The production of Barberton komatiites in an Archean subduction zone. Geophysical Research Letters 28 (13): 2513-2516.

Parman, S.W., Grove, T.L., Dann, J.C., and de Wit, M.J., 2004. South African Journal of Geology 107 (1-2): 107-118.

Patchett, P.J. and Tatsumoto, M., 1980. Hafnium isotope variations in oceanic basalts. Geophysical Research Letters 7 (12): 1077-1080.

Patchett, P.J., Kauvo, O., Hedge, C.E., and Tatsumoto, M., 1981. Evolution of continental crust and mantle heterogeneity: evidence from Hf isotopes. Contributions to Mineralogy and Petrology 78 (3): 279-297.

Patchett, P. J., White, W. M., Feldmann, H., Kielinczuk, S., Hofmann, A. W., 1984. Hafnium/rare earth element fractionation in the sedimentary system and crustal recycling into the Earth's mantle. Earth and Planetary Science Letters **69** (2): 365-378.

Peters, B.J., Carlson, R.W., Day, J.M.D., and Horan, M.F., 2018. Hadean silicate differentiation preserved by anomalous $^{142}Nd/^{144}Nd$ ratios in the Réunion hotspot source. Nature 555: 89-106.

Peters, B.J., Mundl-Petermeier, A., Carlson, R.W., Walker, R.J., and Day, J.M.D., 2021. Combined lithophile-siderophile isotopic constraints on Hadean processes preserved in ocean island basalt sources. Geochemistry, Geophysics, Geosystems 22 (3): e2020GC009479.

1803 Puchtel, I.S., Hofmann, A.W., Mezger, K., Jochum, K.P., Shchipansky, A.A., and Samsonov,
1804 A.V., 1998. Oceanic plateau model for continental crustal growth in the Archaean: A case
1805 study from the Kostomuksha greenstone belt, NW Baltic Shield. Earth and Planetary
1806 Science Letters 155 (1-2): 57-74.
1807 Puchtel, I.S. and Humayun, M., 2000. Platinum group elements in Kostomuksha komatiites
1808 and basalts: Implications for oceanic crust recycling and core-mantle interaction.
1809 Geochimica et Cosmochimica Acta 64 (24): 4227-4242.
1810 Puchtel, I.S., Brandon, A.D., and Humayun, M., 2004a. Precise Pt-Re-Os isotope systematics
1811 of the mantle from 2.7-Ga komatiites. Earth and Planetary Science Letters 224 (1-2): 157-
1812 174.
1813 Puchtel, I.S., Humayun, M., Campbell, A., Sproule, R., and Lesher, C.M., 2004b. Platinum
1814 group element geochemistry of komatiites from the Alexo and Pyke Hill areas, Ontario,
1815 Canada. Geochimica et Cosmochimica Acta 68 (6): 1361-1383.
1816 Puchtel, I.S. and Humayun, M., 2005. Highly siderophile element geochemistry of ^{187}Os-
1817 enriched 2.8-Ga Kostomuksha komatiites, Baltic Shield. Geochimica et Cosmochimica
1818 Acta 69 (6): 1607-1618.
1819 Puchtel, I.S., Brandon, A.D., Humayun, M., and Walker, R.J.., 2005. Evidence for the early
1820 differentiation of the core from Pt-Re-Os isotope systematics of 2.8-Ga komatiites. Earth
1821 and Planetary Science Letters 237 (1-2): 118-134.
1822 Puchtel, I.S., Humayun, M., and Walker, R.J., 2007. Os-Pb-Nd isotope and highly siderophile
1823 and lithophile trace element systematics of komatiitic rocks from the Volotsk suite, SE
1824 Baltic Shield. Precambrian Research 158 (1-2): 119-137.
1825 Puchtel, I.S., Walker, R.J., Brandon, A.D., and Nisbet, E.G., 2009a. Pt-Re-Os and Sm-Nd
1826 isotope and HSE and REE systematics of the 2.7 Ga Belingwe and Abitibi komatiites.
1827 Geochimica et Cosmochimica Acta 73 (20): 6367-6389.
1828 Puchtel, I. S., Walker, R. J., Anhaeusser, C. R., Gruau, G., 2009b. Re-Os isotope systematics
1829 and HSE abundances of the 3.5 Ga Schapenburg komatiites, South Africa: Hydrous
1830 melting or prolonged survival of primordial heterogeneities in the mantle? Chemical
1831 Geology **262** (3-4): 355-369.
1832 Puchtel, I.S., Blichert-Toft, J., Touboul, M., Walker, R.J., Byerly, G., Nisbet, E.G., and
1833 Anhaeusser, C.R., 2013. Insights into early Earth from Barberton komatiites: Evidence
1834 from lithophile isotope and trace element systematics. Geochimica et Cosmochimica Acta
1835 108: 63-90.
1836 Puchtel, I.S., Walker, R.J., Touboul, M., Nisbet, E.G., and Byerly, G.R., 2014. Insights into
1837 early Earth from the Pt-Re-Os isotope and highly siderophile element abundance
1838 systematics of Barberton komatiites. Geochimica et Cosmochimica Acta 125: 394-413.
1839 Puchtel, I.S., Blichert-Toft, J., Touboul, M., Horan, M.F., and Walker, R.J., 2016a. The
1840 coupled ^{182}W-^{142}Nd record of early terrestrial mantle differentiation. Geochemistry,
1841 Geophysics, Geosystems 17 (6): 2168-2193.
1842 Puchtel, I.S., Touboul, M., Blichert-Toft, J., Walker, R.J., Brandon, A.D., Nicklas, R.W.,
1843 Kulikov, V.S., and Samsonov, A.V., 2016b. Lithophile and siderophile element
1844 systematics of the mantle at the Archean-Proterozoic boundary: Evidence from 2.4 Ga
1845 komatiites. Geochimica et Cosmochimica Acta 180: 227-255.

Puchtel, I.S., Blichert-Toft, J., Touboul, M., and Walker, R.J., 2018. ^{182}W and HSE constraints from 2.7 Ga komatiites on the heterogeneous nature of the Archean mantle. Geochimica et Cosmochimica Acta 228: 1-26.

Puchtel, I.S., Mundl-Petermeier, A., Horan, M., Hanski, E.J., Blichert-Toft, J., and Walker, R.J., 2020. Ultra-depleted 2.05 Ga komatiites of Finnish Lapland: Products of grainy late accretion or core-mantle interaction? Chemical Geology 554: 119801.

Puchtel I.S., Nicklas R.W., Slagle J., Horan M., Walker R.J., Nisbet E.G., and Locmelis M., 2022. Early global mantle chemical and isotope heterogeneity revealed by the komatiite-basalt record: The Western Australia connection. Geochimica et Cosmochimica Acta (in press).

Rehkämper, M., Halliday, A.N., Fitton, J.G., Lee, D.-C., Wieneke, M., and Arndt, N.T., 1999. Ir, Ru, Pt and Pd in basalts and komatiites: New constraints for the geochemical behavior of the platinum group elements in the mantle. Geochimica et Cosmochimica Acta 63 (22): 3915-3934.

Reimink, J.R., Chacko, T., Carlson, R.W., Shirey, S.B., Liu, J., Stern, R.A., Bauer, A.M., Pearson, D.G., and Heaman, L.M., 2018. Petrogenesis and tectonics of the Acasta Gneiss Complex derived from integrated petrology and ^{142}Nd and ^{182}W extinct nuclide-geochemistry. Earth and Planetary Science Letters 494: 12-22.

Reimink, J.R., Mundl-Petermeier, A., Carlson, R. W., Shirey, S.B., Walker, R.J., and Pearson, D.G., 2020. Tungsten isotope composition of Archean crustal reservoirs and implications for terrestrial μ^{182}W evolution. Geochemistry, Geophysics, Geosystems 21 (7): e2020GC009155.

Richard, D., Marty, B., Chaussidon, M., and Arndt, N.T., 1996. Helium isotopic evidence for a lower mantle component in depleted Archean komatiite. Science 273 (5271): 93-95.

Richards, M.A., Jones, D.L., Duncan, R.A., and DePaolo, D.J., 1991. A mantle plume initiation model for the Wrangellia flood basalt and other oceanic plateaus. Science 254 (5029): 263-265.

Richter, F.M., 1985. Models for the Archean Thermal Regime. Earth and Planetary Science Letters 73 (2-4): 350-360.

Richter, F.M., 1988. A major change in the thermal state of the Earth at the Archean-Proterozoic boundary: Consequences for the nature and preservation of continental lithosphere. Journal of Petrology, Special Lithosphere Issue: 39-52.

Righter, K. and Drake, M.J., 1997. Metal-silicate equilibrium in a homogeneously accreting earth: new results for Re. Earth and Planetary Science Letters 146 (3-4): 541-553.

Righter, K., Walker, R.J., and Warren, P.H., 2000. Significance of highly siderophile elements and osmium isotopes in the lunar and terrestrial mantles. In: Righter, K. and Canup, R.M. (Eds.). Origin of the Earth and Moon. University of Arizona Press. Tucson, AZ, 291-322.

Rizo, H., Boyet, M., Blichert-Toft, J., Rosing, M., 2011. Combined Nd and Hf isotope evidence for deep-seated source of Isua lavas. Earth and Planetary Science Letters 312 (3-4): 267-279.

Rizo, H., Boyet, M., Blichert-Toft, J., O'Neil, J., Rosing, M.T., and Paquette, J.-L., 2012. The elusive Hadean enriched reservoir revealed by ^{142}Nd deficits in Isua Archaean rocks. Nature 491 (7422): 96-100.

Rizo, H., Boyet, M., Blichert-Toft, J., and Rosing, M.T., 2013. Early mantle dynamics inferred from ^{142}Nd variations in Archean rocks from southwest Greenland. Earth and Planetary Science Letters 377-378: 324-335.

Rizo, H., Walker, R.J., Carlson, R.W., Touboul, M., Horan, M.F., Puchtel, I.S., Boyet, M., and Rosing, M.T., 2016. Early Earth differentiation investigated through ^{142}Nd, ^{182}W, and highly siderophile element abundances in samples from Isua, Greenland. Geochimica et Cosmochimica Acta **175**: 319-336.

Rizo H., Andrault D., Bennett N.R., Humayun M., Brandon A.D., Vlastelic I., Moine B., Poirier A., Bouhifd M.A., and Murphy D.T., 2019. ^{182}W evidence for core-mantle interaction in the source of mantle plumes. Geochemical Perspectives Letters 11: 6-11.

Rosas, J.C. and Korenaga, J., 2018. Rapid crustal growth and efficient crustal recycling in the early Earth: Implications for Hadean and Archean geodynamics. Earth and Planetary Science Letters 494: 42-49.

Roth, A.S.G., Bourdon, B., Mojzsis, S.J., Touboul, M., Sprung, P., Guitreau, M., and Blichert-Toft, J., 2013. Inherited ^{142}Nd anomalies in Eoarchean protoliths. Earth and Planetary Science Letters 361: 50-57.

Roth, A.S.G., Bourdon, B., Mojzsis, S.J., Rudge, J.F., Guitreau, M., and Blichert-Toft, J., 2014. Combined ^{147,146}Sm-^{143,142}Nd constraints on the longevity and residence time of early terrestrial crust. Geochemistry, Geophysics, Geosystems 15 (6): 2329-2345.

Roy-Barman, M. and Allègre, C.-J., 1995. ^{187}Os/^{186}Os in oceanic island basalts: tracing oceanic crust recycling in the mantle. Earth and Planetary Science Letters 129 (1-4): 145-161.

Rubie, D.C., Frost, D.J., Mann, U., Asahara, Y., Nimmo, F., Tsuno, K., Kegler, P., Holzheid, A., and Palme, H., 2011. Heterogeneous accretion, composition and core-mantle differentiation of the Earth. Earth and Planetary Science Letters 301 (1-2): 31-42.

Rudnick, R.L., Barth, M., Horn, I., and McDonough, W.F., 2000. Rutile-bearing refractory eclogites: missing link between continents and depleted mantle. Science 287 (5451): 278-281.

Rudnick, R.L. and Gao, S., 2014. Composition of the Continental Crust. Treatise on Geochemistry: 1-51.

Ryder, G., 2002. Mass flux in the ancient Earth-Moon system and benign implications for the origin of life on Earth. Journal of Geophysical Research 107 (E4): 6.1-6.13.

Saal, A.E., Hauri, E.H., Langmuir, C.H., and Perfit, M.R., 2002. Vapour undersaturation in primitive mid-ocean-ridge basalt and the volatile content of Earth's upper mantle. Nature 419 (6906): 451-455.

Saji, N.S., Larsen, K., Wielandt, D., Schiller, M., Costa, M.M., Whitehouse, M.J., Rosing, M.T., and Bizzarro, M., 2018. Hadean geodynamics inferred from time-varying ^{142}Nd/^{144}Nd in the early Earth rock record. Geochemical Perspectives Letters 7: 43-48.

Salters, V. J. M., White, W. M., 1998. Hf isotope constraints on mantle evolution. Chemical Geology **145** (3-4): 447-460.

Schneider, K.P., Hoffmann, J.E., Boyet, M., Münker, C., and Kröner, A., 2018. Coexistence of enriched and modern-like ^{142}Nd signatures in Archean igneous rocks of the eastern Kaapvaal Craton, southern Africa. Earth and Planetary Science Letters 487: 54-66.

Schoenberg, R., Kamber, B. S., Collerson, K. D., Eugster, O., 2002. New W-isotope evidence for rapid terrestrial accretion and very early core formation. Geochimica et Cosmochimica Acta **66** (17): 3151-3160.

Schubert, G. and Sandwell, D., 1989. Crustal volumes of the continents and of oceanic and continental submarine plateaus. Earth and Planetary Science Letters 92 (2): 234-246.

Shirey, S.B. and Hanson, G.N., 1986. Mantle heterogeneity and crustal recycling in Archean granite-greenstone belts: Evidence from Nd isotopes and trace elements in the Rainy Lake area, Superior Province, Ontario, Canada. Geochimica et Cosmochimica Acta 50 (12): 2631-2651.

Shirey, S. B., Walker, R. J., 1998. The Re-Os isotope system in cosmochemistry and high-temperature geochemistry. Annual Reviews of Earth and Planetary Sciences **26**: 423-500.

Shirey, S.B., Kamber, B.S., Whitehouse, M.J., Mueller, P.A., and Basu, A.R., 2008. A review of the isotopic and trace element evidence for mantle and crustal processes in the Hadean and Archean: Implications for the onset of plate tectonic subduction. In: Condie, K.C. and Pease, V. (Eds.), When Did Plate Tectonics Begin on Planet Earth? Geological Society of America Special Paper 440: 1-29.

Sivell, W.J. and McCulloch, M.T., 1991. Neodymium isotope evidence for ultra-depleted mantle in the early Proterozoic. Nature 354 (6352): 384-387.

Sizova, E., Gerya, T., Stüwe, K., and Brown, M., 2015. Generation of felsic crust in the Archean: A geodynamic modeling perspective. Precambrian Research 271: 198-224.

Smithies, R.H., Champion, D.C., Van Kranendonk, M.J., and Hickman, A.H., 2007. Geochemistry of volcanic rocks of the northern Pilbara Craton, Western Australia. Geological Survey of Western Australia, Report 104. Perth, 47 pp.

Sobolev, A.V., Asafov, E.V., Gurenko, A.A., Arndt, N.T., Batanova, V.G., Portnyagin, M.V., Garbe-Schönberg, D., and Krasheninnikov, S.P., 2016. Komatiites reveal a hydrous Archaean deep-mantle reservoir. Nature 531 (7596): 628-632.

Sobolev, A.V., Asafov, E.V., Gurenko, A.A., Arndt, N.T., Batanova, V.G., Portnyagin, M.V., Garbe-Schönberg, D., Wilson, A.H., and Byerly, G.R., 2019. Deep hydrous mantle reservoir provides evidence for crustal recycling before 3.3 billion years ago. Nature 571 (7766): 555-559.

Sossi, P.A., Eggins, S.M., Nesbitt, R.W., Nebel, O., Hergt, J.M., Campbell, I.H., O'Neill, H.St.C., Van Kranendonk, M., and Davies, D.R., 2016. Petrogenesis and Geochemistry of Archean Komatiites. Journal of Petrology 57 (1): 147-184.

Storey, M., Mahoney, J.J., Kroenke, L.W., and Saunders, A.D., 1991. Are oceanic plateaus sites of komatiite formation? Geology **19** (4): 376-379.

Strom, R.G., Malhotra, R., Ito, T., Yoshida, F., and Kring, D.A., 2005. The origin of planetary impactors in the inner Solar system. Science 309 (5742): 1847-1850.

Tonks, W.B. and Melosh, H.J., 1993. Magma Ocean Formation Due to Giant Impacts. Journal of Geophysical Research 98 (E3): 5319-5333.

Torsvik, T.H., Steinberger, B., Ashwal, L.D., Doubrovine, P.V., and Trønnes, R.G., 2016. Earth evolution and dynamics - a tribute to Kevin Burke. Canadian Journal of Earth Sciences 53 (11): 1073-1087.

Touboul, M., Puchtel, I.S., and Walker, R.J., 2012. ^{182}W Evidence for Long-Term Preservation of Early Mantle Differentiation Products. Science 335: 1065-1069.

Touboul, M., Liu, J., O'Neil, J., Puchtel, I.S., and Walker, R.J., 2014. New Insights into the Hadean Mantle Revealed by ^{182}W and Highly Siderophile Element Abundances of Supracrustal Rocks from the Nuvvuagittuq Greenstone Belt, Quebec, Canada. Chemical Geology 383: 63-75.

Touboul, M., Puchtel, I.S., and Walker, R.J., 2015. Tungsten isotopic evidence for disproportional late accretion to the Earth and Moon. Nature 520 (7548): 530-533.

Trønnes, R.G. and Frost, D.J., 2002. Peridotite melting and mineral-melt partitioning of major and minor elements at 22-24.5 GPa. Earth and Planetary Science Letters 197 (1-2): 117-131.

Turekian, K.K. and Clark, S.P., 1969. Inhomogeneous accumulation of the earth from the primitive solar nebula. Earth and Planetary Science Letters 6 (5): 346-348.

Tusch, J., Sprung, P., van de Löcht, J., Hoffmann, J.E., Boyd, A.J., Rosing, M.T., and Münker, C., 2019. Uniform ^{182}W isotope compositions in Eoarchean rocks from the Isua region, SW Greenland: The role of early silicate differentiation and missing late veneer. Geochimica et Cosmochimica Acta 257: 284-310.

Tusch, J., Münker, C., Hasenstab, E., Jansen, M., Marien, C. S., Kurzweil, F., Van Kranendonk, M. J., Smithies, H., Maier, W., and Garbe-Schönberg, D., 2021. Convective isolation of Hadean mantle reservoirs through Archean time. Proceedings of the National Academy of Sciences 118 (2): e2012626118.

Van Kranendonk, M.J., 2008. Two types of Archean continental crust: Plume and plate tectonics on early Earth. American Journal of Science 310 (10): 1187-1210.

Vervoort, J.D. and Blichert-Toft, J., 1999. Evolution of the depleted mantle: Hf isotope evidence from juvenile rocks through time. Geochimica et Cosmochimica Acta 63 (3-4): 533-556.

Vervoort, J.D., Patchett, P.J., Blichert-Toft, J., and Albarède, F., 1999. Relationships between Lu-Hf and Sm-Nd isotopic systems in the global sedimentary system. Earth and Planetary Science Letters 168 (1-2): 79-99.

Vervoort, J.D., Patchett, P.J., Albarède, F., Blichert-Toft, J., Rudnick, R., and Downes, H., 2000. Hf-Nd isotopic evolution of the lower crust. Earth and Planetary Science Letters 181 (1-2): 115-129.

Viljoen, M.J. and Viljoen, R.P., 1969. The geology and geochemistry of the Lower Ultramafic Unit of the Onverwacht Group and a proposed new class of igneous rocks. Geological Society of South Africa Special Publication 2: 55-86.

Wade, J. and Wood, B.J., 2005. Core formation and the oxidation state of the Earth. Earth and Planetary Science Letters 236 (1-2): 78-95.

Walker, R.J., Shirey, S.B., and Stecher, O., 1988. Comparative Re-Os, Sm-Nd and Rb-Sr isotope and trace element systematics for Archean komatiite flows from Munro Township, Abitibi belt, Ontario. Earth and Planetary Science Letters 87 (1-2): 1-12.

Walker, R.J., Morgan, J.W., and Horan, M.F., 1995. ^{187}Os enrichment in some plumes: evidence for core-mantle interaction? Science 269 (5225): 819-822.

Walker, R.J., Morgan, J.W., Beary, E.S., Smoliar, M.I., Czamanske, G.K., and Horan, M.F., 1997. Applications of the ^{190}Pt-^{186}Os isotope system to geochemistry and cosmochemistry. Geochimica et Cosmochimica Acta 61 (22): 4799-4807.

Walker, R. J., Horan, M. F., Morgan, J. W., Becker, H., Grossman, J. N., Rubin, A. E., 2002. Comparative ^{187}Re-^{187}Os systematics of chondrites: Implications regarding early solar system processes. Geochimica et Cosmochimica Acta **66** (23): 4187-4201.

Walker, R.J., Horan, M.F., Shearer, C.K., and Papike, J.J., 2004. Low abundances of highly siderophile elements in the lunar mantle: Evidence for prolonged late accretion. Earth and Planetary Science Letters 224 (3-4): 399-413.

Walker, R.J., 2009. Highly siderophile elements in the Earth, Moon and Mars: Update and implications for planetary accretion and differentiation. Chemie der Erde - Geochemistry 69 (2): 101-125.

Walker, R.J., 2014. Siderophile element constraints on the origin of the Moon. Philosophical Transactions of the Royal Society of London 372: 20130258.

Walker, R.J., 2016. Siderophile Elements in Tracing Planetary Formation and Evolution. Geochemical Perspectives 5 (1): 1-145.

Walter, M.J., Nakamura, E., Trønnes, R.G., and Frost, D.J., 2004. Experimental constraints on crystallization differentiation in a deep magma ocean. Geochimica et Cosmochimica Acta 68 (20): 4267-4284.

White, W.M. and Patchett, J., 1984. Hf-Nd-Sr isotopes and incompatible element abundances in island arcs: implications for magma origins and crust-mantle evolution. Earth and Planetary Science Letters 67 (2): 167-185.

Widom, E., 1997. Sources of ocean island basalts: A review of the osmium isotope evidence. Physica A: Statistical Mechanics and its Applications 244 (1-4): 484-496.

Willbold, M., Elliott, T., and Moorbath, S., 2011. The tungsten isotopic composition of the Earth's mantle before the terminal bombardment. Nature 477 (7363): 195-198.

Willbold, M., Mojzsis, S.J., Chen, H.W., and Elliott, T., 2015. Tungsten isotope composition of the Acasta Gneiss Complex. Earth and Planetary Science Letters 419: 168-177.

Willig, M. and Stracke, A., 2019. Earth's chondritic light rare earth element composition: Evidence from the Ce-Nd isotope systematics of chondrites and oceanic basalts. Earth and Planetary Science Letters 509: 55-65.

Willig, M., Stracke, A., Beier, C., and Salters, V.J.M., 2020. Constraints on mantle evolution from Ce-Nd-Hf isotope systematics. Geochimica et Cosmochimica Acta 272: 36-53.

Wilson, A.H. and Carlson, R.W., 1989. A Sm-Nd and Pb isotope study of Archaean greenstone belts in the southern Kaapvaal Craton, South Africa. Earth and Planetary Science Letters 96 (1-2): 89-105.

Wyman, D.A., 2013. A critical assessment of Neoarchean "plume only" geodynamics: Evidence from the Superior Province. Precambrian Research 229: 3-19.

Wyman, D., 2019. Do cratons preserve evidence of stagnant lid tectonics? Geoscience Frontiers 9 (1): 3-17.

Wyman, D., 2020. Komatiites From Mantle Transition Zone Plumes. Frontiers in Earth Science **8** (383): 540744.

Yin, Q., Jacobsen, S.B., Yamashita, K., Blichert-Toft, J., Telouk, P., Albarede, F., 2002. A short timescale for terrestrial planet formation from Hf-W chronometry of meteorites. Nature **418** (6901): 949-952.

Yokoyama, T., Walker, D., and Walker, R.J., 2009. Low osmium solubility in silicate at high pressures and temperatures. Earth and Planetary Science Letters 279 (3-4): 165-173.

2064 Young, E.D., Kohl, I.E., Warren, P.H., Rubie, D.C., Jacobson, S.A., and Morbidelli, A., 2016.
2065 Oxygen isotopic evidence for vigorous mixing during the Moon-forming giant impact.
2066 Science 351 (6272): 493-496.
2067 Zindler, A., Jagoutz, E., Goldstein, S. L., 1982. Nd, Sr and Pb isotopic systematics in a three-
2068 component mantle: a new perspective. Nature **298** (5874): 519-523.
2069 Zindler, A., Hart, S. R., 1986. Chemical Geodynamics. Annual Reviews of Earth and
2070 Planetary Sciences **14**: 493-571.
2071
2072

Figure captions

Fig. 1. Variations of model-specific (see the references below for the specific models used), time-integrated Sm/Nd and Lu/Hf ratios in the mantle sources of Archean and Proterozoic komatiite-basalt systems studied to date. The individual models assume a minimum-degree fractionation of Sm/Nd and Lu/Hf in the particular mantle domains from either the chondritic values or values defined by the combined $^{142,143}Nd/^{144}Nd$ systematics (where available) to those required to bring the $\varepsilon^{143}Nd$ and $\varepsilon^{176}Hf$ in the mantle sources to the initial $\varepsilon^{143}Nd$ and $\varepsilon^{176}Hf$ by the times of the respective komatiite formation. The solid line connects Sm/Nd and Lu/Hf ratios inferred for the chondritic uniform reservoir (CHUR) and modern depleted mantle (DMM). Data are from: Ottawa − Blichert-Toft and Arndt (1999); 2.05 Ga Lapland – Puchtel et al. (2020); 2.41 Ga Vetreny − Puchtel et al. (2016b); 2.72 Ga Pyke Hill and Alexo − Dupre et al. (1984), Walker et al. (1988), Blichert-Toft and Arndt (1999); 2.72 Ga Boston Creek − Puchtel et al. (2018); 2.82 Ga Kostomuksha − Puchtel et al. (1998), Blichert-Toft and Puchtel (2010); 3.48 Ga Komati and 3.26 Ga Weltevreden − Puchtel et al. (2013); 3.32 Ga Commondale − Wilson and Carlson (1989), Hoffmann and Wilson (2017); 3.55 Ga Schapenburg − Puchtel et al. (2009a, 2016a); 3.53 Ga Coonterunah, 3.34 Ga Kelly, and 3.18 Ga Ruth Well and Regal – Puchtel et al. (2022). The CHUR and DMM parameters are from Jacobsen and Wasserburg (1980), Hamilton et al. (1983), Goldstein et al. (1984), Vervoort and Blichert-Toft (1999), and Bouvier et al. (2008). All uncertainties are 2SD of the mean.

Fig. 2. (a) Initial $^{187}Os/^{188}Os$ expressed as $\gamma^{187}Os$ and **(b)** initial $^{186}Os/^{188}Os$ expressed as $\mu^{186}Os$ of Archean komatiite systems studied to date, plotted as a function of their age. The blue bars for the modern BSE estimates represent the 2SD of the mean from Meisel et al. (2001) and Brandon et al. (2006) for (a) and (b), respectively. Data are from: 2.05 Ga Lapland − Puchtel et al. (2020); 2.41 Ga Vetreny − Puchtel et al. (2016b); 2.69 Ga Belingwe and 2.72 Ga Pyke Hill − Puchtel et al. (2009a); 2.72 Ga Boston Creek − Puchtel et al. (2018); 2.82 Ga Kostomuksha − Puchtel et al. (2005); 2.88 Ga Volotsk − Puchtel et al. (2007); 3.48 Ga Komati and 3.26 Ga Weltevreden − Puchtel et al. (2014); 3.55 Ga Schapenburg − Puchtel et al. (2009b, 2016a); 3.34 Ga Kelly and 3.18 Ga Ruth Well and Regal − Puchtel et al. (2022). The data for chondritic meteorites are compiled from Walker et al. (2002), Horan et al. (2003), Brandon et al. (2005; 2006), and Fischer-Gödde et al. (2010) and are plotted as an envelope enclosed between the slanting purple lines and corresponding to the entire range of calculated modern $\gamma^{187}Os$ and $\mu^{186}Os$ values projected back to the Solar System initial $^{187}Os/^{188}Os$ and $^{186}Os/^{188}Os$ ratios. All uncertainties are 2SD of the mean.

Fig. 3. Calculated total HSE abundances in the sources of Archean and Paleoproterozoic komatiite systems plotted as *percent* of those in estimates of the modern BSE of Becker et al. (2006). The blue dashed lines correspond to the range for the BSE estimates from Becker et al. (2006). The dark-red arrow represents the regression line through the data. The dark-red vertical arrows represent the projections to the x-axis from the intersections of the regression line with the range for the BSE estimate, thus, illustrating the uncertainties on the average time of homogenization of late accreted materials within the mantle (2.5±0.2 Ga). Data are

from: 2.05 Ga Lapland − Puchtel et al. (2020); 2.41 Ga Vetreny Belt − Puchtel et al. (2016b); 2.69 Ga Belingwe − Puchtel et al. (2009a); 2.72 Ga Pyke Hill and Alexo − Puchtel et al. (2004b, 2009a); 2.72 Ga Boston Creek − Puchtel et al. (2018); 2.82 Ga Kostomuksha − Puchtel and Humayun (2005); 2.88 Ga Volotsk − Puchtel et al. (2007); 3.26 Ga Weltevreden and 3.48 Ga Komati − Puchtel et al. (2014); 3.55 Ga Schapenburg − Puchtel et al. (2009b, 2016a); 3.53 Ga Coonterunah, 3.34 Ga Kelly, and 3.18 Ga Ruth Well and Regal − Puchtel et al. (2022). Uncertainties are 2SD. The data reveal a broad trend of increasing HSE abundances in komatiite mantle sources over geological time. All uncertainties are 2SD of the mean. See text for additional details and the ***Electronic Supplement*** for the algorithm used to estimate the HSE abundances in the sources of the komatiite systems.

Fig. 4. Evolution of the time-integrated $^{147}Sm/^{144}Nd$ and $^{176}Lu/^{177}Hf$ in the calculated sources of the Komati and Weltevreden komatiite systems formed during crystallization of a primordial magma ocean. The differentiation trends (shown by tick marks in percentage) depend on the relative proportions of the fractionating lower mantle mineral phases, *i.e.*, bridgmanite and Ca-Pv. The composition of the magma ocean prior to onset of crystallization is represented by that of the CHUR. The upper part of the panel represents aggregate compositions of magma ocean cumulates, while the lower part of the panel represents compositions of residual liquids after removal of the respective amounts of cumulate bridgmanite and Ca-Pv. All uncertainties are 2SD of the mean. See text for additional details of the model and the ***Electronic Supplement*** for the algorithm used in the calculations.

Fig. 5. Values of $\mu^{182}W$ versus (A) $\mu^{186}Os$ and (B) $\gamma^{187}Os$ in the Kostomuksha komatiites illustrating mixing between the modern BSE and a mantle reservoir preserved from an early magma ocean crystallization event. The Re/Os, Pt/Os, and Hf/W ratios were established by high-pressure and -temperature metal-silicate equilibrium, resulting in $^{187,186}Os$ and ^{182}W enrichments at 2.82 Ga (Touboul et al., 2012). The coupled $^{186,187}Os$ and ^{182}W excesses in the source of the Kostomuksha komatiites (yellow circle) are explained by a ~50% contribution from the isotopically enriched reservoir to the modern BSE. All uncertainties are 2SD of the mean. See text for additional details.

Fig. 6. $\mu^{182}W$ (ppm) versus calculated total HSE abundances in the sources of Archean and Paleoproterozoic komatiite-basalt systems studied to date relative to those in the estimates of the present-day BSE of Becker et al. (2006). This proportion corresponds to the fraction of the total HSE budget of the BSE added during late accretion assuming an HSE-free terrestrial mantle prior to late accretion. The average $\mu^{182}W$ value for the Moon of +25±5 is from Kruijer et al. (2015) and Touboul et al. (2015). The $\mu^{182}W$ of the BSE prior to late accretion is constrained *via Isoplot* regression analysis of the $\mu^{182}W$ and HSE compositions of all komatiite-basalt systems except for those of Kostomuksha and Schapenburg and the present-day BSE to be +17±7. The W isotopic data and estimates of the HSE contents for the komatiite systems are from Puchtel and Humayun (2005), Touboul et al. (2012), and Puchtel et al. (2014; 2009b, 2016a,b; 2018; 2020; 2022). All uncertainties are 2SD of the mean. See text for additional details.

Fig. 7. $^{182}W/^{184}W$ and $^{142}Nd/^{144}Nd$ data for the terrestrial mafic-ultramafic rock record obtained to date. The colored bands represent the 2SD uncertainty on the mean $\mu^{182}W$ and $\mu^{142}Nd$ values for each locality. The red arrows illustrate the change in direction and magnitude of the ^{182}W and ^{142}Nd anomalies. Note the relative scarcity of data for the period between ~2.7 Ga and present day. Data are from: 3.96 Ga Acasta − Roth et al. (2014), Willbold et al. (2015), Reimink et al. (2018); 3.85 Ga Isua − Willbold et al. (2011), Rizo et al. (2013, 2016), Dale et al. (2017), Tusch et al. (2019), Caro et al. (2006), Bennett et al. (2007), Saji et al. (2018); 3.80 Ga Nuvvuagittuq − O'Neil et al. (2012), Touboul et al. (2014); 3.78 Ga Saglek − Liu et al. (2016), Morino et al. (2017); 3.75 Ga Ukaliq − Caro et al. (2017); 3.72 Ga Isua − Rizo et al. (2011, 2016), Tusch et al. (2019), O'Neil et al. (2016); 3.50 Ga Ameralik − Saji et al. (2018); 3.37 Ga Ameralik − Rizo et al. (2012, 2016), Tusch et al. (2019); 3.55 Ga Schapenburg − Puchtel et al. (2016a); 3.53 Ga Coonterunah – Tusch et al. (2021), Puchtel et al. (2021); 3.48 Ga Komati and 3.26 Weltevreden − Touboul et al. (2012), Caro et al. (2006), Puchtel et al. (2013), Schneider et al. (2018); 3.45 Ga Warrawoona – Archer et al. (2019), Rizo et al. (2019), Murphy et al. (2021); 3.35 Ga Kelly – Puchtel et al. (2022); 3.18 Ga Ruth Well and Regal – Archer et al. (2019), Tusch et al. (2021), Puchtel et al. (2022); 3.14 Ga Banasandra − Maya et al. (2017); 2.82 Ga Kostomuksha and 2.69 Ga Belingwe − Touboul et al. (2012), Boyet and Carlson (2006); 2.72 Ga Boston Creek − Puchtel et al. (2018); 2.72 Ga Theo's Flow – Debaille et al. (2013); 2.41 Ga Vetreny Belt − Puchtel et al. (2016b); 2.05 Ga Lapland − Puchtel et al. (2020); modern OIB − Caro et al. (2006), Andreasen et al. (2008), Murphy et al. (2010), Touboul et al. (2012), Mundl et al. (2017), Mundl-Petermeier et al. (2019, 2020), Rizo et al. (2019), Horan et al. (2018), Saji et al. (2018), Peters et al. (2018), Hyung and Jacobsen (2020); modern MORB − Caro et al. (2006), Mundl et al. (2017), Hyung and Jacobsen (2020).

Table 1. Summary of ages, thermodynamic parameters, and chemical features of the komatiite systems considered in this review.

Komatiite-basalt system	Age, Ga	MgO_{liq}	T_{liq}°C	T_p°C	$D_{melt\ init,\ km}$	$D_{plume\ init,\ km}$	Al_2O_3/TiO_2	$(La/Sm)_N$	$(Gd/Yb)_N$	Nb/Nb*	W/Th
Kaapvaal Craton, South Africa											
Schapenburg	3.55	29.1±2.8	1582	1811	443	LM	10.0±0.8	0.93±0.04	1.57±0.10	1.2±0.1	9.7±5.5
Komati	3.48	29.9±0.5	1591	1822	494	LM	10.1±0.7	0.97±0.24	1.39±0.05	1.1±0.2	0.25±0.18
Weltevreden	3.26	31.4±0.9	1606	1841	605	LM	29.2±1.1	0.68±0.06	0.84±0.03	1.4±0.1	1.5±1.4
Pilbara Craton, Western Australia											
Coonterunah	3.53	23.0±0.3	1498	1705	203	MTZ	23.8±1.7	0.80±0.04	0.96±0.04	1.08±0.02	0.91±0.62
Kelly	3.34	27.4±1.0	1561	1786	351	MTZ	22.1±1.7	0.65±0.02	0.91±0.04	1.03±0.04	0.81±0.69
Ruth Well	3.18	29.3±0.7	1584	1814	455	MTZ	11.0±0.5	0.55±0.09† *0.77±0.09*	1.31±0.04† *1.32±0.04*	1.0±0.1† *0.51±0.05*	3.4±2.3
Regal	3.18	29.3±0.7	1584	1814	455	MTZ	11.9±0.8	0.61±0.11† *0.83±0.11*	1.28±0.12† *1.31±0.12*	1.0±0.1† *0.55±0.09*	3.5±2.8
Fennoscandian Shield, northern Europe											
Kostomuksha	2.82	27.6±1.0	1564	1789	361	LM	17.2±1.2	0.48±0.13	1.16±0.02	1.2±0.1	0.84±0.32
Vetreny	2.41	27.0±1.0	1556	1779	333	MTZ	19.7±0.5	0.41±0.10† *2.2±0.1*	1.2±0.1† *1.3±0.1*	1.0±0.1† *0.29±0.03*	0.05±0.02
Lapland	2.05	25.2±0.5	1532	1748	264	LM	13.9±0.4	0.14±0.02† *0.26±0.01*	1.48±0.02† *1.49±0.02*	1.0±0.1† *0.58±0.01*	0.16±0.06
Superior Craton, Canada											
Boston Creek	2.72					MTZ	5.1±0.8	1.9±0.3	2.0±0.2	1.2±0.2	0.9±1.4
Pyke Hill-Alexo	2.72	28.2±0.5	1571	1789	392	MTZ	20.4±0.6	0.53±0.16	0.98±0.03	1.0±0.1	0.15±0.06
Rhodesian Craton, Zimbabwe											
Belingwe	2.69	25.6±0.5	1537	1755	277	MTZ	19.8±0.6	0.68±0.02	1.02±0.04	0.97±0.05	0.20±0.06

†Values corrected for AFC. The italicized values are those measured in the emplaced lavas, before correction for AFC. All uncertainties are 2SD of the mean. **MgO_{liq}** – the MgO content of the original emplaced komatiite magma for each komatiite system compiled from Nicklas et al. (2018, 2019) and Puchtel et al. (1998, 2016a, 2020, 2022). **T_{liq}°C, T_p°C** – liquidus temperatures of the emplaced komatiite magmas and mantle potential temperatures for the studied komatiite systems. $D_{melt\ init}$ – depths of melting initiation. $D_{plume\ init}$ – inferred depths of plume initiation for the studied komatiite systems. $Nb/Nb^* = Nb_N/\sqrt{(Th_N \times La_N)}$, where N are the BSE normalizing values from Hofmann (1988). For sources of the data see Table 2. See text and the ***Electronic Supplement*** for details.

Table 2. Summary of isotopic features and HSE abundances of the komatiite systems considered in this review

Komatiite-basalt system	ε^{143}Nd(T)	ε^{176}Hf(T)	μ^{142}Nd	μ^{182}W	γ^{187}Os(T)	μ^{186}Os(T)	∑HSE	Data source
Kaapvaal Craton, South Africa								
Schapenburg	+2.4±0.5	+5.8±0.8	–5.0±2.8	–8.4±4.1	+3.7±0.3		29±9	[1 – 2]
Komati	+0.46±0.39	+1.9±1.0	–0.9±2.7	+2.7±4.5	+0.3±0.3	–12±8	60±8	[3 – 5]
Weltevreden	+0.54±0.40	+4.7±2.1	+2.5±3.8		–0.1±0.2	+22±7	65±6	[3 – 4]
Pilbara Craton, Western Australia								
Coonterunah	+2.4±0.5	+4.4±0.3		+11.4±4.6			29±6	[6]
Kelly	+0.5±0.6	+1.7±0.6		+8.2±3.3	+0.8±0.4		38±7	[6]
Ruth Well	+1.3±0.7† *+0.6±0.7*	+2.4±0.4† *+1.7±0.4*	–1.8±3.8	+7.7±5.0	–0.4±0.4† *–0.4±0.4*		55±4	[6]
Regal	+1.9±0.3† *+1.0±0.3*	+4.6±0.8† *+4.1±0.8*		+7.7±5.0	+0.9±0.3† *+0.9±0.3*		70±5	[6]
Fennoscandian Shield, northern Europe								
Kostomuksha	+3.0±0.4	+4.9±0.3	+0.4±0.9	+15.0±4.8	+2.5±0.6	+22±6	79±6	[7 – 11]
Vetreny	+3.7±0.4† *–0.9±0.4*	+6.3±0.9† *+0.4±0.9*	+0.5±2.1	–0.5±5.2† *+7.5±5.2*	+1.3±0.2† *+1.7±0.2*	+3.2±1.7	66±10	[12]
Lapland	+4.9±0.3† *+3.7±0.3*	+10.2±0.7† *+8.7±0.7*		–10.0±5.0† *+1.5±3.3*	–0.2±0.3† *–0.2±0.3*	+29±2	120±5	[13]
Superior Craton, Canada								
Boston Creek	+2.5±0.2	+4.3±0.9	–3.8±2.8	+11.7±4.5	+0.1±0.3		35±10	[14]
Pyke Hill-Alexo	+3.0±0.5	+5.5±0.6	+6.8±2.5		+0.4±0.1	–0.1±4.2	85±5	[15 – 19]
Rhodesian Craton, Zimbabwe								
Belingwe	+2.9±0.2		+3.7±7.0		+0.1±0.2	+0.6±2.5	57±7	[20 – 21]

†Values corrected for AFC. The italicized values are those measured in the emplaced lavas, before correction for AFC. All uncertainties are 2SD of the mean. Data sources are as follows: [1] - Puchtel et al. (2009a); [2] - Puchtel et al. (2016a); [3] - Puchtel et al. (2013); [4] - Puchtel et al. (2014); [5] - Touboul et al. (2012); [6] - Puchtel et al. (2022); [7] - Puchtel et al. (1998); [8] - Boyet and Carlson (2006); [9] - Touboul et al. (2012); [10] - Puchtel et al. (2005); [11] - Puchtel and Humayun (2005); [12] - Puchtel et al. (2016b); [13] - Puchtel et al. (2020); [14] - Puchtel et al. (2018); [15] - Blichert-Toft and Arndt (1999); [16] - Puchtel et al. (2004a); [17] - Puchtel et al. (2004b); [18] - Puchtel et al. (2009b); [19] - Debaille et al. (2013); [20] - Puchtel et al. (2009b); [21] - Boyet and Carlson (2006).

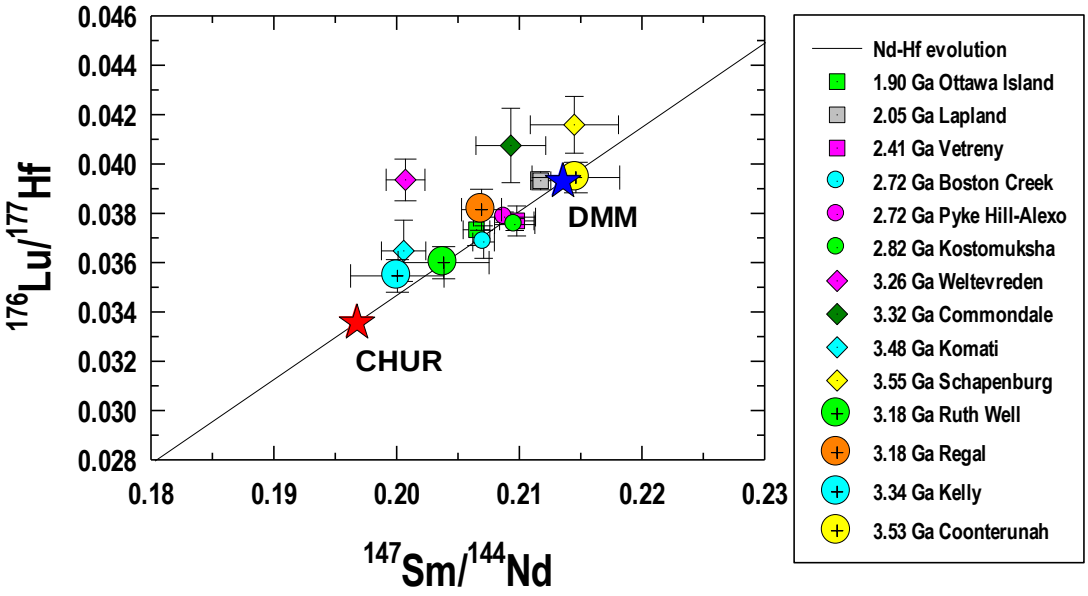

0.046
0.044
0.042
0.040
0.038
0.036
0.034
0.032
0.030
0.028
0.18
0.19
0.20
0.21
0.22
0.23
176Lu/177Hf
147Sm/144Nd
DMM
CHUR
Nd-Hf evolution
1.90 Ga Ottawa Island
2.05 Ga Lapland
2.41 Ga Vetreny
2.72 Ga Boston Creek
2.72 Ga Pyke Hill-Alexo
2.82 Ga Kostomuksha
3.26 Ga Weltevreden
3.32 Ga Commondale
3.48 Ga Komati
3.55 Ga Schapenburg
3.18 Ga Ruth Well
3.18 Ga Regal
3.34 Ga Kelly
3.53 Ga Coonterunah

Fig. 1

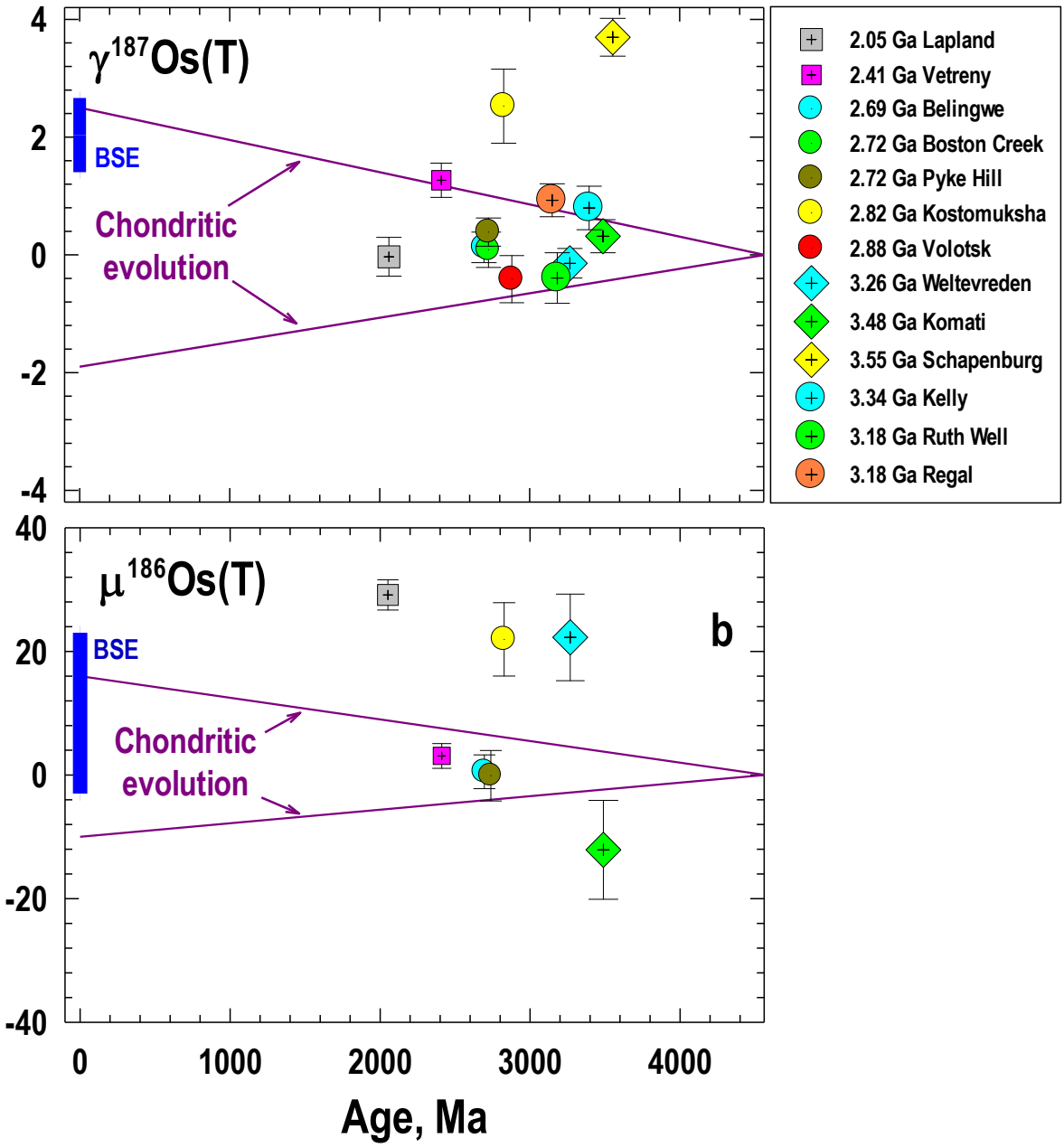
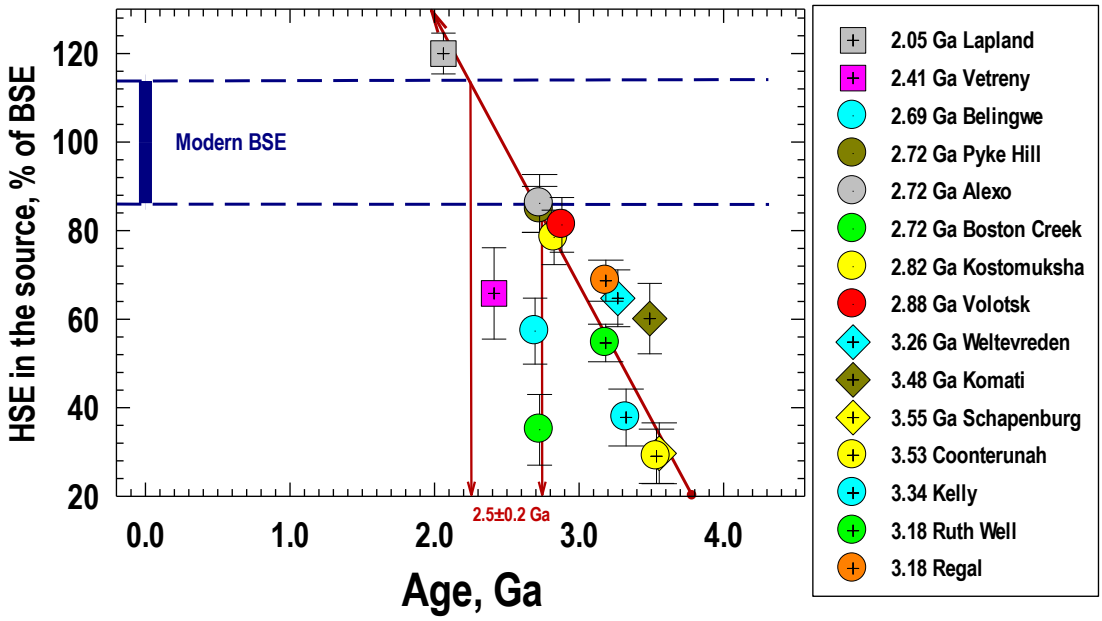

γ187Os(T)
BSE
Chondritic
evolution
μ186Os(T)
BSE
Chondritic
evolution
b
Age, Ma
2.05 Ga Lapland
2.41 Ga Vetreny
2.69 Ga Belingwe
2.72 Ga Boston Creek
2.72 Ga Pyke Hill
2.82 Ga Kostomuksha
2.88 Ga Volotsk
3.26 Ga Weltevreden
3.48 Ga Komati
3.55 Ga Schapenburg
3.34 Ga Kelly
3.18 Ga Ruth Well
3.18 Ga Regal

Fig. 2

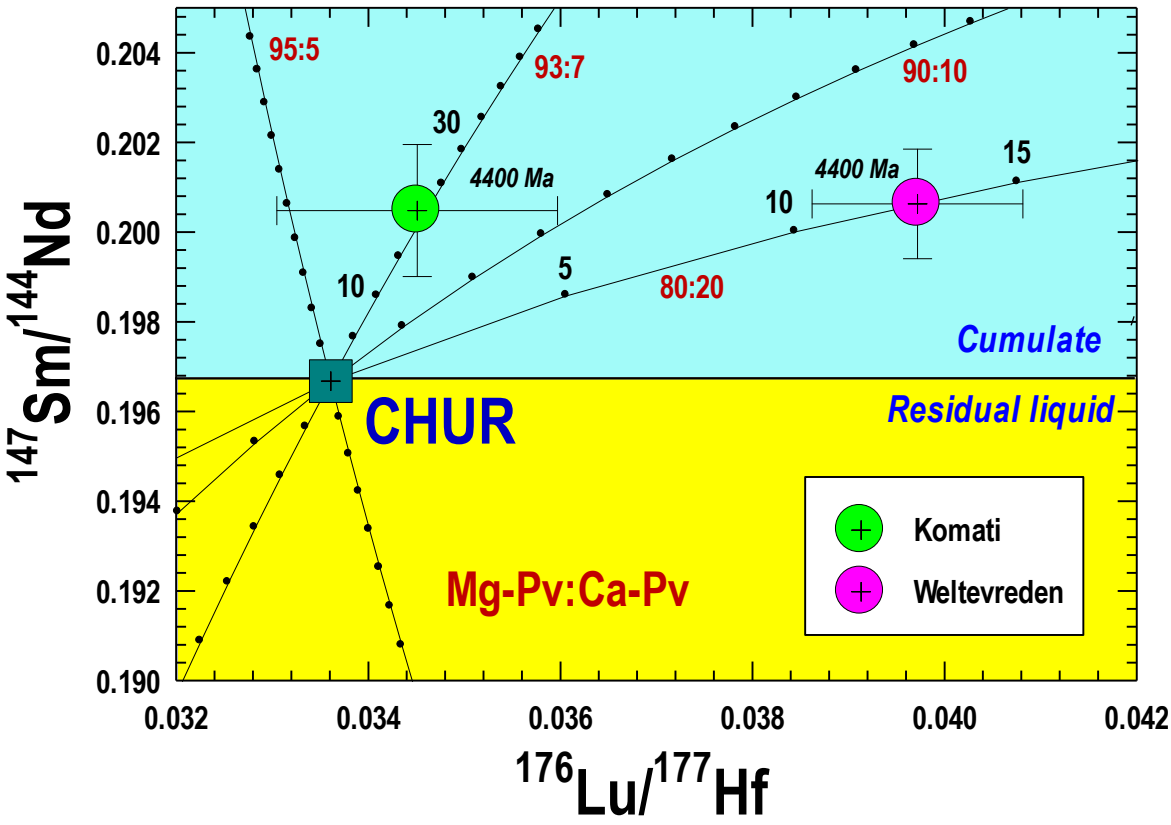


2200

2201

2202 **Fig. 3**

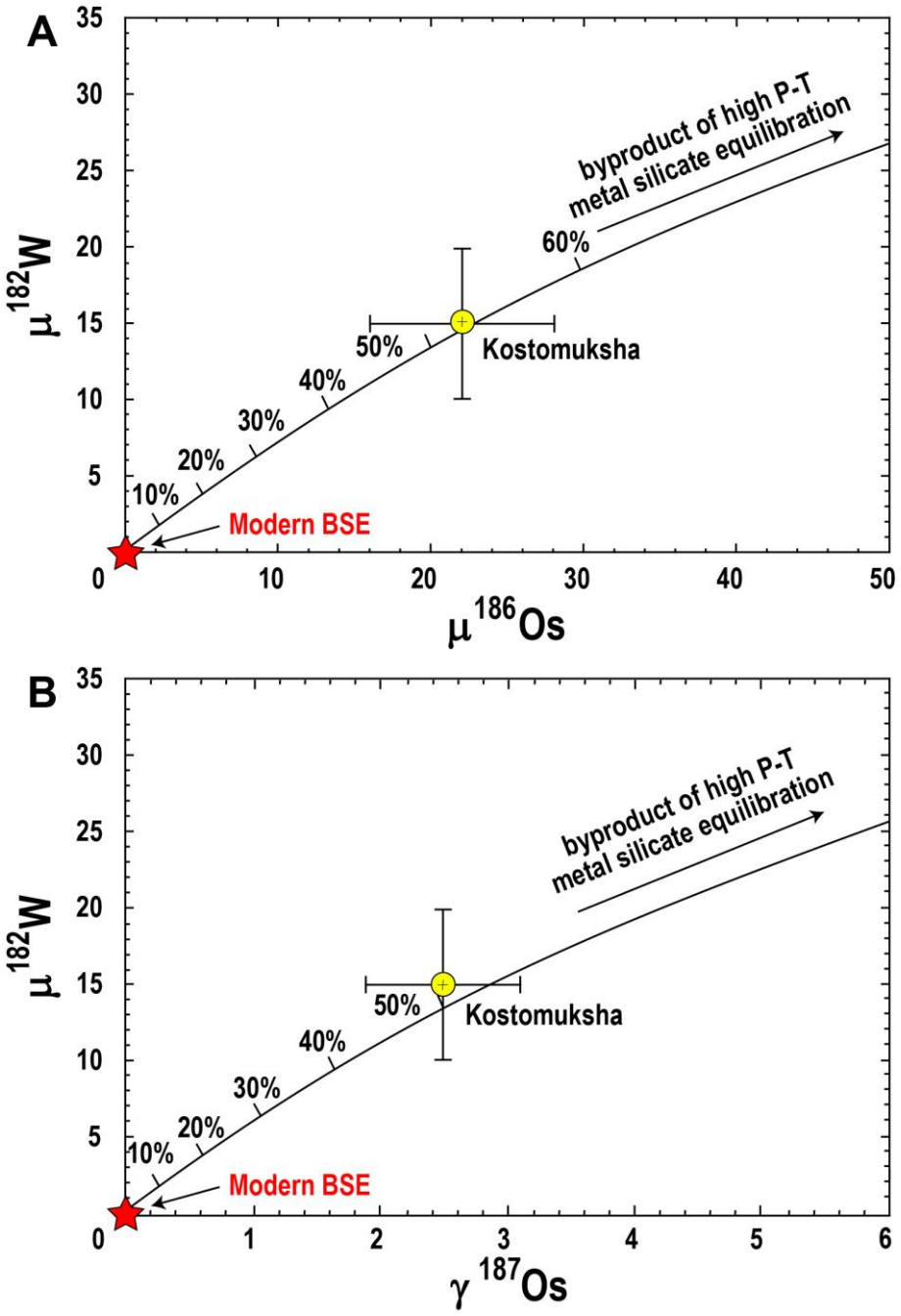
2203



2204
2205

2206 **Fig. 4**

2207



2208

2209 **Fig. 5.**

2210

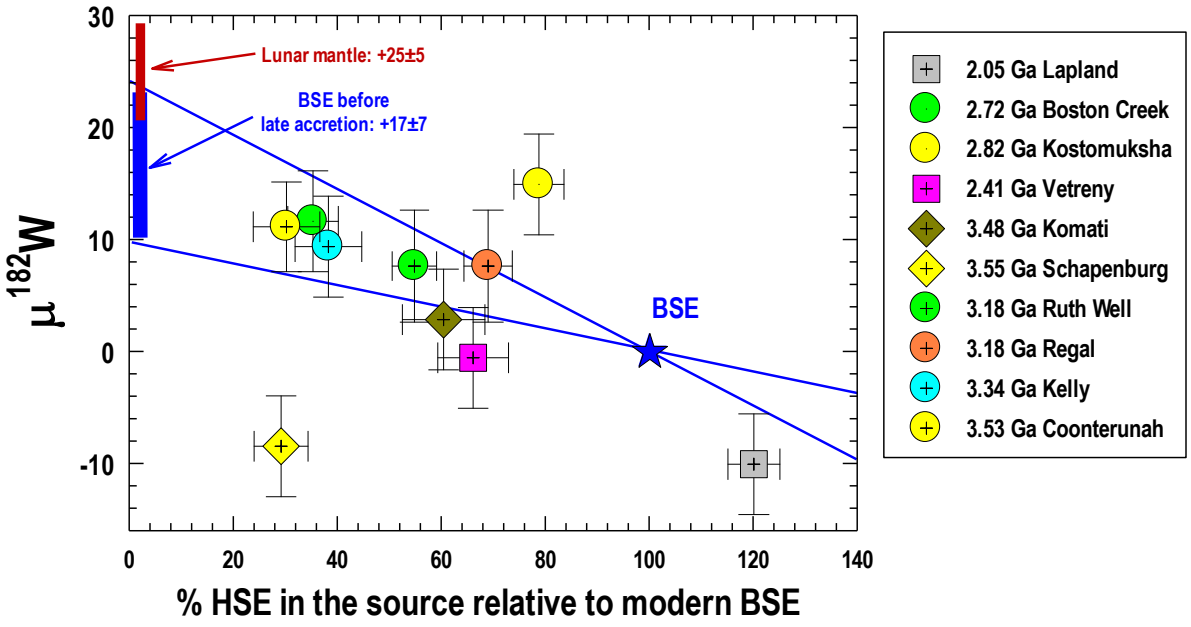

Lunar mantle: +25±5
BSE before
late accretion: +17±7
BSE
μ182W
% HSE in the source relative to modern BSE
2.05 Ga Lapland
2.72 Ga Boston Creek
2.82 Ga Kostomuksha
2.41 Ga Vetreny
3.48 Ga Komati
3.55 Ga Schapenburg
3.18 Ga Ruth Well
3.18 Ga Regal
3.34 Ga Kelly
3.53 Ga Coonterunah

Fig. 6.

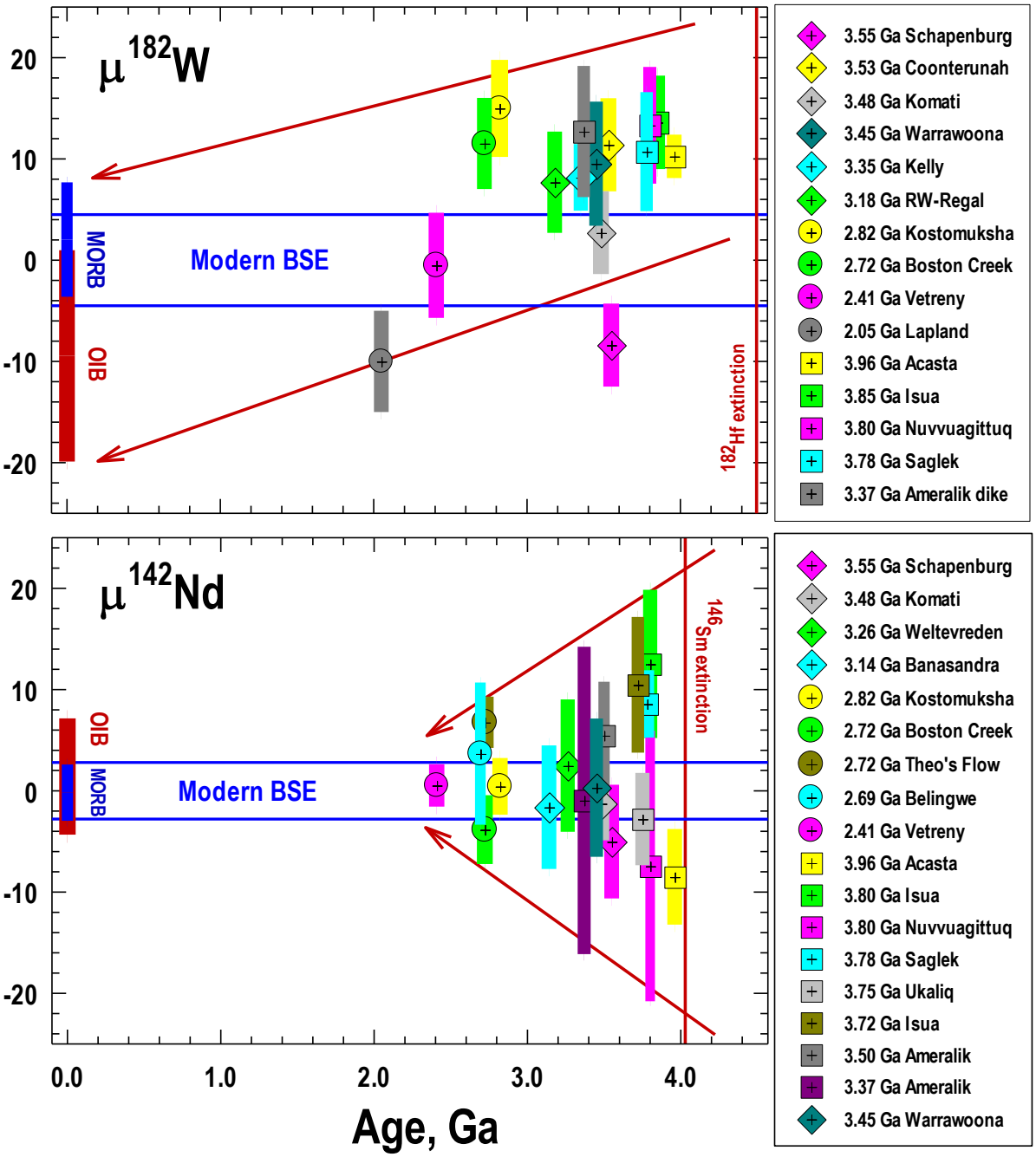

μ182W
20
10
0
-10
-20
MORB
OIB
Modern BSE
182Hf extinction
3.55 Ga Schapenburg
3.53 Ga Coonterunah
3.48 Ga Komati
3.45 Ga Warrawoona
3.35 Ga Kelly
3.18 Ga RW-Regal
2.82 Ga Kostomuksha
2.72 Ga Boston Creek
2.41 Ga Vetreny
2.05 Ga Lapland
3.96 Ga Acasta
3.85 Ga Isua
3.80 Ga Nuvvuagittuq
3.78 Ga Saglek
3.37 Ga Ameralik dike
μ142Nd
20
10
0
-10
-20
OIB
MORB
Modern BSE
146Sm extinction
3.55 Ga Schapenburg
3.48 Ga Komati
3.26 Ga Weltevreden
3.14 Ga Banasandra
2.82 Ga Kostomuksha
2.72 Ga Boston Creek
2.72 Ga Theo's Flow
2.69 Ga Belingwe
2.41 Ga Vetreny
3.96 Ga Acasta
3.80 Ga Isua
3.80 Ga Nuvvuagittuq
3.78 Ga Saglek
3.75 Ga Ukaliq
3.72 Ga Isua
3.50 Ga Ameralik
3.37 Ga Ameralik
3.45 Ga Warrawoona
0.0
1.0
2.0
3.0
4.0
Age, Ga

Fig. 7